TECHNISCHE UNIVERSITÄT MÜNCHEN

Wissenschaftszentrum Weihenstephan für Ernährung,
Landnutzung und Umwelt
Lehrstuhl für Atmosphärische Umweltforschung

Flux Footprint Modeling of Biosphere-Atmosphere Exchange Measurements

Katja Heidbach

Vollständiger Abdruck der von der Fakultät Wissenschaftszentrum Weihenstephan für Ernährung, Landnutzung und Umwelt der Technischen Universität München zur Erlangung des akademischen Grades
eines Doktors der Naturwissenschaften (Dr. rer. nat.)
genehmigten Dissertation.

Vorsitzende: Prof. Dr. Annette Menzel

Prüfer der Dissertation:
1. Prof. Dr. Hans Peter Schmid
2. Prof. Dr. Natascha Kljun
3. Prof. Dr. Hans Christian Bernhofer

Die Dissertation wurde am 28.08.2018 bei der Technischen Universität München eingereicht und durch die Fakultät Wissenschaftszentrum Weihenstephan für Ernährung, Landnutzung und Umwelt am 30.01.2019 angenommen.

Figure 1: Wordcloud generated with Heidbach et al. (2017).

Contents

Abstract

Especially due to climate change, the interest to understand interactions between the biosphere and the atmosphere has increased in the last decades. Thus, more reliable measurements of energy and gas exchange between these two spheres are required. They can be measured by the eddy covariance technique, the most direct method to measure such fluxes. The number of registered sites increased in the last decades, and currently exceeds 517 (October 2015, source: FLUXNET). Even though one assumption of the eddy covariance technique is homogeneous terrain, heterogeneous sites with naturally varying land cover changes are the rule. Over inhomogeneous areas, the measured flux is a function of source- and sink-distributions within the footprint of the respective flux averaging interval. The footprint can be considered as "field of view" of the sensor and reflects the influence of sources of a passive scalar on the flux or concentration measurement at a specific location. Therefore, the footprint provides valuable information that can be used for optimizing measurement locations, the interpretation of flux/concentration data, and up- and downscaling of measurements at different spatial scales.

Different types of models are available to estimate the footprint, ranging from simple and computationally low intensity analytical models, (semi-) empirical parameterizations, to Lagrangian particle models and complex "full flow" LES models. Especially in long-term flux observations, where routine footprint estimates are required, analytical models and parameterizations are the preferential class of footprint models, due to their mathematical simplicity, and hence their low computational expense. This practice also leads to the fact that such models are applied even under measurement conditions where the assumption of horizontally homogeneous turbulence is not fulfilled (i.e. at sites with varying topography or changes in surface roughness or thermal stratification).

In order to show how reliable the results of such computationally less intensive models are at real-world flux sites, this study presents an experimental evaluation of the flux footprint models of Kormann and Meixner (2001) (KM), Schmid (1994) (FSAM), Hsieh et al. (2000) (HS), and Kljun et al. (2015) (FFP) at a grassland site in southern Germany. For this purpose, an artificial tracer gas (methane) was released out of a single surface source of relatively small size (~ 1 m^2). The flux contributions from the tracer source were measured by eddy covariance and compared to those predicted by the footprint models. With different setups we were able to evaluate upwind as well as potential downwind flux contributions, and to analyze the effect of a sharp change in roughness length upstream of the measurement tower on the model performance. Additionally, we quantified footprint model uncertainty resulting from the random error of input parameters.

Our measurements show that all evaluated models match observations roughly, but tend to underestimate the value of the footprint maximum, and overestimate its upstream distance. The analysis of stability dependence of model performances indicates that the HS model clearly underestimates observations for near neutral to stable conditions, while no clear stability dependence could be identified for the performance of the other evaluated models.

Furthermore, we could show that there can indeed be measurable and non-negligible contributions to the flux from downwind sources. Even though flux contributions from the downwind source occurred only intermittently and not continuously, a dependence on along-wind turbulence intensity $\sigma_u/\overline{u}$ could be identified: in periods with low $\sigma_u/\overline{u}$, the downwind contribution is not relevant, whereas for along-wind turbulence intensities of 0.6 and higher, there is a much higher probability that downwind sources contribute to a measured flux.

As expected, model performance is sensitive to an abrupt change in surface roughness and sensible heat flux at a forest edge in the near upwind fetch of the measurement tower. Use of a local apparent roughness length (derived from measured wind speed and friction velocity) only slightly (or negligibly) improved model performance compared to the use of a constant local roughness length (determined from local surface characteristics). Thus, we confirm experimentally that footprint estimates and related data quality assessments should be handled with care at sites with inhomogeneities in surface roughness.

In the second part of this study, we present a pragmatic approach to include the effect of streamwise turbulence fluctuations into simple, similarity-theory based footprint models. For this purpose, we introduce a generic x-diffusion module. This module was then superimposed on the two-dimensional output of the footprint model FSAM (Schmid, 1994), resulting in the extended version FSAMx. With this practicable approach, footprint models describe turbulence more realistically, but remain simple enough for real time footprint analysis. Finally, we compared the new model FSAMx to a model of higher complexity, the backward Lagrangian model LPDM-B (Kljun et al., 2002), and found good agreement for conditions within the validity range of FSAMx.

Zusammenfassung

Durch den fortschreitenden Klimawandel ist auch das Interesse an Austauschprozessen zwischen Biosphäre und Atmosphäre in den letzten Jahrzehnten angestiegen. Für ein besseres Prozessverständnis sind verlässliche Messungen des Energie- und Gasaustauschs zwischen diesen beiden Spähren unerlässlich. Die direkteste Methode, um Gas-Flüsse zu messen, ist die Eddy-Kovarianz Methode. In den letzten Jahrzehnten ist die Anzahl an registrierten Eddy-Kovarianz Standorten bis auf 517 angestiegen (Stand Oktober 2015, Quelle: FLUXNET). Auch wenn die Eddy-Kovarianz Methode homogene Landoberflächen voraussetzt, findet man in der Realität eher komplexe, heterogene Standorte mit natürlich variierenden Landoberflächen. An inhomogenen Standorten hängt der gemessene Austauschfluss bzw. die Konzentration des entsprechenden Gases von der Zusammensetzung der Quellen und Senken innerhalb des Footprints des jeweiligen Messintervalls ab. Der Footprint kann als „Sichtfeld“ des Sensors betrachtet werden. Er gibt an, inwieweit Quellen eines passiven Skalars auf die an einem Ort gemessenen Flüsse oder Konzentrationen des Skalars Einfluss nehmen. Demzufolge liefert der Footprint wertvolle Informationen, die dazu dienen, den Standort einer Messung zu optimieren, Fluss- oder Konzentrationsmessungen besser interpretieren zu können sowie diese Messungen mit Daten in einer anderen räumlichen Auflösung vergleichen zu können.

Es werden verschiedene Modelltypen verwendet, um den Footprint abzuschätzen: von einfachen und weniger rechenintensiven analytischen Modellen und (semi-) empirischen Parameterisierungen bis hin zu Langrangeschen Partikelmodellen und komplexen LES Strömungsmodellen. Gerade in Langzeitstudien, die auf routinemäßigen Footprintberechnungen basieren, werden analytische Modelle und Parameterisierungen aufgrund ihrer geringen mathematischen Komplexität und demzufolge ihrem geringen Rechenaufwand bevorzugt. Das führt dazu, dass solche Modelle auch an Standorten angewendet werden, an denen ihre Bedingung der horizontalen, homogenen Turbulenz nicht erfüllt ist (so zum Beispiel an Standorten mit wechselnder Topographie oder Änderungen der Oberflächenrauhigkeit oder der thermischen Schichtung).

Um zu zeigen, wie verlässlich die Ergebnisse von solch weniger rechenintesiven Footprint-Modellen an realen Messstandorten ist, wurden in dieser Studie experimentelle Evaluierungen der Modelle von Kormann und Meixner (2001) (KM), Schmid (1994) (FSAM), Hsieh et al. (2000) (HS) und Kljun et al. (2015) (FFP) an einem Grünland-Standort im süddeutschen Alpenvorland durchgeführt. Hierfür wurde ein künstliches Tracergas (Methan) aus einer vergleichsweise kleinen Vorrichtung (~ 1 m^2) an der Oberfläche emittiert. Die Beiträge des Tracers zum gemessenen Fluss wurden mit der Eddy-Kovarianz Methode gemessen und anschließend mit den von den Footprint-Modellen errechneten Beiträgen verglichen. Mit Hilfe verschiedener Messaufbauten konnten Flussbeiträge so-

wohl von der Luv- als auch von der Lee-Seite des Sensors evaluiert werden. Desweiteren wurde untersucht, inwieweit eine deutliche Änderung der Rauhigkeitslänge in der Nähe des Messturms die Genauigkeit der Modelle beeinflusst. Darüber hinaus wurde die Unsicherheit der Footprint-Modelle, die aus zufälligen Fehlern der Eingangsparameter resuliert, berechnet.

Alle untersuchten Modelle entsprechen zwar im Großen und Ganzen den Beobachtungen, tendieren allerdings dazu, den Betrag des Footprint-Maximums zu unterschätzen und dessen Distanz zu überschätzen. Untersuchungen über die Modellqualität bei verschiedenen Stabilitäten veranschaulichen, dass das HS Modell die Messungen unter neutraler und stabiler Schichtung deutlich unterschätzt. Für die anderen untersuchten Modelle konnte keine Abhängigkeit von der atmosphärischen Schichtung festgestellt werden.

Des Weiteren konnte gezeigt werden, dass Beiträge von leeseitigen Quellen zum gemessenen Fluss durchaus messbar sind und nicht vernachlässigt werden können. Auch wenn diese Beiträge unregelmäßig und nicht kontinuierlich aufgetreten sind, konnten wir dennoch eine Abhängigkeit von der Turbulenzintensität entlang der mittleren Windrichtung ($\sigma_u/\overline{u}$) feststellen: In Messperioden mit einer geringen Turbulenzintensität spielten leeseitige Flussbeiträge keine Rolle, während die Wahrscheinlichkeit, dass Quellen im Lee der Messung zum gemessenen Fluss beitragen ab einer Intensität von 0.6 deutlich steigt.

Erwartungsgemäß ändert sich die Aussagekraft der Modelle bei einer Waldkante im Luv der Messungen und einer damit verbundenen abrupten Änderung der Oberflächenrauhigkeit und des sensiblen Wärmestroms. Die Berechnung der lokalen Rauhigkeitslänge (berechnet aus Windgeschwindigkeit und Schubspannungsgeschwindigkeit) verbesserte die Aussagekraft der Modelle im Vergleich zu einer konstanten Rauhigkeitslänge (berechnet aus lokalen Oberflächencharakteristiken) nur geringfügig. Demzufolge sollten Footprintberechnungen und damit verbundene Qualitätskontrollen von Daten an Standorten mit inhomogener Oberflächenrauhigkeit mit Vorsicht genossen werden.

Im zweiten Teil dieser Studie wird ein praktischen Ansatz vorgestellt, wie die Turbulenz entlang der mittleren Windrichtung in einfache, auf der Ähnlichkeitstheorie basierende Modelle integriert werden kann. Hierfür wurde ein unabhängiges Modul entwickelt, das zusammen mit dem ursprünglichen Modell FSAM (Schmid, 1994) die erweiterte Version FSAMx bildet. Durch das Modul wird die Turbulenz in FSAMx realistischer beschrieben und gleichzeitig dessen Anwendbarkeit für Footprint Analysen in Echtzeit erhalten. Bei einem Vergleich des neuen Modells FSAMx mit einem komplexeren Modell, dem Lagrangeschen stochastischen Modell LPDM-B (Kljun et al., 2002), wurde für Bedingungen, die im Gültigkeitsbereich von FSAMx liegen, eine gute Übereinstimmung der beiden Modelle gefunden.

1 Introduction

With the progress of climate change, the interest to understand interactions between the biosphere and the atmosphere has increased in the last decades. Therefore, the demand on reliable measurements of energy and mass exchange fluxes between these two Earth system compartments has increased and thus the number of eddy covariance measurement systems. The eddy covariance (EC) technique is the most direct method to measure such fluxes and is nowadays a widespread and established measurement method. In October 2015, 517 active eddy covariance site were registered in FLUXNET, a global network of micrometeorological flux measurement sites (Baldocchi et al., 2001).
Although an EC-flux measurement takes place at a specific point in the atmosphere, measured fluxes originate from an area located mostly upwind of the measurement system. This area is called footprint and can be considered the "field of view" of the sensor. It reflects the influence of the surface on the measured flux (Vesala et al., 2008). The next two sections address the concept and theory of the footprint in more detail, as well as its importance for practical applications.

1.1 The concept of the footprint

Flux measurements at a specific location and height do not only capture the flux exactly below the sensor but represent a spatially weighted average of sources/sinks of the relevant scalar distributed in the surrounding of the sensors. As illustrated in Fig. 2, emitted gas parcels are lifted from the surface and are transported to higher levels of the atmosphere due to turbulence from buoyancy or friction effects. However, only a few of them reach the sensor and are "seen" by the instruments. Here the footprint comes into play, which is something akin to the "field of view" of a flux measurement (Vesala et al., 2008; Schmid, 2002): it represents the probability that a molecule emitted from an elemental surface source reaches the measurement point (Kljun et al., 2002). Thus, the footprint can be interpreted as relative contribution from each elemental surface source to the measured vertical flux (Schuepp et al., 1990). It thus corresponds to a source weight function.
Other frequently used terms in literature are "area of influence" and "source area". However, as these denote not a function, but a specific area, they can be interpreted as the integral of the source weight function over a specified domain (Schmid, 1994), i.e. the smallest possible area responsible for (e.g.) 80% contribution to the flux. The source area and its relation to the source weight function is illustrated in Fig. 3. In some cases, the term "fetch" is erroneously equated with footprint. However, it describes the upstream reach of the (homogeneous) area of interest, which needs to be sufficiently large in order to have a larger extension than any potential source area (Burba, 2013; Leclerc and

Foken, 2014).

The footprint function has a characteristic shape that may be stretched or squeezed, both in along-wind and crosswind direction, depending on atmospheric conditions. The typical shape is illustrated in Fig. 2 (gray areas), and in Fig. 3 in a 2-dimensional and 3-dimensional way, respectively. Eddies that capture gases or energy from sources at small distances to the tower are mostly advected beyond the instruments before reaching the measurement height. Therefore, such sources contribute only little to the measured flux, and are associated with a lower footprint weighting factor. With increasing distance, the probability of surface sources contributing to the measured flux increases, until a maximum is reached. From this point on to longer distances the footprint function decreases again (Fig. 3). Several approaches exist to determine the footprint function f and these are described in more detail in Section 2.4.

Position, size, and shape of the footprint are a function of site and flow characteris-

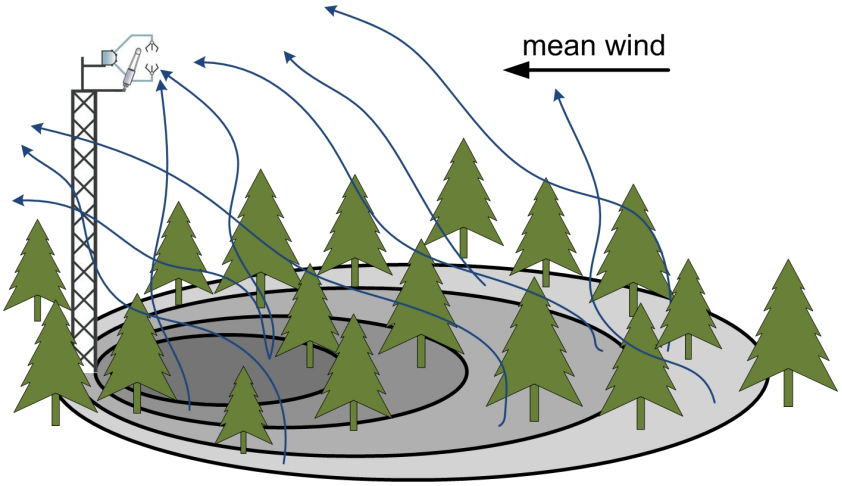

Figure 2: Figure shows an eddy covariance system measuring the flux above forest. Emitted gas parcels are lifted from the surface due to buoyancy or friction and are transported to higher levels of the atmosphere, while only few of them are measured by the sensor. The gray tones on the surface indicate the probability of an emitted molecule to reach the measurement point.

tics. The former include surface roughness and measurement height, while relevant flow characteristics are wind direction and -velocity, turbulence intensity, and atmospheric stability (Schmid, 1994; Burba, 2013; Rannik et al., 2012). During stable conditions, the primary direction of moving air parcels is horizontal, as vertical movement is suppressed. Thus, a long horizontal distance is typically required until the measurement height is reached. However, in an unstable atmosphere, air is carried rapidly to the sensor height which leads to a smaller source area. Even though turbulence and atmospheric stratification are strongly related, there may still be mechanical turbulence in a stable atmosphere. Mechanical turbulence is the consequence of a rough surface and increases

vertical motion, thus reducing the footprint extent. As flow characteristics constantly change in time (and this may also be true for surface roughness, e.g. by canopy growth), footprint size and position vary dynamically and need to be determined separately for every flux averaging interval.

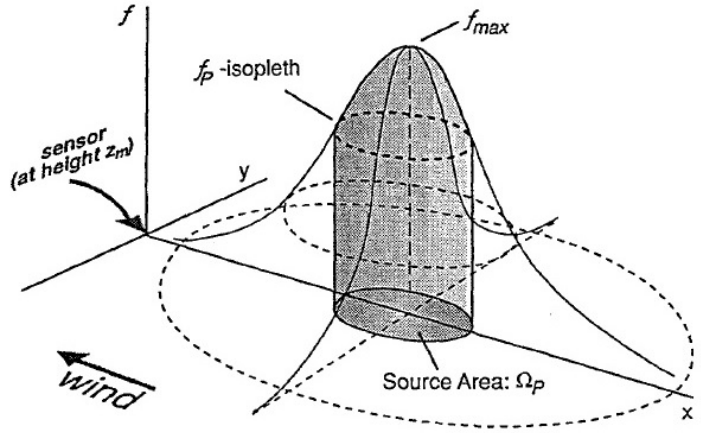

Figure 3: Illustration of the source area and its relation to the source weight function. Dashed isopleths f_P projected to the x-y-plane represent the source area of level P, Ω_P (e.g. P=80%). Mean wind direction is parallel but counter to direction of x-axis. (Figure from Schmid, 1994)

In general, footprints cannot only be determined for flux measurements, but also for concentration measurements. However, flux and concentration footprints differ considerably in size (Kljun et al., 2002). Schmid (1994) concluded that source areas for fluxes are almost an order of magnitude smaller than those of concentrations. From the Lagrangian point of view, the flux footprint value is related to the difference of particles crossing an imaginary horizontal plane at measurement height in upward direction and those crossing it in downward direction (Rannik et al., 2000). At large distances to the measurement point, the number of upward and downward crossings cancel each other out, which reduces the contribution of those particles to the measured flux and thus the footprint weighting factor. However, considering concentration measurements, each crossing (up- and downward) increases the concentration footprint which is particularly noticeable for long transport distances (Rannik et al., 2012). The logical consequence of this fact is that footprints for concentration measurements are generally larger than those for flux measurements.

1.2 Motivation[1]

The two main assumptions of the eddy covariance technique, horizontally homogeneous conditions and stationarity in time, are associated with a homogeneous surface. In this case, fluxes from all parts of the surface can be considered to be equal. Consequently, no footprint estimation is necessary as it always covers the same surface type, irrespective of the location of the measurement system or the footprint (Schmid, 2002). However, since the widespread establishment of the eddy covariance method for scalar flux measurements in the 1980s, the micrometeorological focus has shifted from "ideal" homogeneous conditions to more complex and heterogeneous sites with naturally varying land cover changes (Schmid, 2002). Over inhomogeneous areas, the distribution of individual sources/sinks within the source area varies, depending on footprint size and location. In such cases, footprint estimates are indispensable and valuable for several applications:

a) Optimization of measurement location
   To provide a basis for good quality flux data the location of measurement towers should fulfill the requirements of the EC-method, i.e. homogeneous and flat terrain. However, in most cases a compromise has to be made between the realization of these requirements and real-word conditions with heterogeneous surface and terrain features. Goeckede et al. (2004) developed a source weight synthesis that combines footprint analyses and quality assessment of flux data, to characterize the complexity of measurement sites, and to identify terrain features that may reduce measurement quality. It requires a dataset that is long enough to capture local wind climatology and different stability conditions (Goeckede et al., 2004, 2006; Leclerc and Foken, 2014). Based on the outcome of this method, potentially disturbed wind sectors under different atmospheric stabilities (Rannik et al., 2012), and the most strongly contributing areas can be identified, and tower location can be optimized. In summary, footprint estimates can help to design a field experiment and also to select an appropriate measurement height (Guo and Cai, 2005).

b) Interpretation of flux data
   Furthermore, determining the source area for each flux averaging interval improves the interpretation of flux data, especially in heterogeneous landscapes. In combination with a land cover map, the footprint indicates to what extent the defined area of interest contributes to the measured flux. This is useful in studies analyzing the gas exchange of a specific ecosystem, (e.g., Hommeltenberg et al., 2014b), or in studies investigating the surface energy balance (e.g., Wilson et al., 2002 or Foken

[1] Excerpts of the following section are also contained, almost verbatim, in Heidbach et al. (2017).

et al., 2010). The latter requires the source area of the measured flux to be representative of the surface area captured by the radiation and soil heat flux sensors. By setting a minimum integral footprint contribution of the area of interest, the footprint is also applicable as data rejection criterion.
Averaging several footprints over a longer measurement period (e.g., one year as in Hommeltenberg et al., 2014a, or the duration of a measurement campaign) is a more integrative approach of reflecting the spatial representativeness of a site. It was first introduced by Amiro (1998) as "footprint climatology" and is a useful tool when information about the representativeness of measured fluxes in different periods are required (Leclerc and Foken, 2014).
Furthermore, in fragmented landscapes the measured flux depends on size, location, and orientation of the footprint and, associated therewith, the measurement location. Up to the level of the so-called physical blending height (Claussen, 1989), turbulent fluxes are still inhomogeneous, which means that measurements below this height are affected by a bias depending on the sensor location (Schmid and Lloyd, 1999). This sensor location bias indicates to what extent a flux measured at a given location reflects the ecosystem scale flux. Schmid and Lloyd (1999) determined and analyzed the location bias over a sparse natural dryland forest in the Sahel region, an extremely heterogeneous land cover. It is obvious that the larger the footprint is, the more representative is the sub-sample of the surface that is seen by the sensor. Therefore, as footprint size depends on sensor height and atmospheric stratification, the location bias is expected to decrease with increasing measurement height and stability (Schmid and Lloyd, 1999).

c) Up- and downscaling of flux measurements
Although mass- and energy fluxes can be measured with high temporal resolution by the eddy covariance technique, their spatial scale is limited. By means of the footprint, flux measurements can be spatially assigned to a specific land cover, and thus can be linked to alternative flux observations or model simulations with different spatial resolution. Examples include remote sensing information (e.g., Chen et al., 2010; Kim et al., 2006; Reithmaier et al., 2006), aircraft data (e.g., Metzger et al., 2012; Ogunjemiyo et al., 2003; Kustas et al., 2006), model results (e.g., Song and Wesely, 2003), or observations with a smaller spatial scale like chamber measurements (e.g., Reth et al., 2005; Myklebust et al., 2008). For reliable up- or downscaling, the footprint composition must match the land cover composition of the relevant area of which the flux is intended to be estimated. Therefore, the footprint presents a crucial link between flux measurements and other observations of different spatial scale.

Currently, various models are used to estimate the source area of a flux measurement (see Leclerc and Foken, 2014, for a recent review). In general, researchers are following three different approaches in footprint modeling (for more details about footprint model types see section 2.4): first, simple and computationally less intensive analytical models and (semi-) empirical parameterizations (e.g., Hsieh et al., 2000; Kljun et al., 2015; Kormann and Meixner, 2001; Neftel et al., 2008; Schmid, 1994); second, Lagrangian particle models (forward and backward) that are able to account for three-dimensional turbulent diffusion and (vertically) inhomogeneous turbulence (e.g., Baldocchi, 1997; Flesch et al., 1995; Kljun et al., 2002, based on Rotach et al., 1996); and third, the development towards complex "full flow" LES models which attempt to address spatial heterogeneity and non-ideal topography explicitly (e.g., Leclerc et al., 1997; Steinfeld et al., 2008). All except the "full flow" models assume horizontally homogeneous turbulence, which implies an omnidirectional uniform surface with regard to topography, aerodynamic roughness, and thermal stratification (Rannik et al., 2012). Although this assumption is not usually fulfilled in practical flux measurement conditions, such computationally inexpensive models are often applied at non-ideal, heterogeneous sites, because they are more practical for real time data evaluation and long-term observations. Consequently, such source area estimates contain increased uncertainties and can be used just as a first approximation for real observation conditions (Rannik et al., 2012). This difficulty raises the question of how reliable footprint model results are at real-world flux sites. Therefore, footprint model evaluation experiments under non-ideal surface and atmospheric conditions are required (Foken and Leclerc, 2004).

1.3 State of research in the field of footprint model evaluation

To date, there have been just a few studies that evaluate flux footprint models. They follow mainly four different approaches:

a) The inter-comparison of footprint models
   Models are often compared with pre-existing models (of less complexity) or models of higher complexity, as these are expected to reflect the actual atmospheric dispersion better. The drawback of inter-comparison studies is that a ground truth is missing. Rannik et al. (2000), for instance, compared simulations of their Lagrangian stochastic model with the analytical models of Schuepp et al. (1990) and Horst and Weil (1992, 1994). In order to test model physics, they ran their model with and without along-wind turbulent diffusion and found good agreement with Schuepp et al. (1990) when along-wind turbulence intensity is neglected as assumed by the analytical model.
   Additionally, Kljun et al. (2003) tested flux and concentration footprint estimates

of a backward Lagrangian particle dispersion model (Kljun et al., 2002) against the analytical model of Kormann and Meixner (2001) for an unstable and neutral stratification and two different sensor heights (20/100 m). By running the Lagrangian model with and without longitudinal turbulent diffusion, they could state that, first, the relative importance of longitudinal turbulence is larger in neutral conditions, second, that the peak location of the flux footprint moves closer when along-wind turbulence is included, and third, that small contributions downwind of the receptor are predicted when considering longitudinal wind velocity fluctuations.

Another inter-comparison study was done by Sogachev et al. (2005) who analyzed the higher order closure model SCADIS (**sca**lar **dis**tribution; Sogachev et al., 2002), the analytical models of Kormann and Meixner (2001) and Schuepp et al. (1990) as well as the Lagrangian particle dispersion models of Thomson (1987) and Kurbanmuradov and Sabelfeld (2000). For neutral conditions over a tall homogeneous managed pine forest plantation SCADIS provides footprints quite similar to the Lagrangian approaches and the model of Schuepp et al. (1990). Differences to the model of Kormann and Meixner (2001) were attributed to the divergent determination of the effective mean wind velocity in the analytical models, which is based on the logarithmic vertical wind profile in the Schuepp et al. (1990) model, while in Kormann and Meixner (2001) a power function is applied.

Markkanen et al. (2009) evaluated a Lagrangian model embedded into the LES PALM (Raasch and Schröter, 2001) against two pure Lagrangian simulations, the backward model of Kljun et al. (2002) and a version of the forward model of Rannik et al. (2000) presented in Rannik et al. (2003). For most measurement heights they found moderate to very good performance of the two Lagrangian models in comparison to the LES.

b) The use of wind-tunnel tracer experiments

In wind-tunnel experiments, ideal conditions with stationary turbulence and homogeneous surfaces can easily be generated. This main benefit was used by Kljun et al. (2004b) to evaluate dispersion patterns and concentration footprint predictions of the Lagrangian model LPDM-B of Kljun et al. (2002). They produced a simulated convective boundary layer and released SF_6 from a point source. Several concentration measurements located downwind and crosswind of the source showed that LPDM-B is able to reproduce footprint shape and peak location for various sampling heights throughout the entire boundary layer (Kljun et al., 2004b). Although even heterogeneous surfaces with changes in canopy height (e.g., forest edges) and/or differences in sensible heat production could be simulated with wind-tunnel

experiments, to our knowledge, this is the only experiment using wind-tunnel data for footprint model evaluation.

c) The use of natural tracers
In natural tracer studies, differences in source strength in adjacent fields are used to evaluate footprint models. The measured flux is expected to originate from an area which includes different percentages of the two (or more) fields, depending on footprint location and size (Fig. 4). For each field, the source strength needs to be measured separately in order to have reference measurements. In combination with the ratio of the two land use types in the mixed footprint, a weighted flux average can be determined and compared to the flux with the mixed footprint. This approach was applied by Goeckede et al. (2005), who analyzed the analytical model FSAM by Schmid (1994) and the Lagrangian trajectory model by Rannik et al. (2000, 2003) and found a slightly better performance of the Lagrangian simulation model.
Marcolla and Cescatti (2005) made use of this approach in a different manner. They generated spatially variable carbon sinks by cutting two concentric portions of the footprint at different times. In this way, Marcolla and Cescatti (2005) were able to combine fluxes of two homogeneous footprints (before and after cutting) in order to determine weighted fluxes of the inhomogeneous footprint (between the cuts).

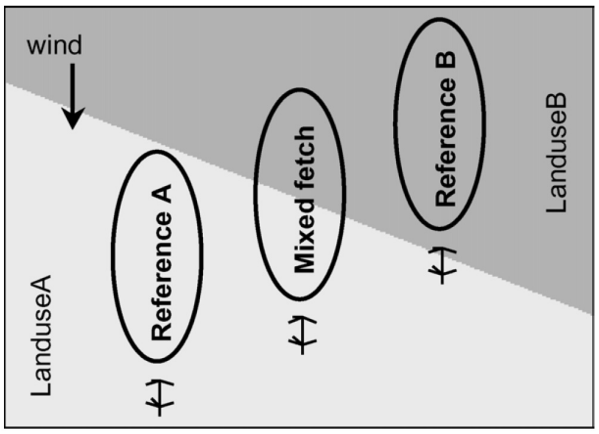

Figure 4: Schematic illustration of the layout for a footprint evaluation approach based on natural tracers (Goeckede et al., 2005).

However, van de Boer et al. (2013) used sensible heat as natural tracer. Over a terrain with different land use types and hence contrasting sensible heat fluxes they made flux measurements with in total seven eddy covariance systems. By

applying two different evaluation approaches, van de Boer et al. (2013) analyzed the analytical models of Kormann and Meixner (2001) and Hsieh et al. (2000) (combined with the crosswind function from the former model and from Detto et al., 2006). They conclude that the model of Hsieh et al. (2000) perform slightly better, but that both models overestimate the location of the peak contribution of the footprint.

Furthermore, by using a combination of two-dimensional lidar scans, measurements of two eddy covariance towers, and footprint analysis, water vapor was used as natural tracer in the study of Cooper et al. (2003). In contrast, Reth et al. (2005) applied another approach with upscaled combinations of chamber measurements (i.e. soil, leaves, stems, and fruit) at a brownfield surrounded by meadows, to allow for the comparison with eddy covariance measurements based on footprint analysis.

In general, model evaluation strategies where known differences in source strength (e.g., of two adjacent fields) are exploited, give only qualitative information on footprint model performance. The significance of such evaluations depends not only on the difference of emission rates between fields, but also on the homogeneity of the source strength within each field.

d) The use of artificial tracers

In contrast, using artificial tracers in model evaluation experiments is a more direct approach and has the advantage that the source strength is known and can be controlled. An ideal tracer gas has no other sources or sinks in the surroundings of the measurement system, has a low water solubility, is chemically inert, and, last but not least, a fast response sensor must be available to measure its flux (Foken and Leclerc, 2004).

Apart from the simplest experimental configuration of installing one source and one measurement system, there are two main methodical approaches in artificial tracer experiments: The "one source - multiple flux sampling points" and the "multiple sources - single flux sampling system" (Leclerc et al., 2003b). Based on the assumption of the inverted plume (see Section 2.4.1) both configurations are mathematically equivalent and result in the same outcome.

Furthermore, not only the experiment setup, but also the form of the tracer source can be designed in different ways. Tracer gases can be released from whole areas, line-, or point configurations. As the definition of a point source is a matter of scale, it needs to be set in relation to the measurement height.

The first study validating flux footprint models based on artificial tracer experiments was conducted by Finn et al. (1996). In that study, they released sulfur hexafluoride (SF_6) from a 400 m line source over a sagebrush canopy and mea-

sured the flux with eddy covariance at four distances aligned perpendicular to the line source. Thus, it is an example for the "one source-multiple flux sampling points" approach. Similar setups were used above a managed pine forest plantation and a peach orchard in the Leclerc et al. (2003a) and the Leclerc et al. (2003b) studies, respectively. Experiment layouts with sufficiently long line sources allow the evaluation of the crosswind integrated footprint with its peak amplitude and position. However, due to its linear configuration and the limited source length, such experiments are wind direction dependent and are exposed to edge effects.
One example of the "multiple sources-single flux sampling system" -configuration is the footprint model evaluation study of Nicolini et al. (2015). Pure CO_2 was progressively released from six distances along the mean wind direction upwind of the measurement system. To release the tracer, a 50 m line source was laid on top of the canopy and placed perpendicular to the prevailing wind direction.
In studies using tracer gases with a natural flux that significantly deviates from zero, high tracer release rates are necessary so that the artificially generated flux is several orders of magnitude larger than the natural flux. This difficulty is circumvented when tracer gases with no background flux are used. To date, there are no footprint evaluation studies using artificial tracers that are able to evaluate the 2-dimensional flux footprint (the crosswind distributed footprint function).

Additionally, footprint models can also be tested implicitly by applying them over areas with small-scale inhomogeneity and analyzing the variability of measured fluxes as a function of flux footprint size and orientation. The difference of this concept to the "natural tracer approach" can be found in the scale of heterogeneity: In the "natural tracer approach" clearly distinguishable fields produce different fluxes, while in this approach fragmented, unstructured surfaces are analyzed. Schmid et al. (1991) measured surface energy balance components over a residential suburban area in Vancouver, Canada. Due to the small-scale spatial variability of this area and the temporally shifting source area they found a link between the temporal and the spatial variability of the measured turbulent fluxes. Schmid (1997) further analyzed the same dataset and found a clear dependence of spatial variability of sensible heat flux on footprint size.

1.4 Objectives of the thesis

The present work addresses three main issues:

In studies which include routine footprint estimates for long-term flux observations, analytical models are the most commonly used class of footprint models, due to their mathematical simplicity, and hence their low computational expense. Although their main assumption of homogeneous turbulence is usually not fulfilled in real measurement

conditions such models are applied to practical flux measurements. Therefore, the question arises whether such footprint models provide reliable results even at real-world flux sites. The first aim of this study is to propose a 2-dimensional flux footprint evaluation method. This method is then used to evaluate the analytical footprint models by Schmid (1994) and Kormann and Meixner (2001), as well as the footprint parameterizations of Hsieh et al. (2000) and Kljun et al. (2015), in real field conditions.

The second issue deals with the effect of along-wind turbulent fluctuations. Within a flux averaging period, air particles may be transported faster, slower or even opposite to the mean wind direction due to along-wind fluctuations. Therefore, it is expected that, depending on along-wind turbulence intensity, downwind sources can have a non-zero probability of contributing to a measured flux. This has already been proven by Lagrangian footprint models which show that downwind contributions are present when along-wind turbulent fluctuations are considered (e.g., Kljun et al., 2002; Rannik et al., 2000; Baldocchi, 1997). While anecdotal evidence exists to support this model result of an upwind-drift (e.g., smelling fragrances or scents slightly upwind from the source), no quantitative flux measurements to verify this effect have been documented in the literature to date. The aim of this study is to experimentally investigate whether contributions to a measured flux from downwind sources are present and measurable.

With the exception of Kljun et al. (2015), the above mentioned analytical models consider crosswind and vertical diffusion, but neglect along-wind turbulent fluctuations. The aim of this study is to present a practicable approach to include streamwise turbulent fluctuations into simple, similarity-theory based footprint models that represents a more realistic description of turbulence, but is still simple enough for real-time footprint analysis. For this purpose, we introduce an extended version of the flux footprint model FSAM (Schmid, 1994), FSAMx, and define a Gaussian along-wind distribution with a standard deviation that increases with particle travel time. Its implementation in the model is realized through a standalone module that is superimposed on the calculation of the original two-dimensional footprint of FSAM. For this reason, this new footprint model extension can be applied to the output of any other footprint model.

Excerpts of this thesis are published in *Agricultural and Forest Meteorology* (Heidbach et al., 2017). K.H. planned and conducted the experiments, processed and analyzed the experimental data, and performed footprint model calculations including uncertainty analyses. K.H. also wrote the paper and designed the figures. HP.S. and M.M. supervised the work and performed an internal review of the paper before publication. Expressed as a percentage, K.H. contributed 95% of the paper while HP.S. and M.M. contributed 5%.

2 Theoretical Background

2.1 Theory of atmospheric dispersion

In general, an emitted gas or pollutant in the atmosphere is dispersed by mainly two processes: advection and diffusion (Chatwin et al., 1996; Stockie, 2011). Advection is the result of moving air, in fact air particles follow the mean wind and are distributed along that axis. However, diffusion allows also for lateral and vertical spread of a plume, by molecular and turbulent mixing. In the atmosphere, the process of turbulent mixing is much more effective than molecular diffusion. Only at the boundary between two media, in this case the boundary between the air and the earths surface or water, molecular diffusion is more relevant, as turbulence is not able to cross this boarder and the turbulent eddy size approaches zero at the surface (Roedel, 2011).
As a result of the stochastic nature of molecular diffusion, the lateral spread of a plume is, according to Taylor (1921), proportional to the square root of time ($\sigma_y \sim \sqrt{t}$) and thus represents a horizontal parable as illustrated in Fig. 5, left. However, turbulent diffusion spreads the plume in the beginning (near-field) with $\sigma_y \sim t$, but for long diffusion times (far-field) with $\sigma_y \sim \sqrt{t}$ (Fig. 5, right). This can be explained by the fact that in the near-field, when the plume size is still smaller than the dominant turbulent eddies, the initial plume is transported instead of diffused (Luhar, 2013). As is shown in Fig. 5, the crosswind distribution due to turbulent diffusion is not uniform or Gaussian, but the gas is arbitrarily transported by turbulent eddies, either in one direction or the other. Therefore, the right panel in Fig. 5 shows a snapshot of the plume which can only be represented by the delineated borderline when considering the time average.

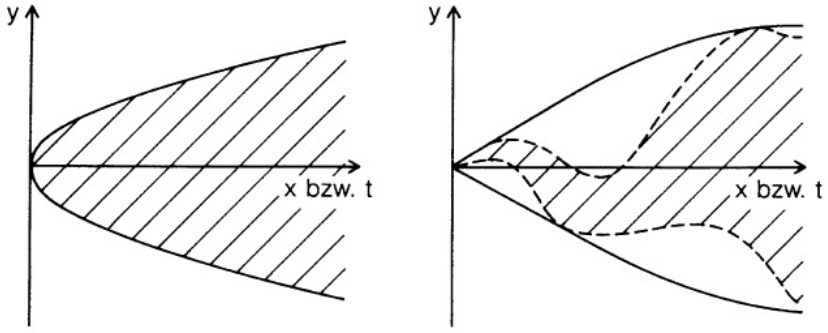

Figure 5: Schematic illustration of lateral plume dispersion as a result of molecular (left) and turbulent (right) diffusion with x and t being the along-wind distance and time, respectively. (source: Roedel, 2011).

The most important parameters that govern atmospheric dispersion are turbulence intensity, stability, and wind velocity. Emitted gases or pollutants are transported along

the mean wind and are dispersed in the lateral and vertical direction mainly by turbulence. If no turbulence is present, air particles would follow the streamlines of the mean wind with only minimal dispersion in other directions due to molecular diffusion.
Stability is a measure of vertical motion tendency in the atmosphere: Stable stratification suppresses vertical motion, and thus turbulent mixing, which leads to a small vertical spread of a plume of released particles even over long distances (Fig. 6, "fanning"). In an unstable atmosphere, vertical displacement of air particles is enhanced and turbulence is increased. As a result, large turbulent eddies bring the plume up, down to the ground, and up again (Fig. 6, "looping"). During neutral conditions, the vertical spread of the plume is much less than in the unstable case but larger than in a stable atmosphere (Fig. 6, "coning"). Therefore, stability is directly related to turbulence intensity and additionally has an influence on atmospheric dispersion.
The wind velocity plays a role in the way that the distance a particle released from the surface travels grows with increasing wind velocity. The higher the wind speed the more effective is the horizontal dispersion from a continuous source. The process of atmospheric dispersion can be described in a simplified form by the advection-diffusion equation, the derivation of which, with its required assumptions, is summarized in section 2.2.

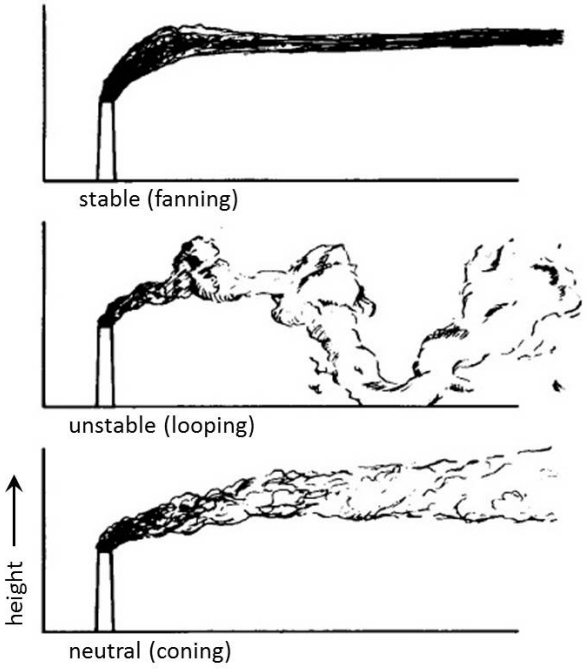

Figure 6: Different types of plumes depending on stratification of the atmosphere (modified after Slade, 1968).

2.2 The advection-diffusion equation

The following derivation of the advection-diffusion equation is based on Stockie (2011). The advection-diffusion equation is based on the law of conservation of mass which can be expressed in differential form as

$$\frac{\partial C}{\partial t} + \nabla \vec{F} = S \tag{1}$$

which describes that the source or sink strength S of a gas is equal to the divergence of the mass flux $\vec{F}$ and the temporal change of its concentration C. The mass flux is the result of the combined effects of atmospheric diffusion and advection. The diffusive component of a flux $\vec{F}_D$ is assumed to be proportional to the concentration gradient as already stated in Fick's law:

$$\vec{F}_D = -K \nabla C \tag{2}$$

with the diffusion coefficient K which, in the 3-dimensional case, is defined as a diagonal matrix $\text{diag}(K_x, K_y, K_z)$. However, the advective component $\vec{F}_A$ can be described as a linear relationship between the wind velocity $\vec{u}$ and the concentration C:

$$\vec{F}_A = C\vec{u}. \tag{3}$$

Therefore, the total flux can be expressed as

$$\vec{F} = \vec{F}_A + \vec{F}_D = C\vec{u} - K\nabla C. \tag{4}$$

Substituting Equation (4) in Equation (1) results in the 3-dimensional advection-diffusion equation

$$\frac{\partial C}{\partial t} + \nabla(C\vec{u}) = \nabla(K\nabla C) + S \tag{5}$$

which can also be written in a more detailed form as

$$\frac{\partial C}{\partial t} + \frac{\partial C}{\partial x}u + \frac{\partial C}{\partial y}v + \frac{\partial C}{\partial z}w = \frac{\partial}{\partial x}\left(K_x \frac{\partial C}{\partial x}\right) + \frac{\partial}{\partial y}\left(K_y \frac{\partial C}{\partial y}\right) + \frac{\partial}{\partial z}\left(K_z \frac{\partial C}{\partial z}\right) + S. \tag{6}$$

In order that Eq. (6) can serve as basis for analytical diffusion models it needs to be analytically solvable. For that purpose, the following assumptions are made (Pasquill and Smith, 1983; Stockie, 2011):

- The gas is emitted at a constant rate from an infinite crosswind line source, i.e. $\frac{\partial}{\partial y}\left(K\frac{\partial C}{\partial y}\right) = 0$.

- $\vec{u} = (u, 0, 0)$, meaning that the wind velocity is parallel to the x-axis.
- The wind velocity and all other parameters are constant so that steady state conditions prevail, i.e. $\frac{\partial}{\partial t} = 0$.
- Advection is much larger than diffusion in x-direction so that the term $\frac{\partial}{\partial x}\left(K\frac{\partial C}{\partial x}\right)$ can be neglected.
- Diffusion is isotropic, meaning that $K := K_x = K_y = K_z$.
- The gas is not absorbed by the ground.
- The surface is flat without variations in topography, i.e. the ground can be described by the plane $z = 0$

Furthermore, by applying the following set of boundary conditions (Equations 7a-7c) given by Pasquill and Smith (1983) Equation (6) simplifies to (8) (Hanna et al., 1982)

$$C \to 0 \quad as \quad x, z \to \infty \tag{7a}$$

$$C \to \infty \quad at \quad x = z = 0 \tag{7b}$$

$$K_z \frac{\partial C}{\partial z} \to 0 \quad as \quad z \to 0, x > 0 \tag{7c}$$

$$\frac{\partial C}{\partial x} u = \frac{\partial}{\partial z}\left(K\frac{\partial C}{\partial z}\right). \tag{8}$$

As Equation (8) presupposes an infinite crosswind line source and therefore excludes the spread in y-direction it serves as initial equation for the crosswind integrated flux footprint function of analytical models (e.g., Kormann and Meixner, 2001, and Schmid, 1994).

2.3 The integral equation of diffusion

Pasquill and Smith (1983) introduced the integral equation of diffusion in order to describe the concentration field that may arise from a single continuous source. They state that the concentration at a specific point is a function of source strength and a probability transfer-function. Schmid (1994) transferred it to the footprint concept: The flux footprint describes the relation between a measured flux and the spatial distribution of sources and/or sinks of this quantity in the surrounding of the sensors. It quantifies the influence of sources/sinks of a passive scalar to the measured flux and can therefore be

considered as a probability function (Schmid, 2002; Horst and Weil, 1994). Following Schmid (1994), the integral equation of diffusion can be expressed as

$$F(r) = \int_R \tilde{Q}(r') \cdot f(r - r')dr' \tag{9}$$

where F is the measured flux at location r, $\tilde{Q}$ is the spatial distribution of stationary surface sources/sinks and f is the footprint or source weight function, the integral is performed over domain R.
Assuming that source/sink distribution is confined to the surface ($z = z_0$) and that diffusion along the mean wind (i.e., the x-axis) can be neglected, Eq. 9 may be written for a measurement point located at $(0, 0, z_m)$

$$F(0, 0, z_m) = \int_{-\infty}^{\infty} \int_{-\infty}^{x} \tilde{Q}(x, y, z = z_0) \cdot f(-x, -y, z_m - z_0)dxdy \tag{10}$$

The footprint function f defines the probability that a passive scalar emitted at (x, y, z_0) contributes to the flux at the measurement location. In other words, it estimates the relative contribution of each individual source to the measurement. The integral of the contributions from all potential sources in the surrounding of the measurement system multiplied with the corresponding source strength results in the flux.
As it is a probability function, the integral of the footprint function equals unity for an infinite area. The actual source weight depends on the distance between source and measurement location as well as on diffusion and transport processes that are relevant for the distribution of the corresponding quantity.

2.4 Classification of footprint models

2.4.1 Analytical footprint models

Analytical footprint models are based on solutions of the 2-dimensional advection-diffusion equation (Eq. 8) and therefore presuppose the assumptions listed in section 2.2. In fact, Equation (8) describes the concentration distribution in the vertical and the along-wind direction of a continuously emitted passive scalar. By coordinate transformation, the resulting concentration distribution can, under certain assumptions, directly be linked to the footprint of a specific measurement position. The underlying concept of this relation is the inverted plume assumption, as is illustrated in Fig. 7. Releasing a tracer from an elemental surface source entails a specific concentration distribution C with a maximum concentration C_{max} located somewhere downwind from the source. The amount of tracer detected at the sensor changes depending on the distance between source and sensor. Under the assumption of horizontally homogeneous turbulence, mov-

ing the source would shift the distribution function in the same way. By adding up the weighted contributions of all potential sources upstream, the total tracer flux measured at the sensor can be estimated. This exactly corresponds to the definition of the flux footprint (Schmid and Oke, 1990).
As the footprint in this case is a geometric translation of the flux distribution, the concept of the inverted plume is only valid in areas where spatial inhomogeneities are inherent in the distribution of source or sink strengths of passive scalars and where variations in mechanical or thermal turbulence production occur only at length scales much smaller than the measurement height. In the latter case, turbulence is assumed to cancel spatial differences by mixing (Schmid, 2002).
Due to their mathematical simplicity and, associated therewith, their low computational expense analytical models are the most commonly used footprint models in studies that include routine footprint estimates for long-term and/or continuous flux observations (Steinfeld, 2009; Leclerc and Foken, 2014).

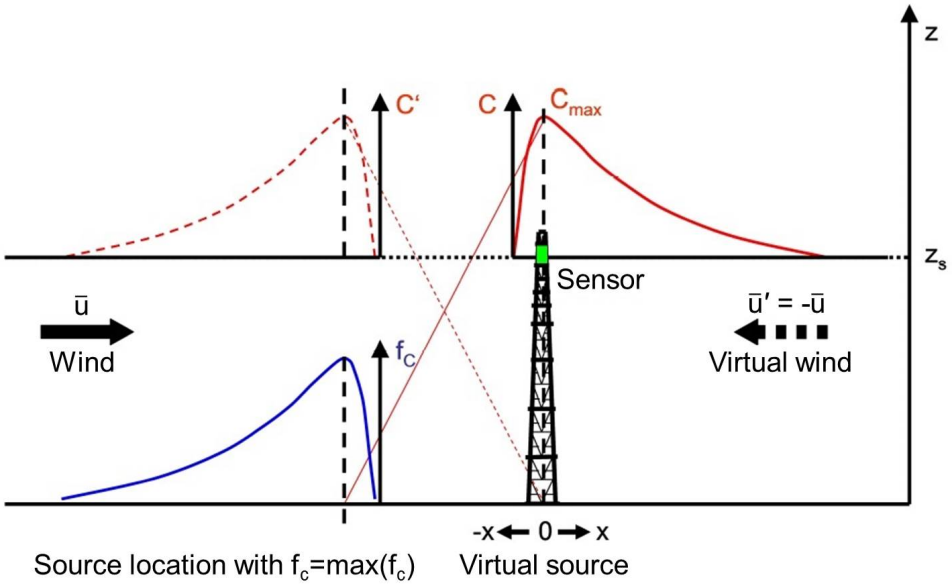

Figure 7: Graphical representation of the inverted plume assumption for a concentration footprint according to Schmid and Oke (1990) (modified after Steinfeld, 2009)

2.4.2 Lagrangian footprint models

Another type of model are Lagrangian simulations (LS) which are based on a stochastic differential equation, the Langevin equation. This equation describes the spatial and temporal evolution of a particle released into the atmosphere by combining a deterministic and a stochastic term (Vesala et al., 2008). The deterministic term provides the linkage of particle velocities between two consecutive time steps while the stochastic part

describes the random contribution to the acceleration of the particles (Steinfeld, 2009). In Lagrangian simulations trajectories of a large amount of released particles are tracked until they reach a specific location. The whole ensemble of particle tracks provides the basis for statistically meaningful estimates of the real dispersion process (Leclerc and Foken, 2014).

In general, there are two modes in Lagrangian footprint modeling: the forward mode (forward in terms of forward in time) and the backward mode. In the forward mode, particles are released at a single surface point and their trajectories are tracked until they reach the measurement location. The footprint is then determined by means of the inverted plume assumption and therefore this concept is restricted to ideal conditions (horizontal homogeneity and stationarity) as given in section 2.4.1. However, Luhar and Rao (1994) showed that Lagrangian models can also be applied for footprint modeling in heterogeneous terrain. In this case, particles are not released extensively from homogeneous terrain, but only from predefined areas/points. In the backward mode, a negative time step is used and particles are tracked from the measurement location back to their origin at the surface (e.g. Flesch et al., 1995; Kljun et al., 2002). The advantage of the backward mode in comparison to the forward mode is that all considered particles cross the measurement point so that less particle trajectories need to be modeled and less computational time is required. Furthermore, backward Lagrangian models are in principal a powerful tool to estimate footprints in an inhomogeneous and non-stationary flow field as no inverted plume assumption is necessary (Leclerc and Foken, 2014).

Lagrangian simulations require a prescribed turbulence field that can be defined differently, depending on height, with the consequence that LS models are not valid exclusively in the surface layer. This was already shown by Baldocchi (1997) and Rannik et al. (2000) for footprint estimates inside and above forests. Another benefit of LS is that they can consider not only Gaussian but also non-Gaussian inhomogeneous turbulence (e.g. Rotach et al., 1996 and Reynolds, 1998), as well as diffusion in along-wind direction.

However, compared to analytical models, LS require much more computational time, due to the large amount of particle trajectories (e.g., $\sim 5 \cdot 10^3$ in Kljun et al., 2002) that need to be determined in order to facilitate statistically reliable estimates of the diffusion process. This explains why Lagrangian models are rarely used in studies with routine footprint estimates, although they are expected to reflect reality better than analytical models. To overcome this drawback Hsieh et al. (2000) and Kljun et al. (2015) developed parameterizations based on the outputs of Lagrangian models which combine the advantages of Lagrangian models with the main benefit of analytical models, the small computational effort.

2.4.3 Large-Eddy simulation models

The most computationally expensive method to estimate footprints is the Large-Eddy simulation (LES). LES is able to compute time-dependent turbulence fields in three dimensions, even above inhomogeneous surfaces or within canopy. It resolves large eddies (of at least twice the grid size) directly by the Navier-Stokes equations, and parameterizes the subgrid-scale (Leclerc and Foken, 2014). This corresponds with the knowledge that a large percentage of the flux is associated with relatively large eddies. Therefore, LES is applicable in the convective boundary layer when eddy sizes are relatively large, but becomes more and more prone to error during stable conditions and for low measurement heights when turbulent eddies are smaller and the subgrid-scale parameterization gains more in importance (Leclerc and Foken, 2014; Schmid, 2002).
There are mainly two ways how Large-Eddy simulation can be used for determining footprints: First, LES models can provide required input parameters for other footprint models. This was done in the study of Hadfield (1994), the first LES study in the context of footprint modeling, with a horizontally homogeneous LES and a forward Lagrangian footprint model. Second, a Lagrangian model can be embedded into an LES which means that particle trajectories are simulated online during an LES run (e.g., Steinfeld et al., 2008 and Markkanen et al., 2010). Furthermore, Leclerc et al. (1997) applied the LES model of Moeng (1984) without using an embedded Lagrangian model, but simulated footprints in an Eulerian framework. This was achieved by running the LES until it reached steady state conditions, and only then a passive scalar from a line source parallel to the axis of the mean wind was released as an instantaneous linear puff.
Although applying LES for routine footprint estimates is impractical, due to its required computational effort, it can provide valuable input-information about flow and turbulence statistics for other footprint models, and can serve as basis for model cross-comparisons and evaluations. Furthermore, LES is an indispensable tool for the characterization of atmospheric flows and footprints above heterogeneous surfaces, within canopy, in the roughness sublayer, and for convective conditions (Schmid, 2002).

2.4.4 Reynolds-averaged models

Aside from Lagrangian simulation and LES there is a third possibility to consider heterogeneous or hilly surfaces in footprint estimations: the Reynolds-averaged models. By using ensemble averages and empirical information, they constitute another way to solve the Navier-Stokes equations. In literature, they are often denoted as RANS models (**R**eynolds **a**veraged numerical **N**avier-**S**tokes simulation) or closure models. As the set of Reynolds equations for turbulent flow contains more unknowns than equations, either parameterizations or additional (prognostic) higher order equations need to be intro-

duced, in order to define the unknowns. The latter introduces even more new unknowns, which leads to a non-closed mathematical description of turbulence. To overcome this "closure problem", the remaining unknowns must be approximated by parameterizations. The order of closure corresponds to the number of prognostic equations that are retained. For more information see Stull (1999).
RANS simulations give no information about instantaneous velocity, temperature, and concentration distributions, they provide time-averaged fields. However, the effect of turbulence on the time averaged fields is implicitly considered by means of parameterizations (Steinfeld, 2009). Therefore, the performance of RANS models depends on the quality of the turbulence parametrization.
Sogachev et al. (2002) first applied a RANS model for estimating footprints. They used their model SCADIS, a one-and-a-half order closure model, to estimate footprints above a non-uniform spruce forest in European Russia. Additionally, Sogachev and Lloyd (2004) determined 3-dimensional footprints over an inhomogeneous forest, while Sogachev et al. (2004) analyzed the 2-dimensional flow over a bell-shaped ridge and applied the SCADIS model to a real flux site in Hyytiälä, Southern Finland, with its complex topography and surface heterogeneities.
Despite their ability to consider non-uniform surfaces, RANS models are rarely used for routine footprint calculations. This can be explained by the relatively high demand for computing effort, especially in complex terrain. Taking Sogachev and Lloyd (2004) as an example, their model requires as many solutions to prognostic equations as source cells are available. This means that, for any source volume, a dispersion calculation needs to be performed in order to determine the corresponding contribution to the measurement (Steinfeld, 2009).

3 Materials and Methods

3.1 Model evaluation approach[2]

In case of a 2-dimensional footprint function, i.e., when it includes not only the crosswind integrated distribution of vertical dispersion effects in along-wind direction, but also the crosswind dispersion, a source-weight density or footprint value for every surface location relative to the flux measurement can be determined. If this footprint function is integrated over a finite elemental surface area, the resulting value reflects the probability of the elemental surface source to contribute to the measured flux. Considering an elemental surface source with a constant emission rate Q, the spatial distribution of stationary surface sources/sinks $\tilde{Q}$ can be expressed as

$$\tilde{Q}(r') = Q \cdot \delta(r'), \tag{11}$$

where δ is the Dirac-delta distribution function. For this special case, equivalent to Equation (4) in Schmid (1994), the integral equation of diffusion (Equation 9) simplifies to

$$F(r) = Q \cdot f(r - r'). \tag{12}$$

Therefore, the measured flux at location r results from the source strength Q multiplied with the footprint weighting factor at the source's location. After transforming Equation (12), the footprint weighting factor can be inferred from the measured flux, divided by the source strength:

$$f(r - r') = \frac{F(r)}{Q}. \tag{13}$$

To obtain the footprint distribution functions for each model used here, we determined the footprint weighting factors on a gridded array of 1 m^2 elemental sources, and assumed the footprint values at the center of each cell to approximate the average over the cell. To test whether a resolution of 1 m^2 is sufficient, we used a configuration in unstable conditions (where the footprint dimensions are relatively small, and thus limited resolution may be important), and determined the crosswind integrated footprint with resolutions of 0.5, 1 and 2 m. Comparing the sums of weighting factors up to a distance of 3 times the distance of the footprint maximum (x_{max}), multiplied with the corresponding step-size, reveals a deviation of the sums by less than 2.4% for all models. For the experimental tracer release setup, we constructed a diffuser apparatus of approximately 1 m^2 size (see Section 3.6) as a finite elemental surface source. As it perfectly matches the dimension of our chosen footprint model array resolution we henceforth refer

[2]Excerpts of the following section are also contained, almost verbatim, in Heidbach et al. (2017).

to it as a "point source". Figure 8 shows a schematic illustration of a footprint grid and indicates that the tracer release point (orange arrow) can be assigned to a specific cell in the footprint matrix (blue cell). With the assumption that no other sources or sinks of the tracer gas are present in the vicinity of the measurement system, Eq. (13) can be applied directly to evaluate the experimentally determined flux footprint contribution as the measured flux relative to the tracer source. This experimental footprint evaluation was done for each flux averaging interval and the outcome was directly compared with the corresponding footprint estimate of each model.

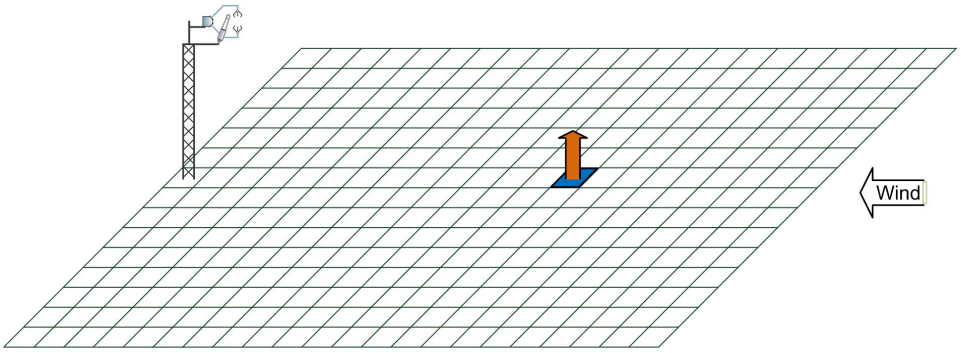

Figure 8: Illustration showing the model evaluation approach. Both, the EC station as well as the point source can be assigned to a specific cell of the footprint grid with 1 m^2 cell size. At the center of each cell the footprint value was determined, which was assumed to reflect the average over the cell. The blue cell indicates the footprint cell at which the tracer diffuser is located, while the arrow shows the artificial tracer release.

3.2 Footprint model implementation

In this study, the analytical flux footprint models of Kormann and Meixner (2001) (hereinafter referred to as KM) and Schmid (1994) (FSAM), as well as the empirical footprint parameterizations based on Lagrangian simulation results of Kljun et al. (2015) (FFP) and Hsieh et al. (2000) (HS) are evaluated. In the following chapters each of the models is described and principal formulae are presented. For consistency, notations of variables in the original publications are modified in some cases.

3.2.1 FSAM (Schmid, 1994)[3]

Schmid (1994) first introduced the extension to two dimensions in flux footprint modeling. The original model SAM (source area model; Schmid and Oke, 1990) also included two dimensions, but was valid only for concentration footprints. FSAM follows the theoretical approach of Horst and Weil (1992) but uses the dispersion model of Gryning

[3]Excerpts of the following paragraph are also contained, almost verbatim, in Heidbach et al. (2017).

et al. (1987) to include buoyancy and a realistic wind profile (Schmid, 1994).
Relating the crosswind integrated flux $\overline{F^y}$ to the crosswind integrated concentration $\overline{C^y}$ and the mean wind speed profile $\overline{u}(z)$ through the 2-dimensional advection diffusion equation leads to

$$\overline{u}(z) \cdot \frac{\partial}{\partial x}\overline{C^y} = -\frac{\partial}{\partial z}\overline{F^y}. \tag{14}$$

Applying the boundary condition $\overline{F^y}(x, z_0) = \overline{F_0^y} \cdot \delta(x)$, when $\overline{F_0^y}$ is a crosswind integrated unit point source at ground level, and considering that the crosswind integrated flux $\overline{F^y}$ is equal to the crosswind integrated footprint $\overline{f^y}$, Eq. (14) can be written as

$$\overline{F^y}(x) = \overline{f^y}(x) = -\int_{z_0}^{z_m} \bar{u}(z) \cdot \frac{\partial}{\partial x}\overline{C^y}(x, z)dz \tag{15}$$

with the integral from the roughness length z_0 to the measurement height z_m. For simplicity, and to save computation time, Eq. (15) is determined following the parameterization of Horst and Weil (1994):

$$\overline{f^y}(x) \approx \frac{d\bar{z}}{dx}\frac{\partial}{\partial \bar{z}}\left(\frac{z_m}{\bar{z}}\right)\left(\frac{\bar{u}(z_m)}{U(\bar{z})} \cdot A \cdot exp\left(-\frac{z_m}{b \cdot \bar{z}}\right)^r\right). \tag{16}$$

The parameterization includes the mean plume height $\overline{z}$, the plume advection velocity U. The definitions of parameters A, b and r can be found in Horst and Weil (1994) and Gryning et al. (1987). The mean plume height is calculated according to Equation (16) in Van Ulden (1978) by integrating its inverse function with respect to $\overline{z}$ until a specific upwind distance is reached:

$$\frac{d\overline{z}}{dx} = \frac{k^2}{[ln(p\overline{z}/z_0) - \psi(p\overline{z}/L)]\Phi_h(p\overline{z}/L)} \tag{17}$$

where z_0 denotes the roughness length, $k(= 0.4)$ is the von Kàrmàn constant, L the Obukhov length, $p = 1.55$ following Van Ulden (1978), and ϕ_h and ψ surface-flux-layer functions correcting the eddy diffusivity for sensible heat and the wind profile for stability, respectively. The stability function for momentum ψ was defined following Paulson (1970) for unstable conditions and Holtslag and De Bruin (1988) for a stable stratification (see Equations (33) and (34), below), while Φ_h was determined according to Dyer (1974) (Equation 18):

$$\Phi_h\left(\frac{z}{L}\right) = \begin{cases} \left(1 - 16\frac{z}{L}\right)^{-0.5} & \text{for } \frac{z_m}{L} < 0 \\ 1 + 5\frac{z}{L} & \text{for } \frac{z_m}{L} \geq 0 \end{cases} \tag{18}$$

The crosswind distribution is treated independently from vertical dispersion and is as-

sumed to be Gaussian and height-independent. It is defined as D_y (Gryning et al., 1987):

$$D_y(x,y) = \frac{1}{\sqrt{2\pi}\sigma_y} exp\left(-\frac{y^2}{2\sigma_y^2}\right), \tag{19}$$

where x and y are defined as along-wind and crosswind distance, respectively. The standard deviation is defined as $\sigma_y = \sigma_v x/U$, with the standard deviation of the lateral wind component σ_v and the effective plume velocity U. The 2-dimensional footprint f follows as

$$f(x,y) = D_y(x,y)\overline{f^y}(x). \tag{20}$$

As the parameterization in Equation (16) is only an approximate solution of Equation (15), its integration with respect to x (upwind distance) does not equal unity exactly. To force the computed integral footprint to unity, discrete footprint function increments are sorted according to their value and then summed to where the footprint function decreases to 1% of its maximum. The footprint function is then scaled by this sum. At this point, we should mention that versions of FSAM distributed after December 1996 contained an error that affected the shape of the computed footprint function. This error in FSAM was fixed for the present analysis.

3.2.2 Kormann and Meixner (2001)

The KM model is based on the analytical solution of the advection-diffusion equation of Van Ulden (1978) and Horst (1979). In order to achieve this solution analytically, power law profiles for the horizontal wind velocity and the eddy diffusivity are applied. The power laws are related to the semi-logarithmic profile functions from Monin-Obukhov similarity theory by an analytical approach of Huang (1979). In this way, the model includes the effects of buoyancy but is restricted to surface layer measurements.
The model provides a 2-dimensional flux footprint, is applicable for all stability conditions and can be routinely applied due to its small computing effort (Kormann and Meixner, 2001). However, as the model is not able to incorporate surface characteristics it presupposes horizontally homogeneous and stationary flow conditions (Kljun et al., 2003). The crosswind integrated footprint function of the KM model is described as (Neftel et al., 2008)

$$\overline{f^y}(x) = \frac{1}{\Gamma(\mu)} \frac{\xi^\mu}{x^{1+\mu}} exp\left(-\frac{\xi}{x}\right), \tag{21}$$

where Γ is the Gamma-function, ξ is a length scale incorporating the vertical profiles for the horizontal wind velocity and the eddy diffusivity, and μ a constant. Their explicit

definition can be found in Kormann and Meixner (2001). The 2-dimensional footprint is then defined by multiplying $\overline{f^y}$ with a Gaussian distribution according to Equations (19) and (20).
As for all other existing analytical footprint models, along-wind velocity fluctuations are neglected and thus, downwind flux contributions are not considered in the KM model. Due to its simplicity, and because it exclusively requires micrometeorological parameters provided by eddy covariance measurements, the KM model is widely used in current surface gas exchange research. Its input parameters are the aerodynamic measurement height z_m, mean horizontal wind velocity $\overline{u}$, friction velocity u_*, Obukhov length L, and the standard deviation of the lateral wind component σ_v.
Neftel et al. (2008) developed a tool for footprint calculations based on the model by Kormann and Meixner (2001). They provide an online-software[4] which determines the integral contribution of different fields in the surrounding of the measurement tower to the measured flux.

3.2.3 Hsieh et al. (2000)[5]

To overcome the main weakness of Lagrangian stochastic footprint models of long computation times, Hsieh et al. (2000) developed an analytic footprint model based on the simulation outputs of the Lagrangian model of Thomson (1987) and similarity theory (dimensional analysis). They estimate the crosswind integrated footprint by

$$\overline{f^y}(x) = \frac{1}{k^2 x^2} D z_u^p |L|^{1-P} exp\left(\frac{-1}{k^2 x} D z_u^p |L|^{1-P}\right) \tag{22}$$

where k is the von Kármán constant, L the Obukhov length, D and P are similarity constants depending on stability, and z_u is a length scale incorporating the aerodynamic measurement height z_m and the roughness length z_0. The one-dimensional model of Hsieh et al. (2000) is fully determined by three parameters: z_m, z_0, and L.
Since our evaluation strategy with the given experiment concept (see Section 3.6) requires a 2-dimensional source weight function we expanded the crosswind integrated footprint of HS with the crosswind component of the FSAM model (Equation 19). This was also done by van de Boer et al. (2013) who applied the crosswind component of FSAM as well as the one proposed by Detto et al. (2006) to the originally 1-dimensional model of Hsieh et al. (2000) and found no difference between these two based on their natural tracer experiment. As other analytical footprint models, HS also does not include along-wind diffusion and consequently is not able to consider flux contributions from regions downwind of the measurement system.

[4] http://www.agroscope.admin.ch/art-footprint-tool/, access on 2nd Feb 2017
[5] Excerpts of the following paragraph are also contained, almost verbatim, in Heidbach et al. (2017).

3.2.4 Kljun et al. (2015)

As Hsieh et al. (2000), Kljun et al. (2015) also developed a parametrization of a Lagrangian footprint model (from now on referred to as FFP). The model is an corrected and expanded version of the first parameterization of Kljun et al. (2004a). Both are derived from the backward Lagrangian particle dispersion model LPDM-B of Kljun et al. (2002). For more details of the original model please refer to Rotach et al. (1996), De Haan and Rotach (1998), and Kljun et al. (2002).
To obtain the 2-dimensional footprint function, a non-dimensional upwind distance X^* is determined:

$$X^* = \frac{x}{z_m}\left(1 - \frac{z_m}{h}\right)\left(\frac{\overline{u}(z_m)}{u_*}k\right)^{-1}, \tag{23}$$

where x is the upwind distance, z_m is the measurement height, h the boundary layer height, $\overline{u}(z_m)$ the mean wind velocity, u_* the friction velocity, and k the von Kármán constant. The non-dimensional upwind distance serves as input for the parameterized crosswind-integrated footprint F^{y*} and the scaled crosswind dispersion σ_y^*:

$$F^{y*} = a(X^* - d)^b exp\left(\frac{-c}{X^* - d}\right) \tag{24}$$

with $a = 1.452$, $b = -1.991$, $c = 1.462$, and $d = 0.136$, and

$$\sigma_y^* = a_c\left(\frac{b_c\,(X^*)^2}{1 + c_c X^*}\right)^{1/2} \tag{25}$$

with $a_c = 2.17$, $b_c = 1.66$, and $c_c = 20.0$. The crosswind integrated footprint in real dimensions $\overline{f^y}$ results from

$$\overline{f^y}(x) = \frac{F^{y*}\left(1 - \frac{z_m}{h}\right)u_*}{z_m\overline{u}(z_m)k} \tag{26}$$

and

$$\sigma_y = \frac{\sigma_y^* z_m \sigma_v}{p_{s1} u_*} \tag{27}$$

where p_{s1} is a proportionality factor depending on stability, and σ_v is the standard deviation of the lateral wind component. The extension to 2 dimensions is achieved by multiplying $\overline{f^y}$ with the Gaussian crosswind distribution (Equation 19)

$$f(x,y) = \overline{f^y}(x)\frac{1}{\sqrt{2\pi}\sigma_y} exp\left(-\frac{y^2}{2\sigma_y^2}\right) \tag{28}$$

In summary, the footprint of FFP is fully determined by the six parameters measurement height, Obukhov length, friction velocity, standard deviation of the lateral wind component, either roughness length or wind velocity, and boundary layer height. As the latter is available only rarely, Kljun et al. (2015) analyzed the sensitivity of their model output as a function of boundary layer height and found only minor shifts and changes in footprint size for variations up to 20% in h. Due to very clean air in the Graswang valley, boundary layer heights derived from ceilometer measurements in clear sky conditions are not reliable. As variations in h have only slight effects on footprint estimates of FFP, we set h to 1000 m for all measurement periods (see also Section 3.10.2). For changes of 20% in z_0, Kljun et al. (2015) also found only minor alterations of the resulting footprint. However, as wind speed measurements are available at our site, z_0 doesn't have to be determined for the FFP model. All other input parameters are measured at the site in Graswang and usually by default at eddy covariance sites.
Like the original Lagrangian model LPDM-B, the parameterization is applicable for a broad range of boundary layer stratifications ranging from convective to stable conditions and for measurement heights over the entire boundary layer. In contrast to its predecessor of Kljun et al. (2004a), the optimized parameterization predicts the peak location of the footprint to be closer to the measurement system (Kljun et al., 2015) and is able to predict flux contributions from sources downwind of the measurement tower. The latter is accomplished when another set of fitting parameters specifically derived for convective conditions is applied (see Appendix A in Kljun et al., 2015). Furthermore, FFP provides not only the crosswind integrated footprint (as is the case in the older parameterization of Kljun et al., 2004a), but also width and shape of footprint estimates (Kljun et al., 2015). Nevertheless, such parameterizations are simpler and easier accessible compared to more sophisticated, but highly computationally expensive, Lagrangian stochastic particle dispersion footprint models.

3.3 Research site[6]

The tracer experiments were conducted near Graswang, a small village within the prealpine region in southern Germany, approximately 90 km south of Munich (47.57° N, 11.03° E, 870 m a.s.l.). Graswang is located in a flat ∼1 km wide U-shaped east-west valley that is flanked by steep sides (up to 1800 m a.s.l., see Fig. 9 and 10a).
As part of the TERENO (**Ter**restrial **En**vironmental **O**bservatories, www.TERENO.net; Zacharias et al., 2011) preAlpine Observatory, eddy covariance measurements in Graswang are conducted above an extensively managed grassland with two cuts per year. For more information about Graswang and the other two sites of the TERENO-preAlpine Obser-

[6]Excerpts of the following section are also contained, almost verbatim, in Heidbach et al. (2017).

vatory, Rottenbuch and Fendt, the reader is referred to Zeeman et al. (2017).
The grass was cut right before and in between the experiments for the present study (July 25 and August 13 in 2013 and June 05 and August 07 in 2014) so that the mean grass height in Graswang varied between 0.08 m and 0.25 m. These grass heights are associated with a median roughness length of 0.03 m determined by wind-speed measurements and the logarithmic wind profile (see Equation 32, below). A forest with tree heights ranging between 13-29 m (estimated by visual inspection) is located $\sim$ 230 m east of the measurement tower, its edge extends in north-south (cross-valley) direction. Due to the terrain characteristics, local winds are typically characterized by a mountain-valley-breeze pattern, with prevailing easterly winds during day and westerlies at night (Fig. 10b). Hence, the site in Graswang behaves akin to a natural wind tunnel. Wind systems with such predictable direction changes facilitate tracer experiments, as up- and downwind regions can be estimated a-priori, and a fixed tracer release setup can be implemented.

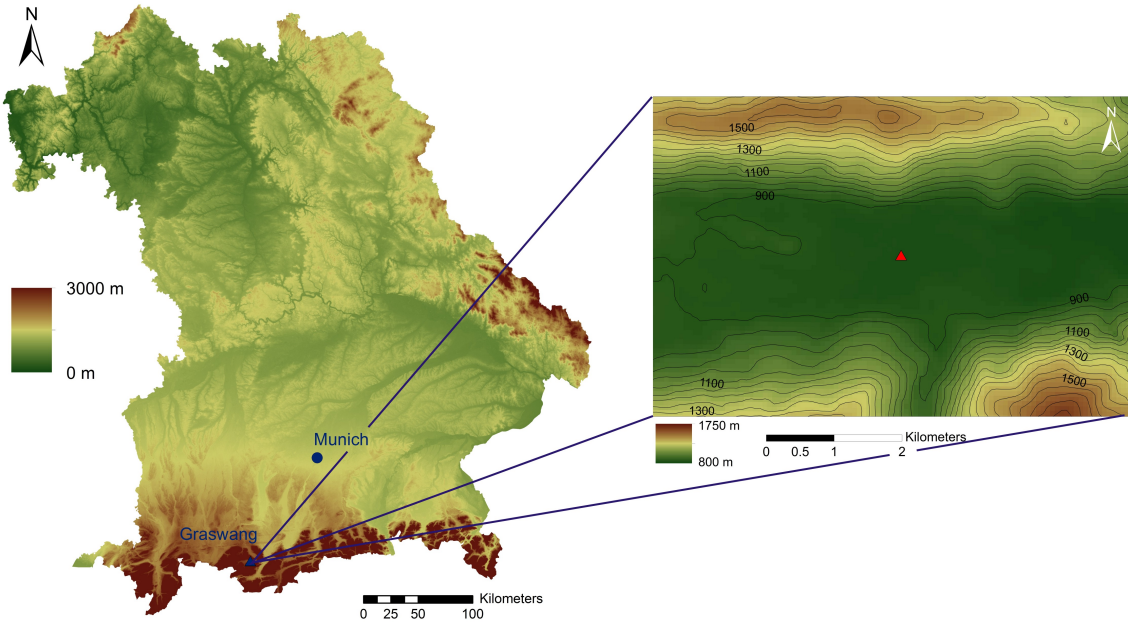

Figure 9: Topographic map of Bavaria, Germany, (left) and the Graswang-valley (right). The maps were produced using an ASTER DEM (ASTER Global DEM, U.S. Geological Survey (USGS), 2014).

3.4 Instrumentation

The TERENO measurement site in Graswang was established in October 2009. Since then, fluxes of energy and CO_2 were continuously measured with an eddy covariance system, including an open path CO_2/H_2O analyzer (IRGA, LI7500, Li-Cor Biosciences Inc., Lincoln, NE, USA) and a 3-D sonic anemometer (CSAT-3, Campbell Scientific,

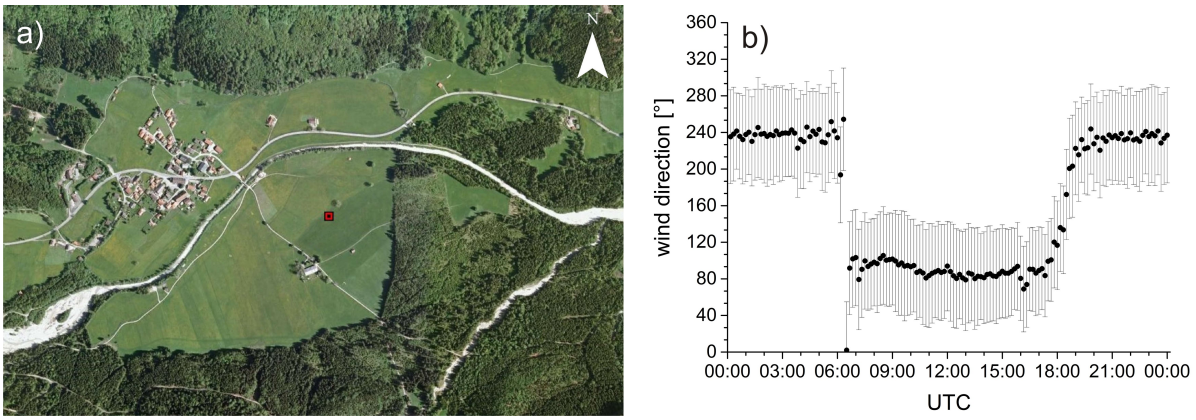

Figure 10: a) Satellite image of the measurement area in Graswang, area roughly 2.2 km x 1.4 km, the red square represents the eddy covariance tower (Google, 2013), b) mean daily cycle of wind direction in Graswang with the vertical bars showing the standard deviation, determined with vectorial analysis. Time period from July 02 to September 30 in 2013, data of precipitation periods are rejected. Figure from Heidbach et al. (2017).

Inc., Logan, Utah, USA). From June to November 2013 and from June to August 2014, the existing eddy covariance setup was temporarily extended with an open path CH_4 analyzer (LI7700, Li-Cor). The measurements were conducted on top of a radio-antenna-type tower of 3.25 m height with a sampling frequency of 20 Hz (Fig. 11).

Since the measurement site was not installed especially for the present study, but for the long-term TERENO-preAlpine observatory, a number of complementary parameters are routinely measured at the research site in Graswang: air temperature and relative humidity are measured by the HMP45C (Vaisala, Helsinki, Finland), surface temperature by an infrared radiometer (IR100, Campbell Scientific), the four components of the net radiation by the CNR4 (Kipp and Zonen, Delft, The Netherlands), diffuse, global radiation and sunshine duration are recorded by a separate pyranometer (SPN1, Delta-T Devices Ltd, Cambridge, UK), while photosynthetically active radiation is measured by a quantum sensor (SKP215, Skye Instruments Ltd, Llandrindod Wells, UK). Precipitation is detected by a weather transmitter (WXT520, Vaisala) that counts the impact of every drop separately and generates a signal proportional to the impact and therefore to its volume. Additionally, the weather transmitter captures horizontal wind velocity and direction, air temperature and humidity as well as atmospheric pressure. Measurements of the ground heat flux in 0.08 and 0.09 m depth by three heat flux plates (HFP01, Hukseflux Thermal Sensors B.V., Delft, The Netherlands) are supplemented by 18 temperature probes (T107, Campbell Scientific) and the same number of water content reflectometers (CS616, Campbell Scientific), placed in three profiles with six depths (0.02, 0.06, 0.12, 0.25, 0.35, 0.5 m). Finally, an acoustic sensor (SR50A, Campbell Scientific) provides

either snow depth or vegetation height.
The sensors of the eddy covariance system, including the HMP45C are connected to a CR3000 data logger (Campbell Scientific) that scans sensors and stores data with an interval of 20 Hz. The other instruments are scanned with an interval of 1 min and are stored to a second CR3000 data logger. All data are additionally stored on an onsite minicomputer (MPC21A, Kontron AG, Eching, Germany) and, by means of the existing internet connection, transferred to an institute-server on a daily basis.
In autumn 2013 and summer 2014, an additional mobile mast (tripod CM110, Campbell Scientific, Fig. 12), also equipped with a LI7700 CH_4 analyzer and a CSAT-3 sonic, was used for a more detailed evaluation of the model performance, as described in Section 3.7.

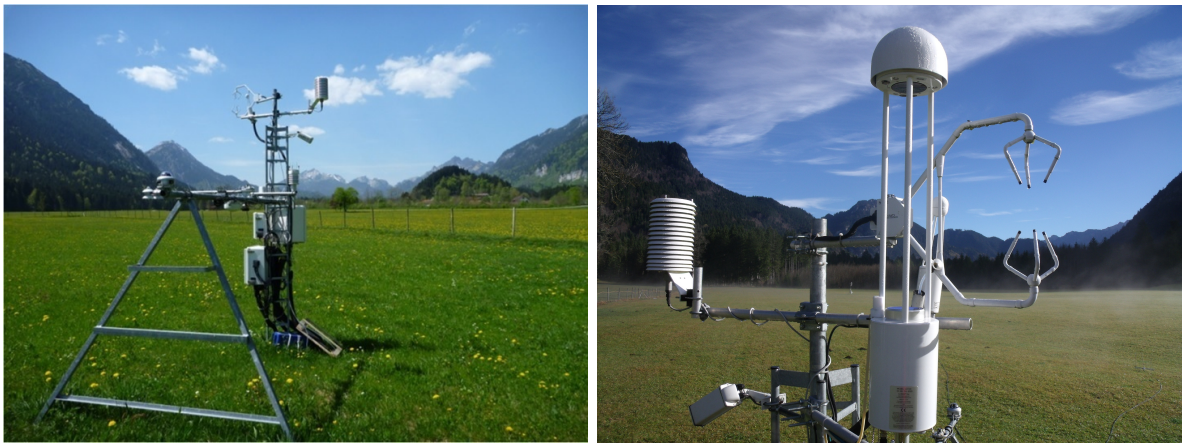

Figure 11: Left: Photograph of the measurement tower in Graswang towards the west; Right: Photograph towards the east with the eddy covariance system consisting of a sonic anemometer (CSAT3), and two gas analyzers (LI7700 and LI7500); for more details see Section 3.4.

3.5 Eddy covariance technique

Currently, the eddy covariance technique is one of the most direct and least interfering methods to measure turbulent fluxes of momentum, heat and trace gases between the Earth's surface and the atmosphere (Mauder et al., 2010; Burba, 2013). Therefore, since first scalar flux measurements appeared in the 80's, the eddy covariance method developed to an established long-term measurement technique with currently more than 700 sites worldwide (as of July 2015, source: FLUXNET, http://fluxnet.ornl.gov/). The mathematical derivation is described in the following, more detailed descriptions of the eddy covariance method can be found in the literature, e.g., Baldocchi et al. (1988), Foken (2008), Aubinet et al. (2012), and Burba (2013).
In general, the vertical flux F of any gas in turbulent flow is defined as the mean product

Figure 12: Photograph of the mobile mast in the front and the permanent eddy covariance mast in the background.

of air density ρ_a, vertical wind speed w, and the dry mole fraction of the corresponding gas c (Burba, 2013):

$$F = \overline{\rho_a w c} \tag{29}$$

With Reynolds decomposition, each fluctuating variable can be divided into its mean and deviations from this mean, i.e., the turbulent part, as illustrated in Figure 13.

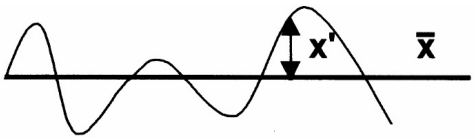

Figure 13: Schematic illustration of the Reynolds decomposition of a process x (Foken, 2008).

To consider turbulent motions in the flux calculation, this concept is applied to each variable in Equation (29), which results in

$$F = \overline{(\overline{\rho_a} + \rho_a')(\overline{w} + w')(\overline{c} + c')}, \tag{30}$$

where overbar (e.g., $\overline{w}$) represents the mean and prime (e.g., w') the fluctuating and random part. To simplify Equation (30), air density fluctuations are assumed to be negligible for the duration of an EC averaging period. This is reasonable in the lower atmosphere and over flat terrain.

By transforming and considering the assumption, Equation (30) results in the Equation for the flux:

$$F = \underbrace{\overline{\rho_a}\overline{w'c'}}_{i} + \underbrace{\overline{\rho_a wc}}_{ii} \tag{31}$$

with the eddy flux (i) and the mean flux (ii).
A summary of further assumptions for applying the eddy covariance technique can be found in Aubinet et al. (2012). Despite the difficulties that may occur to satisfy all assumptions, the eddy covariance technique is widely used to estimate exchange processes between ecosystems and the atmosphere, as it combines several advantages: First, it does not disturb natural exchange conditions, secondly, although it measures at a single point it represents an average flux of a specific area (the flux footprint; Schmid and Oke, 1990), and thirdly, it can be used to measure fluxes continuously over different time scales, ranging from hours to years (Baldocchi et al., 2001).

3.6 Experimental concept[7]

By releasing a tracer gas from extensive sources, a portion of the integral of the footprint function can be evaluated. However, it is not possible to examine the shape of the footprint, such as the along-wind and crosswind distributions. Furthermore, using tracer sources which extend over a specific area (this may also be a line or a circular line source) presupposes that the released tracer from any part of the source reaches the sensor in order to derive the effective emission rate that can be compared with the measured flux. Footprint evaluation experiments with linear line sources or extensive sources are highly wind direction dependent, which inevitably leads to edge effects.
For these reasons, we conducted validation experiments with a single, small finite surface source of an artificially released tracer gas. We constructed a tracer-source diffuser of approximately $\sim$1 m^2, corresponding to the size of one footprint matrix cell, so that it can be considered as an elemental source. In addition to practical advantages, such a small source provides the possibility to attribute the measured tracer flux to a specific cell in the footprint exactly.
We chose methane (CH_4, 99.5% purity) as tracer gas for two reasons: first, because it is measurable with a fast-response sensor, so that the eddy covariance method can be applied to estimate the flux, and second, because its natural flux in Graswang is negligible (see Section 4.3.1).
The tracer flux that is actually measured, is the result of the interplay between tracer release rate, footprint, and the source location within the footprint. Since the region

[7] Excerpts of the following section are also contained, almost verbatim, in Heidbach et al. (2017).

close to the footprint maximum is the most influential and relevant area for flux measurements, the tracer experiments were designed in such a way that especially this region could be evaluated. Accordingly, the tracer source was aimed to be located as close as possible to the footprint's maximum contribution. For this purpose, we identified typical daytime flux footprints by applying the model of Kormann and Meixner (2001) to input data from the permanent mast, prior to the experiments. These calculations resulted in an along-wind distance of ∼20-35 m, at which the footprint maximum is located most likely during daytime. Based on this position and by using the same model output we determined an appropriate emission rate. The latter was kept constant over each experimental averaging period (fluctuations less than 0.9%), but was adapted between the experiments, so that it varied between 6 and 8.5 l/min. The release was started one minute before the actual flux averaging period began, in order to avoid start-up effects during the time the tracer plume is approaching the measurement system. The experiments were conducted during daytime, when the source area is generally small compared to nighttime, and therefore the proportion of tracer molecules reaching the measurement system is much higher and a lower tracer release rate is required.

The tracer was released at the grass-canopy top from a diffuser apparatus: a stainless steel tubing manifold in a six-prong star arrangement (inner tube diameter: 0.015 m; diffuser diameter: 0.88 m; Fig. 14c). This star-shaped construction served to avoid spurious advection of the tracer plume in the near-field. This may occur when the plume in the near-field is smaller than the smallest eddies and may be transported by a single eddy. Distributing the gas to several turbulence elements increases the statistical representativeness of our experiments. As the construction is adjustable in height, it was adapted according to vegetation height.

We used two mass flow controllers (type 1179A and 1259CC, MKS Instruments, Inc., Andover, Massachusetts, USA) to set and record the flow rate, and electric valves (type 0300 and 0200, Bürkert, Ingelfingen, Germany) to start and stop the gas flow instantaneously, in case of changing wind direction (Fig. 14d). All devices were connected with tubes made of PTFE (0.635 cm outer diameter). To regulate the mass flow controller, we used a control unit (type I-7024, ICP DAS, Reutlingen, Germany) that is able to output a defined voltage, while a second control unit with a power relay switch (type I-7063, ICP DAS) was used to open and close the valves. The control units were operated via the on-site computer with the software DCON Utility. As the computer is connected to the internet, we were further able to monitor the wind situation, as well as the weather conditions in real-time, and to operate the experiments by remote control. In this way, methane was released only during periods without rain and suitable wind directions.

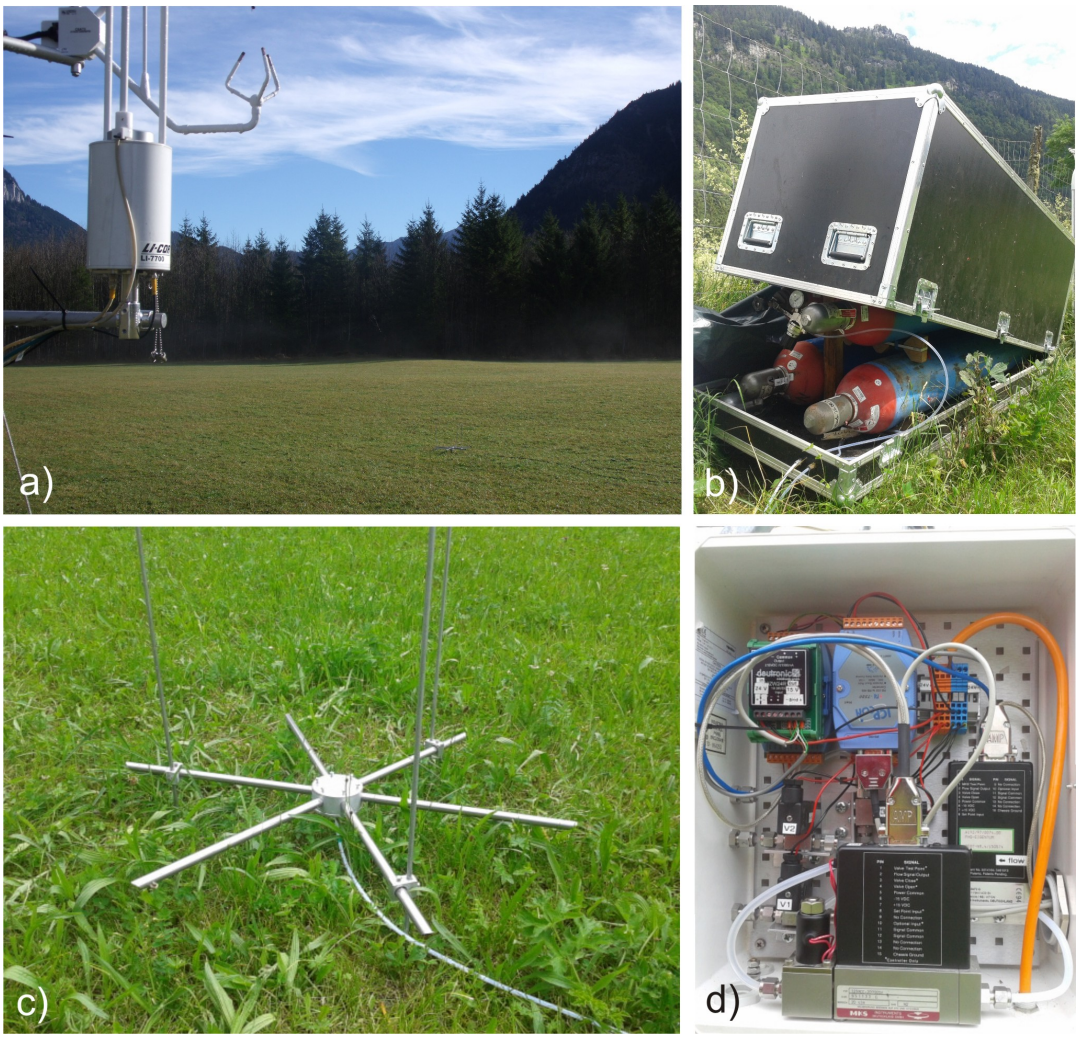

Figure 14: a) Eddy covariance system with the tracer diffuser in the background, b) storage of the gas bottles, c) diffuser with its six openings, d) electronics for the remotely controllable tracer release system, including three electric valves, two mass flow controllers and two control units.

3.7 Experiment setups

In total, the evaluation experiments were conducted in 4 different setups:

- Configuration A: a simple setup with only one flux measurement and a single tracer source placed in the upwind region of the mast (Fig. 15a)
- In configuration B we combine two similar setups, each with two flux towers simultaneously measuring the flux downwind of one single methane source: First, the two masts were placed in the expected along-wind direction (specific notation:

configuration B_{al}, Fig. 15b) and subsequently in the expected crosswind direction (configuration B_{cr}, Fig. 15c)

- Configuration C: same devices as in the first setup, but with the tracer source placed in the downwind region of the mast (Fig. 15d)
- Configuration D: Two masts, each with a single tracer source, but placed so far apart that they can be considered as independent systems. One of these systems was located close to the forest edge, in order to evaluate whether upwind changes in surface roughness and sensible heat flux have an influence on the performance of the footprint models (Fig. 15e).

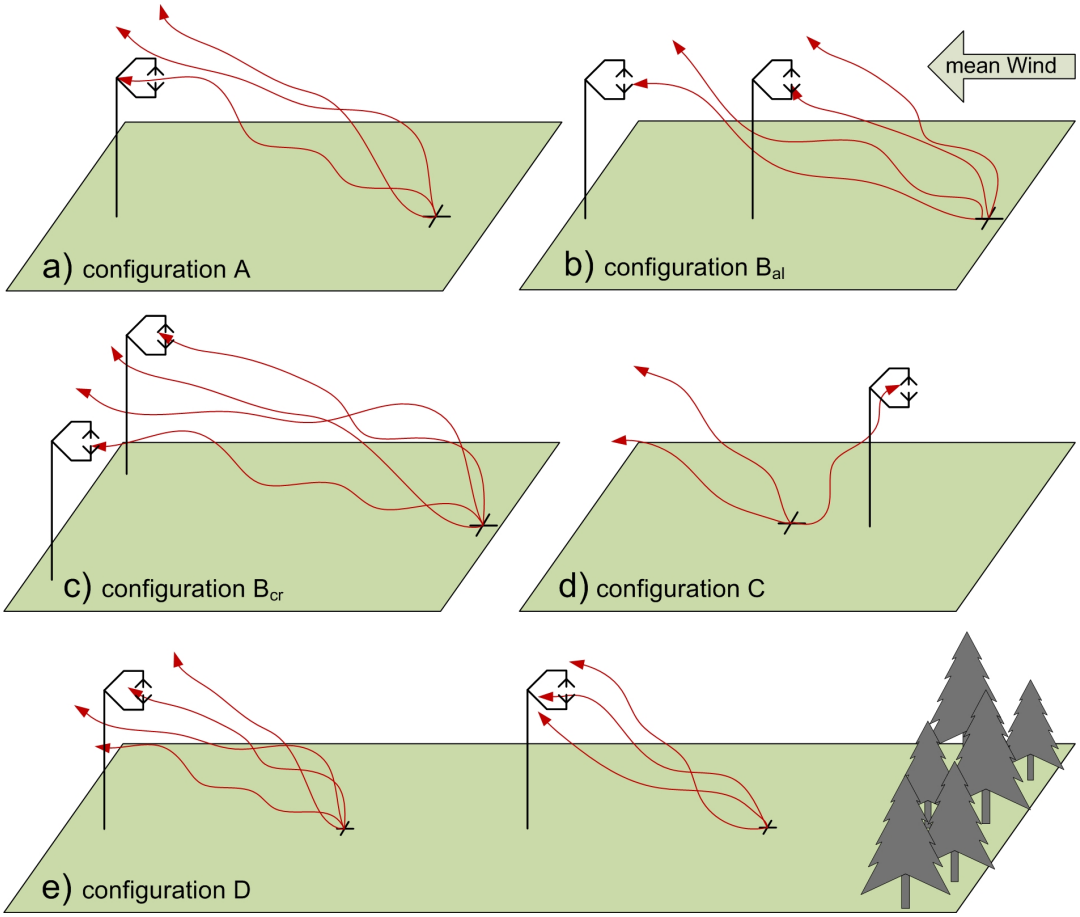

Figure 15: Sketches of experimental setups with up to two eddy covariance masts and either one or two point sources depicted as crosses. Red arrows represent potential paths of the released methane molecules that may or may not reach the eddy covariance system. Detailed descriptions of panels a), b), c), d), and e) can be found in the text.

Upwind and downwind sectors could be determined relatively easily due to the distinct and consistent mountain-valley-breeze, with prevailing easterly winds during day and

westerlies at night. As the tracer experiments were conducted only during daytime, the upwind sector was mostly east, and the downwind side west of the measurements. During the experiments, the tracer diffuser was installed at a fixed position and was not moved within a flux averaging period. In some cases, the source location was adapted, when a better position was ascertained during the experiments. Nevertheless, the relative location of the source within the footprint is not fixed, but varies dynamically, since location and size of the source area vary with changes in atmospheric stability, turbulence intensity, wind direction, and -velocity.
A more detailed description of the chosen setups can be found in the following Sections.

3.7.1 Setups with upwind source

Flux measurements at one location
Our experiments started with tracer flux measurements at the permanent mast and the tracer diffuser located in the expected upwind region east of the tower (hereinafter referred to as configuration A). We started the experiments with a sensor-source distance of 35 m and moved to 20 m after three weeks of measurements. Measurements with this setup were conducted from July 02 to July 30 in 2013. Figure 18a illustrates the position of the tracer diffuser relative to the flux measurement, and, in addition, the considered wind sector which was included in our evaluation analysis. Time periods with a mean wind direction outside the sector around the tower-diffuser-axis $\alpha \pm 40°$ were discarded, as the measured tracer flux is expected to be negligible in such cases.

Flux measurements at two locations
As a next step, we extended setup A with a second, mobile mast which was first placed between the permanent mast and the tracer diffuser (configuration B_{al}, Fig.18b). In this setup, the "along-wind experiment", the distance between the tracer source and the permanent mast was 35 m. The mobile mast, with its slender design, was chosen to be located in-between, at a distance of 20 m to the source, in order to minimize flow distortion at the permanent mast. The two masts and the source were arranged in one line with an alignment of 103° from north. This angle results from the expected easterly winds during daytime so that the wind most likely blows parallel to this axis. The experiments took place from June 12 to July 6 in 2014.
From July 10 to August 03 in 2014, the mobile mast was placed exactly south of the permanent mast at a distance of 10 m, while the tracer source was located 20 m east of the two towers (configuration B_{cr}, Fig. 16a+b and Fig. 18c). The main purpose of these two-tower setups was to facilitate the simultaneous evaluation of two locations in the footprint, to increase data availability for model evaluation. However, the main benefit of configuration B_{al} is that, in combination with an appropriate wind direction,

the along-wind distribution of the footprint, i.e. the centerline, can be evaluated. The centerline combines the crosswind integrated footprint (which expresses the along-wind variation), and the crosswind distribution (see Eq. 20).
Such a multi tower setup with only a single tracer source is equivalent to an experiment with multiple sources but only one flux measurement. However, by using several sources, different tracer gases would be required in order to facilitate the allocation of the measurements to each source. Therefore, our chosen setup is logistically and technically more feasible. Finn et al. (1996) already used a similar setup with even four flux towers along a line normal to a line source. However, as they released the tracer from a line source a meaningful interpretation of the measurements was strongly dependent on wind direction.

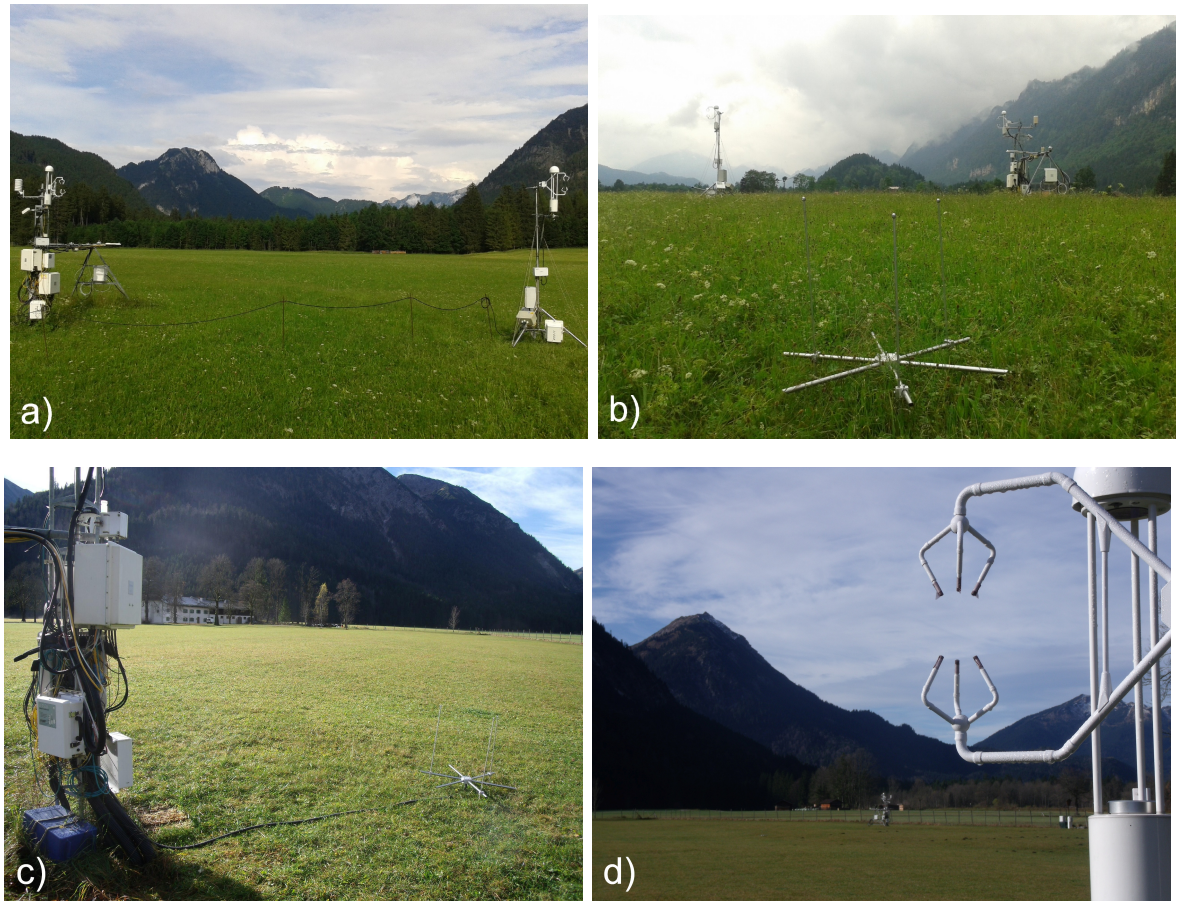

Figure 16: Pictures showing the experimental setups: a) configuration B_{cr} with the two eddy covariance masts next to each other; b) configuration B_{cr} with the point source in the front; c) configuration C with the point source next to the permanent mast; d) configuration D with the eddy covariance system of the additional mobile mast in the front and the permanent mast in the background.

3.7.2 Setup with downwind source

Setup D comprises the same devices as in Setup A, namely one flux measurement and one tracer source. However, in this case the tracer diffuser was placed in the anticipated downwind region, west of the permanent mast. In combination with the typical easterly winds during the day, we were able to analyze the presence of flux contributions from the downwind side of the mast (Fig.18d, configuration D). Due to the low measurement height, the distance between mast and diffuser was set to only 3 m (Fig. 16c). Measurements with this setup took place from July 22 to September 30 in 2013. Data rejection was implemented in the same way as for the upwind-experiments, i.e., measurement periods with a mean wind direction outside the 80°-wide sector centered on the main upwind azimuth α (prolonged tower-diffuser-axis) were discarded. Periods with winds blowing from outside this sector could not be used to investigate downwind flux contributions.

3.7.3 Setup at forest edge

In addition, we investigate the extent to which footprint model performance is affected, when upwind turbulence is disturbed by abrupt changes in surface roughness and sensible heat flux. For this purpose, supplementary to configuration A (in this setup referred to as X_{far}), we placed the mobile tower (in this setup referred to as X_{close}), paired with a second tracer source, at a distance of 88 m to the forest edge and released the tracer simultaneously from both point sources (Fig. 18e, configuration D). The separation between source and sensor was identical for the two systems, but the proximity to the forest edge was different: 88 m of the mobile mast in comparison to 230 m of the permanent mast (Fig. 16d). These experiments were conducted from October 11 to November 05 in 2013.
In principle, downwind of a forest-to-grass (or rough-to-smooth) transition, a surplus of increased turbulence kinetic energy (TKE) persists far into the "smooth" region. As Schmid and Bunzli (1995) stated, surface shear stress is drastically reduced after the transition, which results in a less efficient momentum transfer from higher levels to the surface. Consequently, the readjustment of the flow to the local surface roughness, and the recovery of equilibrium conditions, are slower than in a smooth-to-rough transition. In the case of a forest-to-grass transition, the roughness change is combined with geometric flow effects, due to the step-change in canopy height and the reduction of the height of the aerodynamic zero-plane. The flow characteristics at and downstream of the forest-to-grass edge is thus akin to flow over a backward-facing step (Le et al., 1997). According to Liu et al. (1996), there is a "quiet zone" downwind of a forest edge, with reduced wind speed, and reduced turbulence, followed by a "wake zone", characterized by increased turbulent exchange and a still lower, but increasing wind speed (Fig. 17).

With this setup, we specifically intended to violate the footprint model assumption of horizontally homogeneous turbulence, and thus the second tower was located in the expected "wake zone", at a distance of 88 m to the forest edge. At X_{close}, we expect that the turbulence within the footprint is more disturbed by the forest edge than at X_{far}. This hypothesis is evaluated in Section 4.3.5.

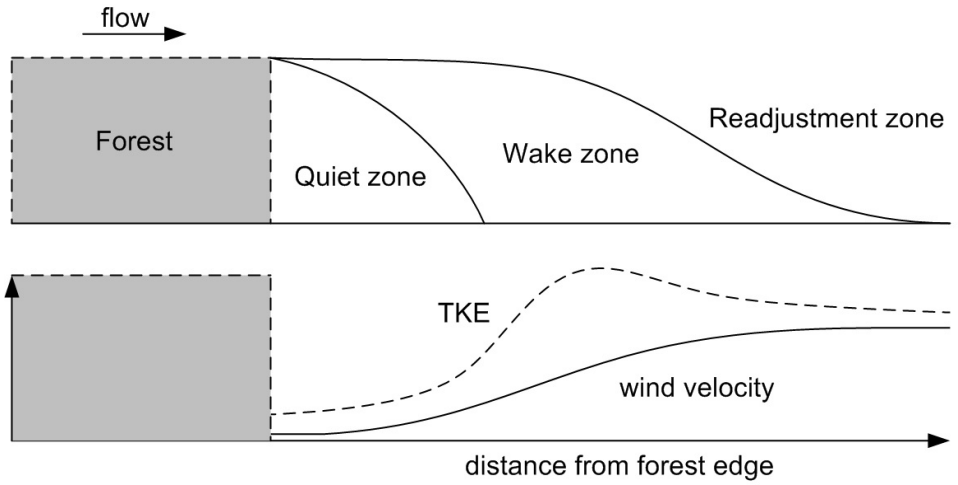

Figure 17: Schematic illustration of the flow over a backward-facing step and a rough-to-smooth transition. Course of turbulence kinetic energy (TKE) and wind velocity downwind of the forest edge are shown in the lower panel (following Liu et al., 1996). Figure from Heidbach et al. (2017).

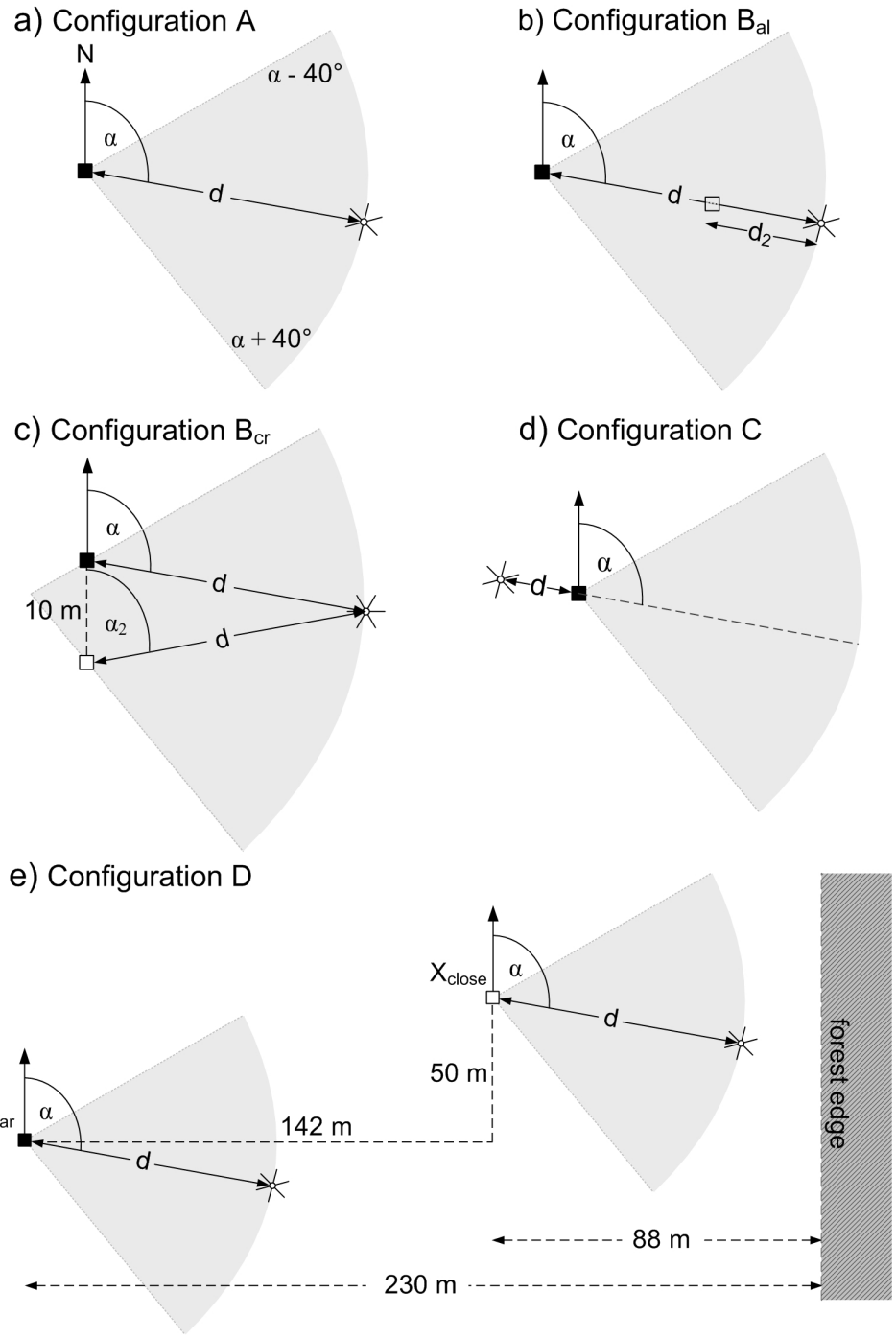

Figure 18: Schematic illustration of the five experimental configurations. Filled and open squares represent the permanent and mobile tower, respectively, while the star shows the location of the point source. The separation distance between tower and point source, d, as well as the main upwind azimuth, α, were adjusted to the prevailing flow conditions for each experiment. Shaded areas show the wind sector that was deemed acceptable for an experiment. a) Point source upwind of tower at d=20 m/35 m and $\alpha = 90°/100°$; b) point source upwind of two towers at d=35 m, d_2=20 m, and $\alpha = 103°$; c) diffuser upwind of two towers at d=20 m, $\alpha = 112°$ and $\alpha_2 = 67°$; d) diffuser downwind of tower at d=3 m and $\alpha = 100°$; e) simultaneous measurements with two identical systems, d=20 m and $\alpha = 100°$, but different proximity to the forest edge. The schematics are not true to scale. Figure modified after Heidbach et al. (2017).

3.8 Flux measurements

3.8.1 CH_4 flux calculation[8]

Methane fluxes were calculated from 20 Hz raw data using the data processing software package EddyPro (version 5.0.0, Li-Cor Biosciences Inc., Lincoln, NE, USA). To increase the number of independent flux samples, EC-fluxes were determined for an averaging interval of 10 minutes. A test showed that any low frequency losses compared to the more common interval of 30 minutes were negligible. The test is based on regression results between 30-minute blocks of 10 minutes fluxes, F_{10}, vs. 30-minute fluxes, F_{30} ($F_{10} = 1.00F_{30} - 0.02$, where the flux values are given in μmol m^{-2} s^{-1}, $R^2 = 0.97$, $N = 231$, relative RMSD in % of the mean 30-minute flux is 0.10, Figure 19).

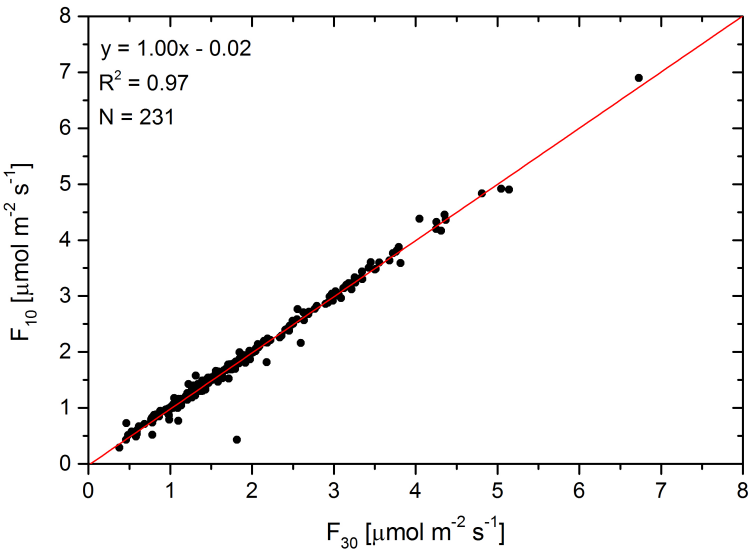

Figure 19: Regression between 30-minute CH_4 fluxes, F_{30}, and the corresponding 30 min blocks of 10-minute fluxes, F_{10}. Only data of the permanent mast of experiment configurations A, B_{al}, and D were used. The number of reliable 30-minute periods amounts to 231.

We applied the following standard corrections and data adjustments:

- Potential time lags between the 20Hz time series of the vertical wind component and the concentrations of methane and water vapor are determined and compensated with covariance maximization. In this way, we correct for an potential electronic delay that can be different for each sensor as well as for the sensor separation in along-wind direction. The lateral separation can only be compensated for via spectral correction (but this was not done).

[8]Excerpts of the following paragraph are also contained, almost verbatim, in Heidbach et al. (2017).

- To fulfill the prerequisite of the eddy covariance method of a vertical wind component of zero, we applied the double rotation method to our data. The main benefit of this method is that it nullifies each averaging interval separately and can be applied for short term experiments (Kaimal and Finnigan, 1994).
- The spectral correction in the low frequency range was performed following Moncrieff et al. (2004) which uses analytical cospectra formulations according to Moncrieff et al. (1997), a modification of the Kaimal formulation (Kaimal et al., 1972). To correct for the high frequency loss we applied the method after Moncrieff et al. (1997).
- We applied the methods after Webb et al. (1980) to account for density fluctuations (termed as WPL-adjustment following the last names of the authors Webb, Pearman amd Leuning) resulting from thermal expansion and/or dilution of the air. The WPL-adjustment at the mobile tower without water vapor measurements was performed with the available IRGA at the permanent tower.

The artificially generated emissions in this study produce highly fluctuating concentration measurements (not shown). However, as this is expected and sharp fluctuations are not necessarily an indication of bad data quality, we did not apply a de-spiking routine (such as in Mauder et al., 2013). In this way, we prevent removing high, but in our case valuable, concentration measurements that are more persistent than spurious spikes.

3.8.2 Quality assurance

Despite the above mentioned corrections and adjustments, data can still be of bad quality or inappropriate for the purpose of this study. Therefore, additional quality tests were performed and data selection criteria were defined.
To screen the data for steady state conditions and well developed turbulence, we applied the quality flagging scheme after Mauder and Foken (2004), which follows the protocol of the second CarboEurope-IP QA/QC workshop held in Spoleto, Italy (2004). We rejected fluxes with a flag of 2 (out of the 3 possible categories 0,1, and 2), indicating lowest data quality. Furthermore, an instrumental diagnostic value of the open path methane laser (RSSI: Received Signal Strength Indicator smaller than 35%) was used to detect periods with insufficient data quality.
In some particular cases, we measured non-negligible negative methane fluxes (see Figure 22). Most likely, in these time periods the methane plume rose beyond the measurement height before passing the sensors, which led to a reversed concentration gradient and therefore to downward directed fluxes. Since this relates to only 1% of the data we removed such cases for further analysis. However, negative fluxes measured during

experiments with setup C were not rejected as those reflect the natural methane flux fluctuating around zero in case of no downwind contribution.
To avoid unnecessary methane emissions, the tracer was released only in periods with an appropriate wind direction. Nevertheless, in some cases the wind unexpectedly changed direction, so that the tracer no longer reached the sensor and the corresponding time interval was unsuitable. Therefore, we screened data according to wind direction and included only time periods when the mean wind direction was within a 80° wide sector centered on the upwind azimuth α (see Fig.18).
Table 1 summarizes the number of 10-minute fluxes for each experimental setup that remained after data screening and were used for this study. Overall, we could use 2037 out of 2789 (corresponding to 73%) tracer release periods in total.

Table 1: Data availability for each experiment setup. Numbers correspond to the number of 10-minute fluxes that remained after data screening and were used for this study.

Setup	A	B_{al}	B_{cr}	C	D	$\sum$
Permanent mast	259	325	211	199	254	1248
Mobile mast	–	316	244	–	229	789
$\sum$	259	641	520	199	483	2037

3.9 Determination of roughness length[9]

For FSAM and the HS model, the roughness length z_0 is required as input parameter. FFP utilizes either the roughness length as input, or the mean wind speed at measurement height and derives an apparent roughness length by the aerodynamic method similar to the one presented below.
A common and simple way to parameterize the local roughness length is to set it at 10% of the canopy height following Foken (2008). This method is questionable, particularly for the mobile tower close to the forest edge (X_{close}), as some influence of the upwind forest is expected to play a role in a "true" effective roughness length at that location. Although the effective roughness length at X_{close} is thus expected to be higher than at the permanent tower (X_{far}), we first determined the footprints for both measurement towers with the same roughness length, i.e. $z_0 = 0.01$ m (thus ignoring the presence of the forest), for a straightforward comparison of the model performance in homogeneous vs. inhomogeneous conditions.
Additionally, footprints of X_{close} were calculated with the apparent roughness length determined from measurements of wind speed u, friction velocity u_*, and Obukhov length

[9]Excerpts of the following section are also contained, almost verbatim, in Heidbach et al. (2017).

L, according to the surface layer wind profile in standard Monin-Obukhov similarity theory:

$$z_0 = \frac{z_m}{exp\left(\frac{u(z_m)k}{u_*} + \Psi\left(\frac{z_m}{L}\right)\right)} \tag{32}$$

where k is the von Kármán constant (k=0.4) and Ψ is a stability correction function for a non-neutral atmosphere following Paulson (1970) for unstable conditions, and an empirical fit by Holtslag and De Bruin (1988) for stable conditions:

$$\Psi\left(\frac{z_m}{L}\right) = \begin{cases} 2ln\left(\frac{1+\zeta}{2}\right) + ln\left(\frac{1+\zeta^2}{2}\right) - 2tan^{-1}(\zeta) + \frac{\pi}{2} & \text{for } \frac{z_m}{L} < 0 \\ -a\left(\frac{z_m}{L}\right) - b\left(\frac{z_m}{L} - \frac{c}{d}\right) exp\left(-d\frac{z_m}{L}\right) - \frac{bc}{d} & \text{for } \frac{z_m}{L} \geq 0 \end{cases} \tag{33}$$

with $a = 0.7$, $b = 0.75$, $c = 5$, $d = 0.35$ and

$$\zeta = \left(1 - 16\frac{z_m}{L}\right)^{0.25} \tag{34}$$

This approach was not applied to KM and FFP since these models do not require z_0 as input parameter. Internally, KM and FFP use a similar similarity approach to relate z_0 to the mean wind speed at measurement height and u_*.

3.10 Uncertainty estimation

To investigate whether the model results differ significantly from the measurements, it is indispensable to quantify uncertainties of both the measurements and the models. In the following two Sections we summarize the sources of systematic, as well as random errors, and explain how we quantify uncertainties of flux measurements and footprint model results.

3.10.1 Uncertainty estimation of flux measurements[10]

According to Richardson et al. (2012) the uncertainty of flux measurements includes systematic as well as random errors. The latter result from turbulence sampling errors (ϵ_t), errors due to the instrument system (ϵ_i), and uncertainties associated with spatial representativeness affected by variability of the source field within the footprint (ϵ_f).
The turbulence sampling error includes potential flux losses as a result of not-captured large eddies and the uncertainty in the calculation of the (eddy-) covariance. It results from the fact that the number of independent samples of a flux averaging period is limited, and can be minimized by increasing the number of independent observations,

[10]Excerpts of the following paragraph are also contained, almost verbatim, in Heidbach et al. (2017).

i.e., either measuring at several locations, and/or extending the flux averaging interval (Mauder et al., 2013; Finkelstein and Sims, 2001). However, this leads to practical difficulties and other problems, such as the violation of stationarity.
The error due to the instrument system includes instrumental noise, and technical issues that may have an influence on the actual measurement process, or that may disturb the natural flow (Dragoni et al., 2007). It can be estimated with a paired measurement approach, i.e., measuring a flux with at least two eddy covariance systems next to each other, as was already done by Eugster et al. (1997) and Dragoni et al. (2007).
The uncertainty attributable to the variable footprint results from the fact that, usually, in real field conditions the land cover type within the changing footprint is not homogeneous, and/or the flux magnitudes are not (permanently) uniform within a homogeneous land cover type (Mauder et al., 2013). The magnitude of this error clearly depends on the degree of heterogeneity in the source distribution at a specific site. In general, random errors cannot be eliminated, but minimized by proper site selection and data handling. However, the systematic error of flux measurements includes errors due to unmet assumptions of the eddy covariance method (ϵ_{EC}), instrument design and calibration errors (ϵ_c) as well as errors resulting from data processing (ϵ_p) (Richardson et al., 2012). Uncertainties attributable to instrument design comprise a potential misalignment of the anemometer, flow distortion due to sensor construction, and high-frequency losses as a result of limited time response, sensor separation, and volume averaging (Richardson et al., 2012). Data corrections, such as detrending, coordinate rotation, high- and low-frequency corrections, and gap filling, can be applied in order to compensate for such errors. However, these in turn produce another uncertainty, as they are based on imperfect data and theoretical considerations.
Therefore, following Richardson et al. (2012), the total uncertainty of observations ϵ_{obs} can be expressed as:

$$\epsilon_{obs} = function(\epsilon_t, \epsilon_i, \epsilon_f, \epsilon_{EC}, \epsilon_c, \epsilon_p) \tag{35}$$

Janina Klatt (personal communication) investigated the instrument error of two LI7700 sensors by measuring the methane flux side by side with the same sonic anemometer (CSAT-3). In their bog forest, they found an RMSD (root mean square deviation) between the two sensors of 6.7 nmol m^{-2} s^{-1} for a flux range of [56; 97] nmol $m^{-2}s^{-1}$ and a mean flux of 10.5 nmol m^{-2} s^{-1}. As the artificially generated fluxes of our experiments are mostly more than one order of magnitude higher (Figure 22), and assuming that the instrument error does not depend on the flux magnitude, we neglect ϵ_i in our study. Furthermore, as the fluxes from an artificially generated point source are measured, the spatial representativeness of fluxes does not play a role here, and ϵ_f can be set to zero. However, the turbulence sampling error of fluxes was estimated by the variance of the

covariance following Finkelstein and Sims (2001). This is a statistical approach, and a direct method that can be applied to estimate the uncertainty of a measured flux. It includes all terms contributing to the variance of a flux, i.e., auto- and cross-covariance functions. Considering two variables x and y, the variance of their covariance, and thus the turbulence sampling error, can be determined from Equation (36) (following Finkelstein and Sims, 2001):

$$\epsilon_t = \sqrt{\frac{1}{n}\sum_{p=-m}^{m} \overline{x'x'_p} \cdot \overline{y'y'_p} + \overline{x'y'_p} \cdot \overline{x'_p y'}} \tag{36}$$

The auto-covariance functions are denoted as $\overline{x'x'_p}$ and $\overline{y'y'_p}$ while $\overline{x'y'_p}$ and $\overline{x'_p y'}$ represent the cross-covariances with lag p. According to Finkelstein and Sims (2001) the parameter m is the number of samples contained in one integral time scale (ITS). The ITS is a measure for the auto-correlation duration of a process, which approaches zero for longer time lags. Therefore, a threshold defining when correlation is zero cannot unambiguously be determined. Several approaches can be applied to objectively define the ITS: The time lag at which the cross- or auto-correlation function first crosses zero or 1/e (selectable options in the software application EddyPro, or even a fixed value (e.g., $n/2$ with n being the number of samples) as proposed in Mauder et al. (2013) and Finkelstein and Sims (2001), can be used to define the ITS. However, Finkelstein and Sims (2001) selected an m of 200 (representing 20 s for 10 Hz data) and showed that for m between 100 and 400 the results varied by only 1-2%. Under the assumption that there is no trend in the data, selecting m too high does not have a relevant influence on the determination of ϵ_t, as all terms in Equation (36) approach zero for a larger m. In our study, we used a fixed m of $n/2$ and an m at which the cross- or auto-correlation function first crosses 1/e for the calculation of ϵ_t of the friction velocity, constituting covariances ($\overline{u'w'}$ and $\overline{v'w'}$), and the sensible heat and methane flux, respectively.

Since systematic errors cannot be quantified without an absolute reference, their effect can be minimized only by instrument calibration, including the application of pertinent corrections and adjustments of eddy covariance fluxes (Mauder et al., 2013), and by assuring that such systematic errors are kept constant over the experimental period. Consequently, such systematic errors contribute to the overall bias of the measurements, but not to the error variance. We therefore excluded ϵ_{EC}, ϵ_c, and ϵ_p in the estimation of measurement uncertainty, and, as ϵ_i and ϵ_f are assumed to be negligible, equate the uncertainty of observations with the turbulence sampling error ϵ_t:

$$\epsilon_{obs} \approx \epsilon_t \tag{37}$$

3.10.2 Uncertainty estimation of footprint model results[11]

In general, the uncertainty of a footprint model (ϵ_{model}) consists of uncertainties resulting from an incomplete or deficient model theory (ϵ_{th}), the violation of model assumptions (ϵ_a) (e.g., horizontally homogeneous turbulence and Monin-Obukhov similarity), and from the uncertainty of input parameters (ϵ_{in}):

$$\epsilon_{model} = function(\epsilon_{th}, \epsilon_a, \epsilon_{in}) \tag{38}$$

Our study is designed to investigate the sum of the first two components, while we can determine the third component by error propagation of the random errors of the input parameters. Input parameters of the evaluated footprint models are the aerodynamic measurement height z_m, roughness length z_0, mean horizontal wind velocity $\bar{u}$, standard deviation of the lateral wind component σ_v, wind direction, boundary layer height (h, only FFP) and two parameters that are based on fluxes (covariances), namely friction velocity u_* ($\overline{u'w'}$ and $\overline{v'w'}$) and Obukhov length L ($\overline{w'T'}$).
As not only the boundary layer height, but also the width of the valley (∼1 km) is a limiting factor for the eddy size we set h to 1000 m for all measurement periods. The flux contributions estimated by the FFP model varied not more than 1% by applying boundary layer heights of 500 - 2000 m. This little variation can be attributed to the low measurement height, as only the relative difference between measurement height and boundary layer height (h-z_m)/h is relevant. We therefore neglected the uncertainty of the boundary layer height in the uncertainty analysis of the FFP model.
Furthermore, the random uncertainties of z_m, $\bar{u}$, σ_v, and wind direction are assumed to be small and mainly systematic, and thus are neglected as well. As the uncertainty of z_0 cannot be estimated appropriately we calculated footprints of FSAM and HS with different roughness lengths for the measurements of the mobile tower in configuration D and analyzed whether an effect on model quality is apparent (see Section 4.3.5).
We suspect that the uncertainty of the friction velocity and the Obukhov length can produce large random errors in the footprint, so that we define the random error of a footprint model as a result of turbulence sampling errors of those input parameters that contain fluxes (covariances). For each covariance we estimated the random error following Finkelstein and Sims (2001) and numerically determined the model uncertainty resulting from the uncertainty of input parameters ϵ_{in} based on error propagation:

$$\epsilon_{in} = \sqrt{\left(\frac{\partial f}{\partial u_*} \cdot \sigma_{u_*}\right)^2 + \left(\frac{\partial f}{\partial \overline{w'T'}} \cdot \sigma_{\overline{w'T'}}\right)^2} \tag{39}$$

[11] Excerpts of the following paragraph are also contained, almost verbatim, in Heidbach et al. (2017).

where f is the 2-dimensional footprint function, $\sigma_{\overline{w'T'}}$ and σ_{u_*} are the random errors of the sensible heat flux $\overline{w'T'}$, and the friction velocity u_*, respectively, while σ_{u_*} results from error propagation of the random errors of $\overline{u'w'}$ and $\overline{v'w'}$.
The uncertainty of the KM model was additionally determined by solving the partial derivatives in Equation (39) analytically. The results were compared with the numerically determined uncertainties, to verify consistency between the two.

4 Results and Discussion

4.1 Uncertainty of flux measurements

In this section, we analyze the measurement uncertainty, in our study quantified by the turbulence sampling error following Finkelstein and Sims (2001) (see Section 3.10.1). We analyzed the random errors separately for measurements close to the forest edge (mobile mast in setup D) and the "undisturbed" open field measurements of both masts in all configurations. However, we excluded fluxes measured during the downwind experiments (configuration C) in this analysis, as they fluctuate around zero in most cases and thus produce tremendous relative uncertainties. The median of the relative uncertainties for the open-field flux measurements is 26%, while the lower and upper quartile range from 21 to 34% (Fig. 20). The statistics of the measurements close to the forest edge show slightly higher relative uncertainties, with a median of 33% and a lower and upper quartile of 26% and 42%, respectively. However, it needs to be considered that the number of available measurements is significantly lower for the forest edge boxplot (N=229 in contrast to N=1609). This estimate of the turbulence sampling error assumes stationary conditions that are clearly not likely in the fast concentration time series emerging from a point source. Therefore, we compare the random uncertainties of the artificially generated fluxes in this study to the results in Mauder et al. (2013), who analyzed the random flux errors of momentum, sensible heat, latent heat and CO_2 at 5 different sites. On average, the random errors were around 20-30% for most of their selected sites and fluxes. Mauder et al. (2013) further differentiated between highest-quality data (flag 0, using the same flagging scheme as described in Section 3.8.2) and medium-quality data (flag 1). In their study, random errors of highest-quality data are typically smaller than 20% while those of medium-quality data range between 15% and 50%. Therefore, lacking a better choice, we consider the variance of a covariance as adequate estimate of the random uncertainty here.

4.2 Uncertainty analysis of the footprint estimates[12]

In the following, we examine the uncertainty of the footprint estimates resulting from the most uncertain model input parameters, friction velocity and Obukhov length. To allow a visualization of an ensemble of footprints and their uncertainties, we normalized the flux contribution, and the along-wind distance of 259 (configuration A) footprint centerlines with the footprints maximum contribution f_{max}, and its distance x_{max}, respectively. The footprint centerline corresponds to the along-wind axis of the crosswind distributed footprint. Those standardized centerlines were binned and the median flux contribution,

[12]Excerpts of the following section are also contained, almost verbatim, in Heidbach et al. (2017).

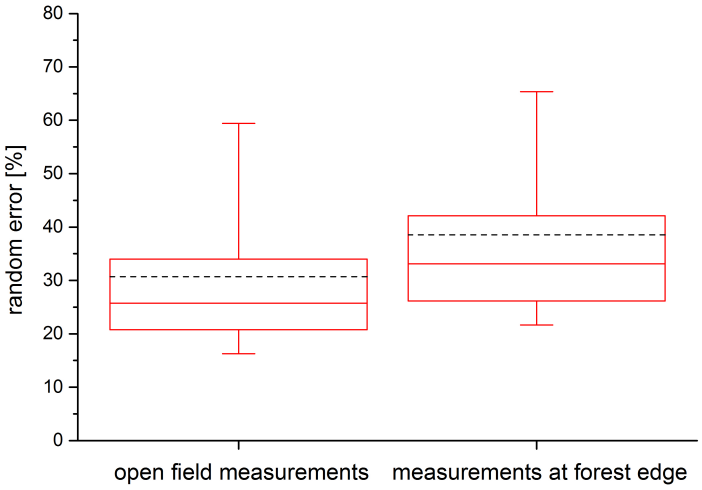

Figure 20: Boxplots of the random error of measured CH_4 fluxes. The left boxplot includes fluxes measured in the open field at the permanent and mobile mast during the experiment configurations A, B_{al}, B_{cr}, and D (only permanent mast) while the right boxplot is based on data of the mobile mast of setup D. Shown are the lower and upper quartile (box range), the 5^{th} and 95^{th} percentile (whiskers), the median (solid line), and the mean (dashed line) of the random errors. Only random errors of fluxes remaining after data screening as described in section 3.8.2 are considered.

as well as the median uncertainty for each bin was determined. Due to the normalization, f_{max} amounts to 1 and is located at a normalized distance of 1, and this applies to all four models (Fig. 21a). As a result, the footprint centerlines of the four models look very similar. In the most influencing part of the source area around f_{max}, up to a normalized distance of 1.5 from the tower (equal to 1.5 times x_{max}) FSAM shows the smallest relative uncertainty while HS shows the largest (Fig. 21b). At the location of the footprint maximum the uncertainty of FSAM amounts to only 13%, while for KM, HS, and FFP it is 27%, 48%, and 40%, respectively. Such potentially large errors of footprint regions that contribute to a major part to the measured flux can cause non-negligible differences in the extent of the footprint. This is of importance particularly for studies that use integrated flux contributions of a specific area of interest (e.g., a specific ecosystem), e.g., as described in Neftel et al. (2008), to screen their data. Shortly beyond the maximum, at a distance of 1.4 times x_{max}, the relative uncertainty of FSAM has a minimum of only 9%. The uncertainties of KM, HS, and FFP also show minima of 5%, 3%, and 0.5%, but further upwind at normalized distances of 1.9, 2.5, and 4, respectively. The uncertainty minimum for the KM model was also found by solving the partial derivatives in Equation (39) analytically (not shown). Behind the minima the uncertainties of the KM, HS, and FSAM stabilize at around 5-20%, while the uncertainty of FFP levels off to an uncertainty of only 1% further upwind.

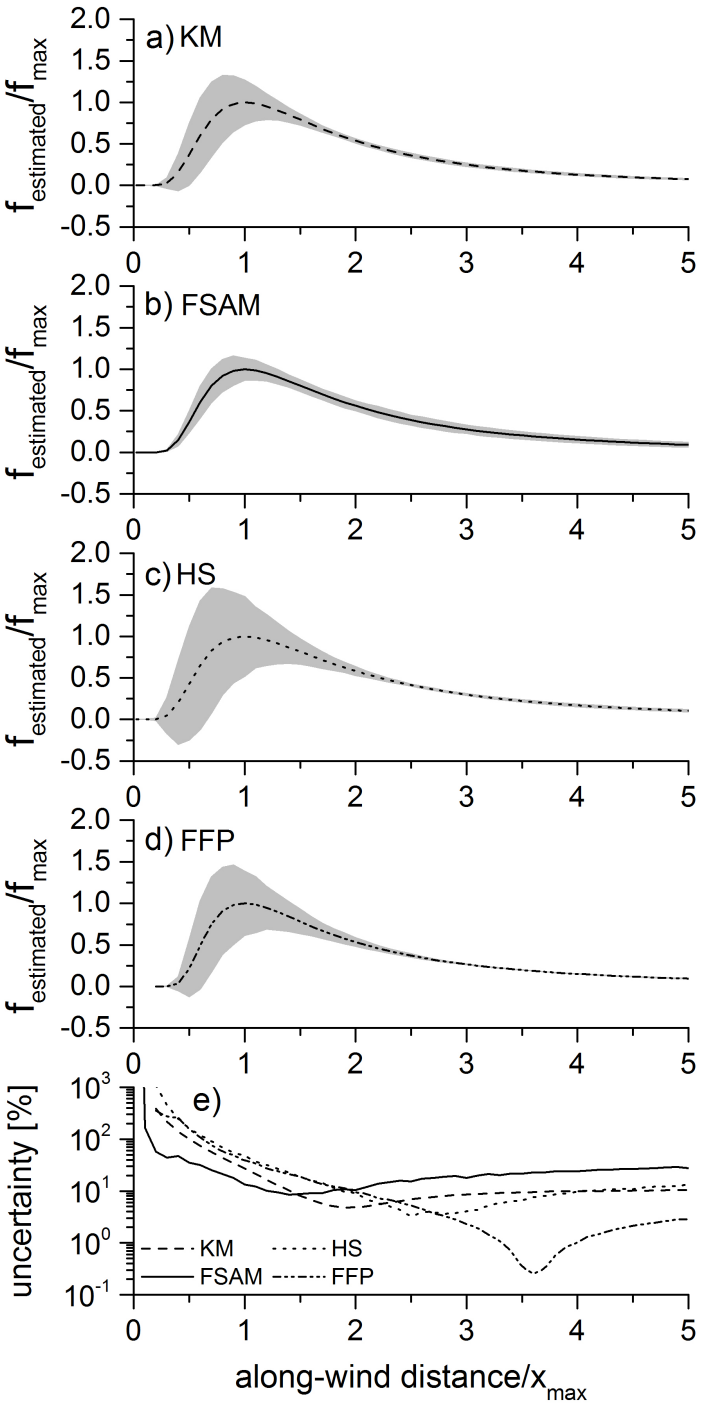

Figure 21: a-d) Median of 259 (configuration A) footprint centerlines of a) KM, b) FSAM, c) HS, and d) FFP. Estimated flux contributions $f_{estimated}$ and along-wind distance were normalized by f_{max} and x_{max}, respectively. Footprints were binned according to their normalized distance, and median flux contributions were determined for each bin of 0.05 width. Shadings of gray denote the binned and normalized medians of model uncertainties. e) shows the relative median model uncertainty $\epsilon_{in}/f_{estimated}$ (in %) as a function of the normalized along-wind distance for all analyzed models. Figure from Heidbach et al. (2017).

4.3 Experiments

4.3.1 Artificial CH_4 flux compared to the natural flux in Graswang[13]

In general, the main prerequisite for experiments with artificially released tracers is a negligible natural flux of the tracer gas. In Graswang, the natural flux of methane fluctuates around zero with a median of -0.001 μmol m^{-2} s^{-1} and the 95%-confidence interval from 0.08 to 0.08 μmol m^{-2} s^{-1} (Fig. 22a). However, the fluxes we measured during tracer release periods are mostly more than one order of magnitude higher (Fig. 22b). For that reason, we didn't apply any correction concerning the natural flux. In some particular cases we measured non-negligible negative methane fluxes (as mentioned above).

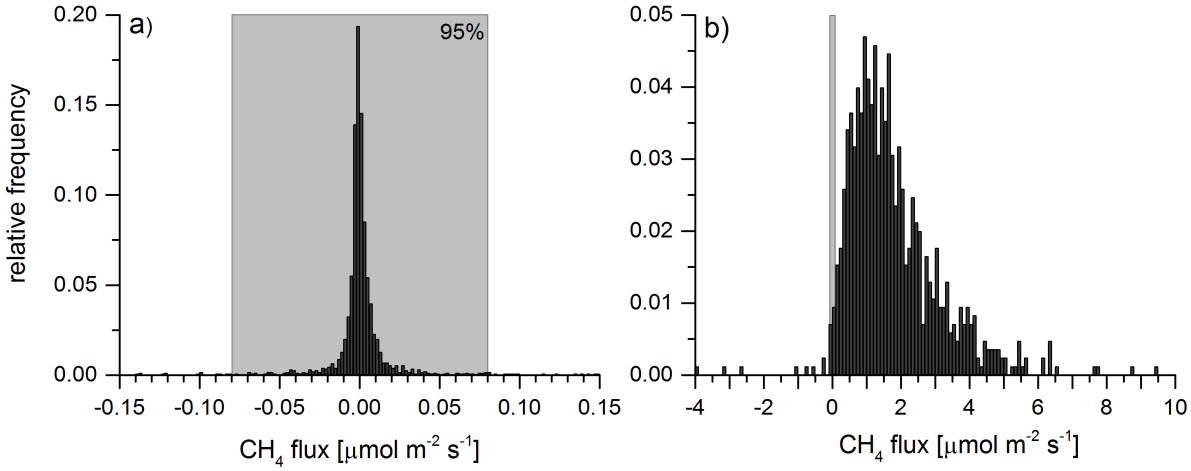

Figure 22: Frequency distributions of quality controlled data of a) the natural methane flux measured from Mar 1 to June 11, 2014 and b) the artificial CH_4 flux measured at the permanent tower during experiments A, B_{al} and D. Please note the difference in the horizontal axis scales between the two panels. In both panels, the gray background represents the 95%-confidence interval of the natural methane flux. Figure from Heidbach et al. (2017).

4.3.2 Meteorological flow conditions[13]

We conducted the tracer experiments during daytime in the summer and autumn months of 2013 and 2014. Consequently, the mountain-valley-breeze patterns and wind directions were very consistent. In 90% of the relevant time periods, the wind direction was within the sector of 67°-120° (Fig. 23a). Accordingly, the position of the tracer source was suitable for both the upwind experiments with the tracer diffuser at 90° and 100° (azimuth, clockwise from north) as well as the downwind experiments with the tracer source at

[13]Excerpts of the following paragraph are also contained, almost verbatim, in Heidbach et al. (2017).

280°. Due to the channeling of the wind in the valley, the wind velocities during the experiments were comparatively high, with a median of 2.9 m s^{-1} (Fig. 23b). As the tracer experiments took place only during daytime, the friction velocity u_* was in most cases relatively high, with the mean and the median at 0.23 m s^{-1} indicating well-developed turbulent conditions (Fig. 23c). Additionally, the distribution of the stability parameter z_m/L shows that, in 89% of the experiments, unstable conditions ($L<0$) were dominant (Fig. 23d). The standard deviation of the lateral wind component σ_v is relevant for the width of the footprint. On average it amounts to only about one third of the mean wind speed (Fig. 23e). This is consistent with Rannik et al. (2012) who pointed out that lateral diffusion is typically less pronounced for high wind speeds.

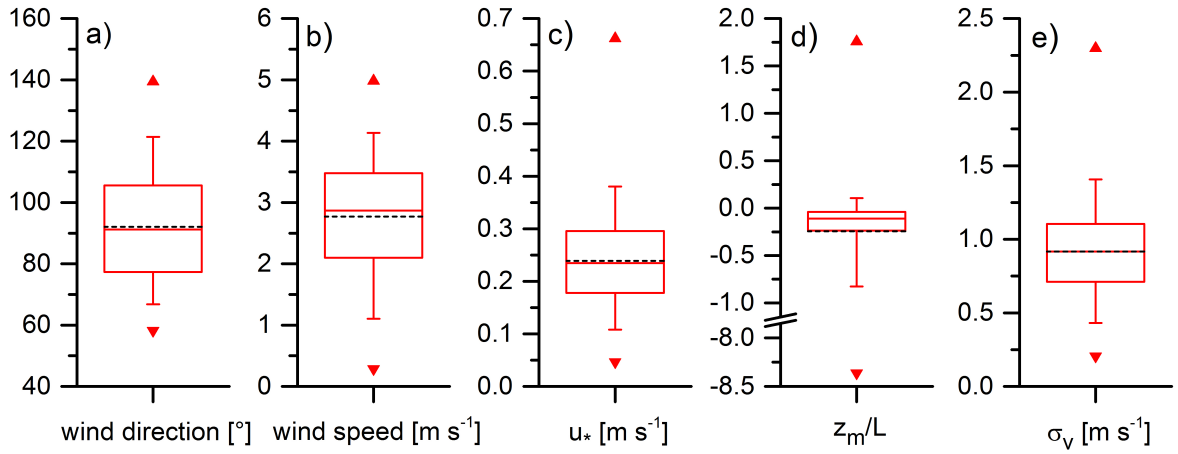

Figure 23: Boxplots of a) wind direction, b) wind speed, c) friction velocity u_*, d) the stability parameter z_m/L, and e) the standard deviation of the lateral wind component σ_v during periods of tracer release (July 02 – Nov 07, 2013 and June 12 – July 06, 2014). Only data of periods with high quality fluxes are shown. The box reflects the range between 25th and 75th percentiles while the whiskers indicate the 5th and 95th percentiles. Also shown are the median (solid line), mean (dashed line) as well as minimum and maximum of the data (triangles). Figure from Heidbach et al. (2017).

4.3.3 Experiments with upwind source[14]

The data shown in this section are from measurements at the permanent tower during experiments A (July 02 – 30, 2013) and D (Oct 11 – Nov 05, 2013), and from those of both towers in configuration B_{al} (Jun 12 – August 03, 2014). During the experiments, the tracer source was located at fixed distances of 20 and 35 m from the tower, i.e., a distance of 6 – 11 times the aerodynamic measurement height, which was expected to be close to the estimated footprint maximum and thus the most influencing part of the

[14]Excerpts of the following paragraph are also contained, almost verbatim, in Heidbach et al. (2017).

footprint.
The overall performance of the four footprint models is shown on the left panel in Fig. 24, expressed as the ratio of estimated to measured flux contributions ($f_{estimated}/f_{measured}$). The frequency distributions reflect a tendency of KM, FSAM, and HS to underestimate the measurements for the range of meteorological boundary conditions prevalent during our experiments (Fig. 23). KM and FSAM underestimate the measurements in 71% and 69% of the cases, respectively, while HS is more balanced and underestimate only 62% of the cases. The frequency distribution of FFP is exactly balanced, with 50% under- and overestimation. Furthermore, the mode of the distribution, corresponding to the most likely value, for HS and FFP is 0.8, while for KM and FSAM it is 0.4. An underestimation of the footprint region around its maximum goes along with an overestimation of regions further upwind, since the integral of the footprint over the whole domain must amount to unity. This "flattening" of the footprint results in an overestimation of the footprint extent.
In their natural tracer study, Goeckede et al. (2005) found a high correlation between observations and fluxes estimated by FSAM. In addition, Hsieh et al. (2000) compared their own model with water vapor flux measurements downwind of a transition from a desert to a potato field, and found reasonably good agreement. However, model evaluations with natural tracer experiments give only qualitative information that depends not only on the difference of emission rates from each field, but also on the homogeneity of source strength within each field. By knowing the exact tracer release rate, we are able to evaluate flux footprint models quantitatively, and therefore a comparison of our study with natural tracer experiments is not straightforward.
In addition, we examine whether the model performances depend on stability. Our data show that the HS model clearly underestimates observations for near neutral to stable conditions (Fig.24g). This finding, and the fact that our experiments mainly were conducted during unstable conditions (89%), shed a different light on the overall good performance of HS. However, we could not identify a clear dependence of the performance of KM on z_m/L (Fig.24e). FSAM (Fig.24f) appears to exhibit a linear dependence of its performance on stability, with a tendency to overestimate in unstable and underestimate in stable conditions. However, as with the other models, because of the increasing scarcity of data away from slightly unstable conditions, no clear picture of stability dependence emerges. Although the four models behave similarly in near neutral to unstable conditions KM, FSAM, and FFP perform better than HS in near neutral to stable conditions. Our results partly agree with the outcome of the study of Marcolla and Cescatti (2005), who utilized the variability of CO_2 sink strength as natural tracer. They generated a spatially and temporally heterogeneous CO_2 sink by cutting grass within an area of 30 m distance from their 2.5 m high measurement system. In their study, HS performs well

for z_m/L in the range of $[0.15, 0.08]$, but underestimates the measurements in more neutral conditions, while KM underestimates observations in neutral and slightly unstable conditions, and overestimates in strongly unstable conditions.
Since the experiments were conducted during daytime, with mainly unstable and highly turbulent conditions, our results are not transferrable to nighttime conditions with a stable and less turbulent atmosphere. In case of typical nighttime conditions, the footprint becomes very large and only a small percentage of tracer gas would reach the measurement system. With respect to our experimental setup, this would require a very large amount of released tracer gas. This difficulty limits the applicability of artificial tracer experiments, but it is not necessarily a limiting factor in natural tracer experiments.

To analyze model performances in along-wind direction, and thus the location of the footprint maximum, we screened data according to wind direction and only considered periods with a mean wind direction along the tower-diffuser-axis $\pm 5°$. The qualifying 190 data points were directly compared with the estimated footprint centerlines. By considering wind directions that are not exactly parallel to the tower-diffuser-axis, the diffuser may not necessarily lie exactly on the estimated footprint centerline. As a result, we introduce an uncertainty that, however, does not exceed 7% of the footprint maximum for our dataset.
The left panel of Fig. 26 shows measured flux contributions (dots) in relation to estimated centerlines. Both measured and estimated values are normalized as in Fig. 21a-d. KM, FSAM, and HS considerably underestimate most of the measured flux contributions in regions closer than x_{max} (normalized distance < 1), while at x_{max} the underestimation is less ($f_{estimated}/f_{measured}$ closer to 1) (Fig. 26e-g). Furthermore, measured flux contributions closer than x_{max} mostly even exceed the maximum flux contribution estimated by the models (Fig. 26a-c). Therefore, we can state that KM, FSAM, and HS tend to underestimate the value of the footprint maximum, as well as overestimate its distance. Our results coincide with the outcome of the natural tracer study of van de Boer et al. (2013). They came to the same conclusion that KM and HS overestimate the distance of the footprint maximum.
This bias is likely due to the fact that KM, HS, as well as FSAM neglect along-wind turbulent diffusion. Rannik et al. (2000) and Kljun et al. (2003) investigated the distance of the peak contribution of the footprint by comparing analytical models with Lagrangian simulations. Both demonstrated that considering along-wind turbulent diffusion in the Lagrangian models moves x_{max} closer to the tower. Moreover, disregarding streamwise turbulence results in an underestimation of flux contributions close to the measurement system (Rannik et al., 2000), and to an increase of the footprint extent (Schmid, 2002).

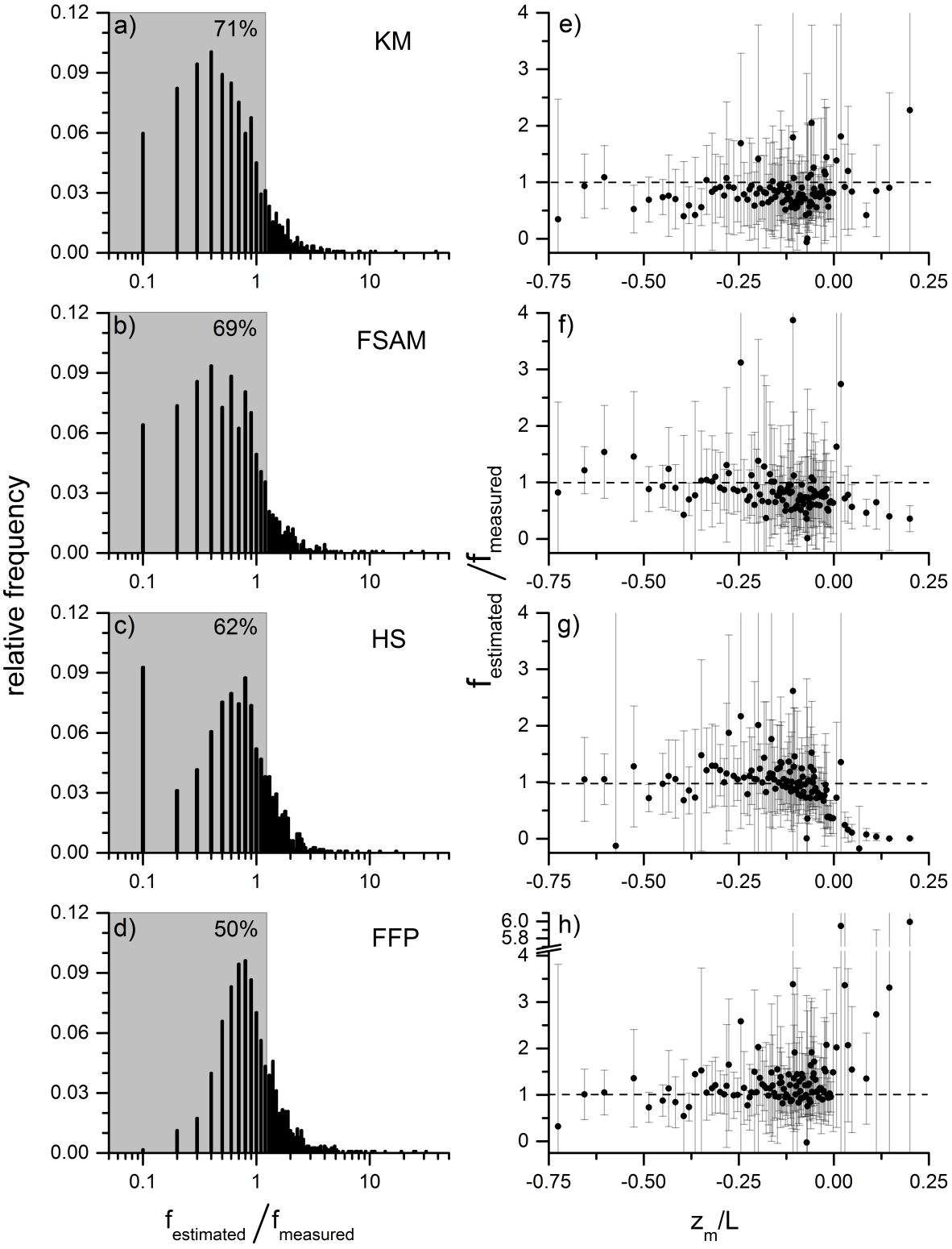

Figure 24: Left (a-d): Frequency distributions of the ratio of estimated to measured flux contributions. The left-most bar combines all ratios ≤ 0.15. Right (e-h): Binned averages with standard deviation of $f_{estimated}/f_{measured}$ as a function of z_m/L for a+e) KM (number of observations: 1154), b+f) FSAM (1153), c+g) HS (1154) and d+h) FFP (1154). Figure from Heidbach et al. (2017).

However, the FFP model mostly predicts the peak location closer to the measurement system than the other models, as illustrated in Fig. 25 for typical daytime conditions in Graswang. Therefore, Fig. 26d shows only a few periods in which the normalized distance is less than 1. Nevertheless, as for the other three models, measured flux contributions occasionally exceed the estimated footprint maximum of the FFP model (Fig. 26d). This leads to the conclusion that FFP underestimates the footprint maximum contribution as well. Due to the small amount of data in regions downwind and around the predicted x_{max}, we are not able to evaluate the footprints peak location estimated by the FFP model.

The large underestimations of HS (Fig. 26c) at normalized distances up to 0.5 are exclusively characterized by near neutral to stable conditions ($z_m/L>0$). In such periods, the distance of the maximum moves further upwind and consequently the normalized distance of the point source decreases below 1. In contrast, KM, FSAM and FFP model performances for convective and stable conditions are not disparate (Fig. 26a+b+d).

It should be noted here that all footprint estimations in this study refer to the 2-dimensional footprint, combining the crosswind integrated footprint (which expresses the along-wind variation), and the crosswind distribution (see Eq. 20). The experimental setup in this study does not lend itself for separate evaluations of these two footprint distribution components.

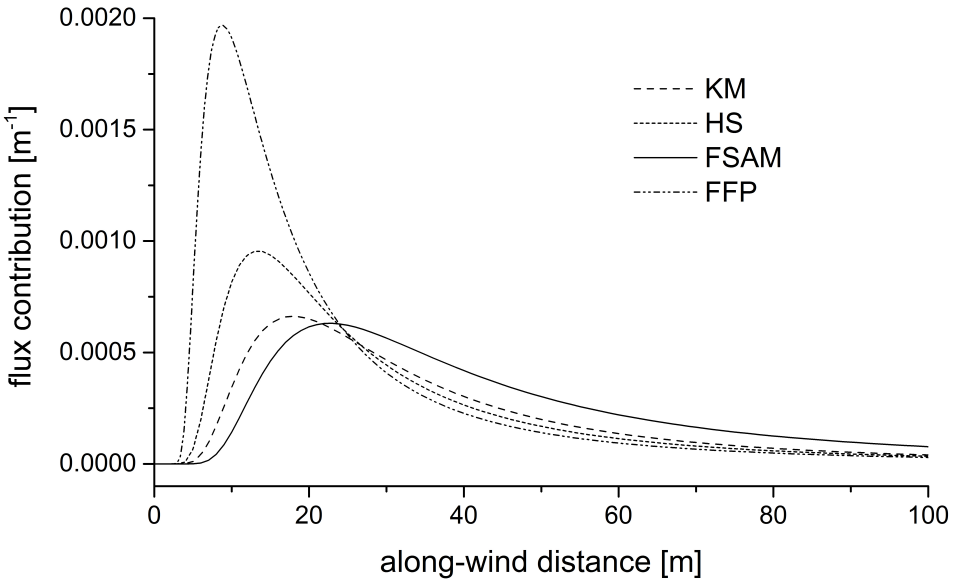

Figure 25: Exemplary footprint centerlines of the four different models KM, HS, FSAM, FFP for typical daytime conditions in Graswang: $z_m/L = -0.11$, $u_* = 0.28$, $u = 2.6$. Figure from Heidbach et al. (2017).

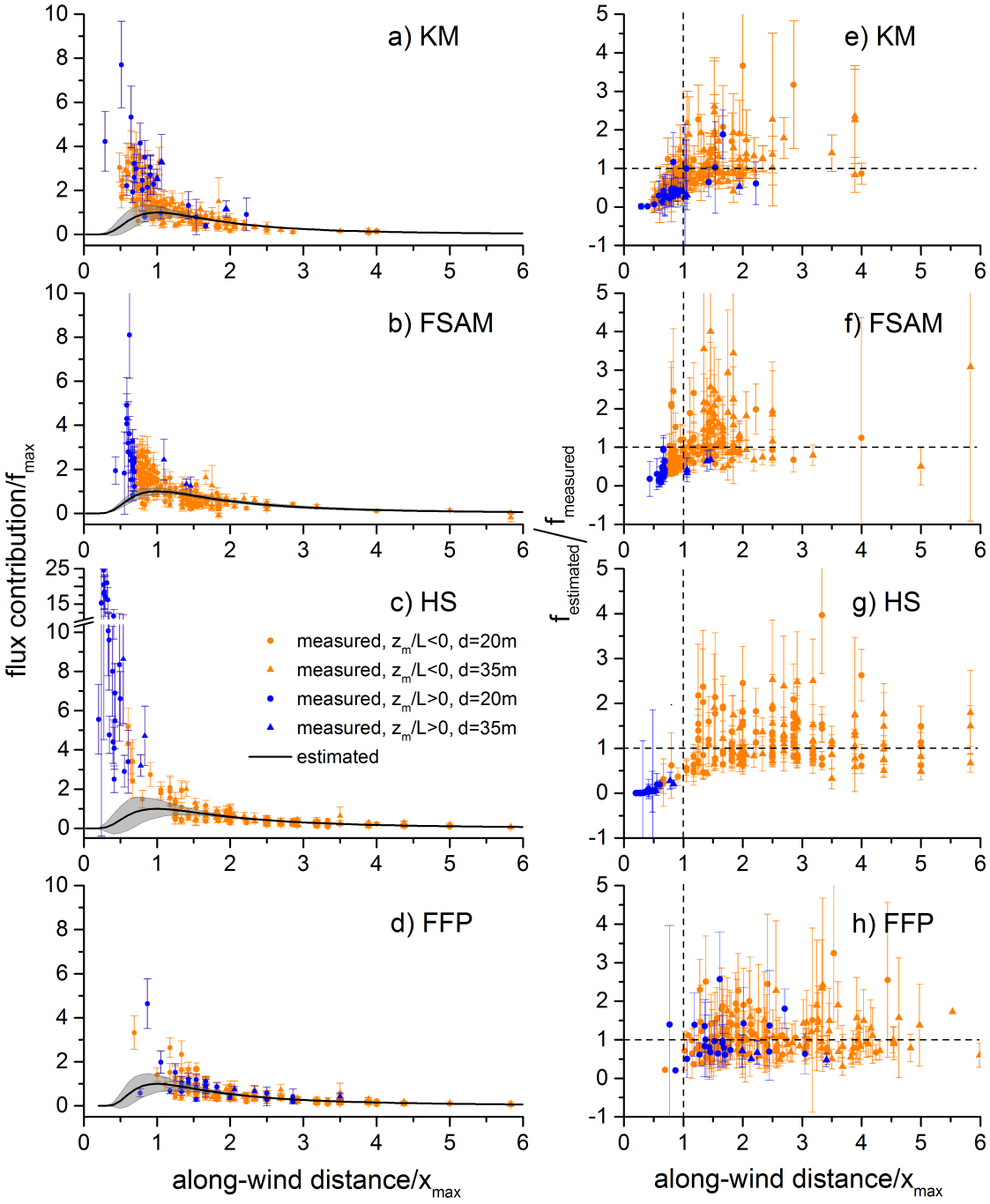

Figure 26: Left: Measured (points, triangles) and model-estimated (lines) normalized flux contributions as a function of normalized along-wind distance. Vertical bars denote the turbulence sampling error estimates following Finkelstein and Sims (2001). Right: Ratio of estimated to measured flux contributions as a function of normalized along-wind distance of the point source. Vertical bars represent the propagated errors of measurement and model after Finkelstein and Sims (2001) for a+e) KM, b+f) FSAM, c+g) HS, and d+h) FFP. Blue color indicates periods with $z_m/L>0$, while points and triangles reflect measurements at d=20m and d=35m, respectively. In all panels, only periods with the mean wind direction within the sector of the source location ±5° are included, which leads to a data reduction from 1154 to 190 data points. Figure from Heidbach et al. (2017).

4.3.4 Experiments with downwind source

To examine potential contributions to a measured flux from downwind sources, we conducted the tracer experiments described in Section 3.7 from July 22 to September 30 in 2013. Although methane was continuously released during experiments, we also measured minor negative fluxes when the tracer didn't reach the sensor, because the natural flux of methane varied slightly around zero with a median of -0.001μmol m^{-2} s^{-1}.
After data screening, 199 10-minute periods of tracer release in the downwind-source configuration remained for our analysis. In most time periods, the measured flux fluctuates around zero and is not markedly different from the natural flux. However, a few events confirm that downwind sources can contribute considerably to a flux measurement (Fig. 27).

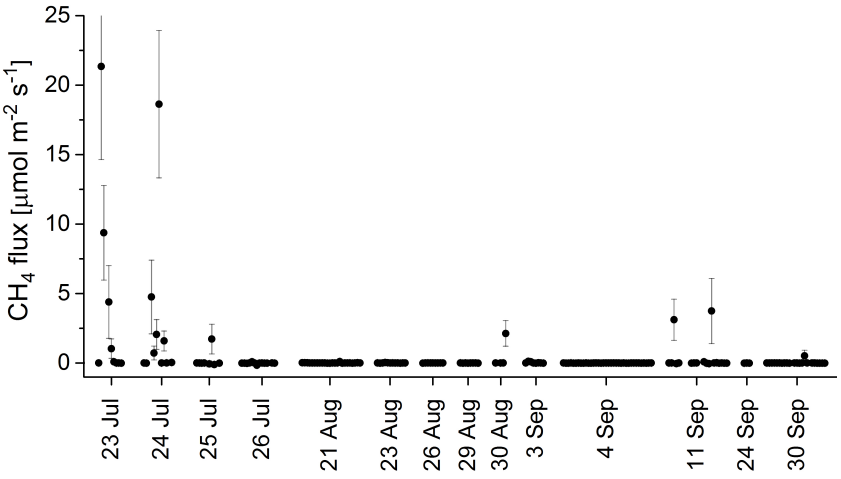

Figure 27: Discontinuous time series of the CH_4 flux measured while CH_4 was released from downwind source. Vertical bars denote the turbulence sampling error according to Finkelstein and Sims (2001).

The magnitude of the CH_4 fluxes that are influenced by the downwind source is of the same order of magnitude (or even larger) as fluxes measured during similar experiments with an upwind tracer source. Nevertheless, with our setup of a fixed and small downwind tracer source, we are not able to determine integrated flux contributions from downwind sources, nor the distance up to which downwind sources are relevant for flux measurements.
Footprint studies based on Lagrangian models (Kljun et al., 2002; Rannik et al., 2000) come to the conclusion that downwind contributions are a function of along-wind turbulent diffusion. Rannik et al. (2000) analyzed the effect of horizontal turbulence on downwind contribution by running their Lagrangian stochastic simulation with and without along-wind diffusion. They state that the relevance of downwind contribution decreases with measurement height, and that along-wind turbulence mainly plays a role for sources

close to the sensor. For a measurement height of 40 m over a 35 m high forest and a high intensity of along-wind turbulence Rannik et al. (2000) found a cumulative contribution of downwind sources of 10%. Similarly, the Lagrangian footprint model of Kljun et al. (2003) predicts a small flux contribution downwind of the measurement for unstable and neutral stratification that can also be attributed to along-wind diffusion.
The role of along-wind turbulence intensity in association with downwind flux contributions is schematically explained in Fig. 28. Downwind sources contribute to the measured flux when the instantaneous flow temporarily turns in opposite direction of the mean wind. The probability that this occurs (hatched area in Fig. 28) increases with rising along-wind turbulence intensities $\sigma_u/\bar{u}$.

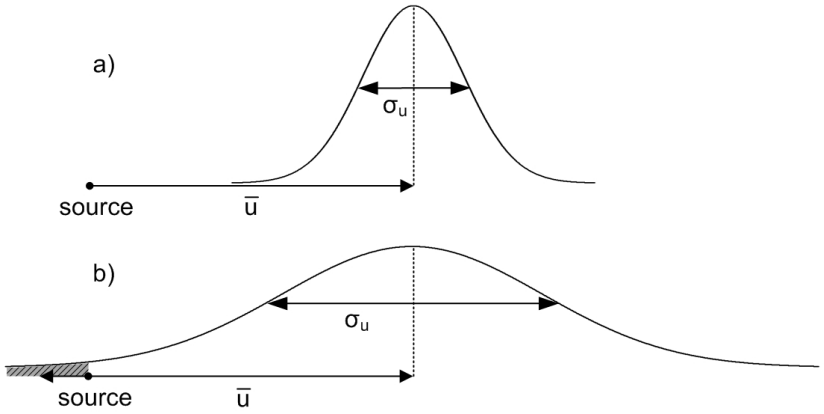

Figure 28: Relevance of the along-wind turbulence intensity $\sigma_u/\bar{u}$ on downwind flux contribution. a) small standard deviation and b) large standard deviation of the along-wind component σ_u. The hatched area reflects the probability that the instantaneous flow direction is opposite to the mean flow.

As expected, we found that the magnitude of measured downwind flux contribution is constrained by the along-wind turbulence intensity $\sigma_u/\bar{u}$ (Fig. 29). Our measurements in Graswang show that in periods with a low $\sigma_u/\bar{u}$ downwind flux contributions are not relevant, whereas there is a much higher probability that the downwind source contributes to the flux measurement for along-wind turbulence intensities of 0.6 or higher. Due to the stochastic nature of turbulence sampling, it may also occur that, even at high turbulence intensities, downwind contributions do not play a role. Hence, the parameter $\sigma_u/\bar{u}$ is a helpful and simple tool to assess the relevance of downwind contribution at a measurement site. However, at high measurement levels downwind sources will likely become negligible as $\sigma_u/\bar{u}$ is expected to decrease with height (Leclerc and Foken, 2014). We should state here that our site is very special due to its location in a deep valley. In Graswang, on fair weather days the mountain-valley-breeze becomes more pronounced, and thus the flow is aligned with the valley axis and becomes more organized. However, at other sites unorganized flow direction fluctuations become more likely when free con-

vection increases during fair weather conditions. Therefore, downwind flux contributions at sites that are not affected by organized wind systems (e.g., land-sea-breeze) might be even more important than in Graswang.

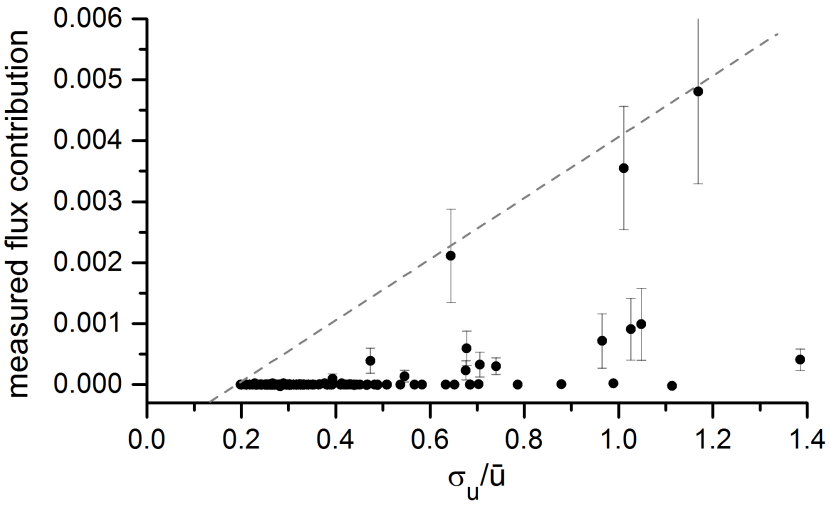

Figure 29: Flux contributions measured while CH_4 was released from downwind source as a function of along-wind turbulence intensity $\sigma_u/\bar{u}$. Vertical bars denote the turbulence sampling error estimated following Finkelstein and Sims (2001). The dashed line (hand drawn) indicates an approximate envelope of maximum downwind flux contributions with increasing along-wind turbulence intensity.

4.3.5 Experiments at a forest edge[15]

The experiments with a second tower close to the forest edge (X_{close}, configuration D) were conducted from October 11 to November 05 in 2013. This two-tower setup was chosen to investigate the extent to which inhomogeneous turbulence due to the forest edge, with its changes in surface roughness and sensible heat flux, affects the model performance. In principle, footprint considerations in the presence of horizontal inhomogeneity in turbulence or flow (e.g., a forest edge) should be evaluated with a full flow model that can resolve the inhomogeneity explicitly (e.g., Leclerc et al., 1997; Sogachev and Lloyd, 2004). However, in practice, standard simple footprint models of the kind evaluated in the present work are used even at sites where the flow-homogeneity condition is clearly violated. Clearly, the variety of potential inhomogeneities is infinite, but an upwind edge is one of the more typical cases encountered at field sites.
To evaluate the hypothesis that turbulence within the footprint of the permanent mast (X_{far}) is less disrupted than in the footprint of X_{close}, and whether an influence of the forest on the turbulence structure is apparent in measured wind statistics, we compared

[15]Excerpts of the following paragraph are also contained, almost verbatim, in Heidbach et al. (2017).

turbulence parameters from the two towers in Fig. 30. The mean horizontal wind velocity, measured at the tower close to the forest edge (X_{close}) was consistently lower than at X_{far} (Fig. 30a). In contrast, the friction velocity was quite similar, with a tendency to be higher closer to the forest edge (Fig. 30b). Therefore, the ratio u/u_*, a parameter which is often used to characterize momentum adjustment across a roughness transition (Sogachev et al., 2008), was in most cases lower at X_{close} (Fig. 30c), likely caused by a plume of surplus turbulence propagating from the forest to the grass surface downwind of the forest edge, as is characteristic in the wake zone (Liu et al., 1996). With regard to the surface layer wind profile relation, this local reduction of wind speed at a relatively high u_* is accounted for by an increased apparent roughness length (see Eq. 32-34). In almost all periods the local apparent roughness length at X_{close} was higher than at X_{far} (Fig. 30f). This finding confirms the expectation that the forest influences the measurements downwind from its edge to some degree. Furthermore, the integral turbulence characteristics σ_u/u_* and σ_w/u_* of the two towers are compared in Fig. 30d,e. The characteristic of the streamwise turbulence component σ_u is slightly increased at X_{far}, while for the vertical wind component no clear pattern is apparent. Panofsky et al. (1982) found that higher frequencies in the turbulence spectra adapt more quickly to a new surface roughness than lower frequencies. As the horizontal turbulence components scale with h, they are dominated by larger eddies (lower frequencies), whereas the vertical components scale with measurement height (leading to higher frequencies). Therefore, our results are consistent with Panofsky et al. (1982). Our measurements also agree with the findings of Gash (1986) who investigated changes in wind statistics downwind of a forest-heath transition. In summary, the selected wind statistics show differences between the two towers, and thus indicate different effects of the forest edge on the two towers. Clearly, turbulence is not likely completely homogeneous within the footprint of X_{far}, but it is at least less disturbed by the forest edge than in the source area of X_{close}.

As Fig. 30f already indicates, an unambiguous determination of the apparent roughness length is sensitive to upstream surface characteristics, and remains uncertain (van de Boer et al., 2013). We calculated the footprints for both towers with, first, a constant roughness length of 0.01 m, corresponding to that of the local short grass surface, and second, with the local apparent z_0 determined by Equations (32-34) at each tower. The latter determination of z_0 was only made for HS and FSAM; no distinction of z_0 was made for the KM and the FFP models, as these models determine z_0 internally, based on similarity relations similar to Equations (32-34) (FFP requires either a roughness length or mean wind speed at measurement height as input).

Table 2 summarizes the statistics of the model performances at the two towers. The RMSE and the ratio of the systematic and the unsystematic RMSE, $RMSE_s/RMSE_u$

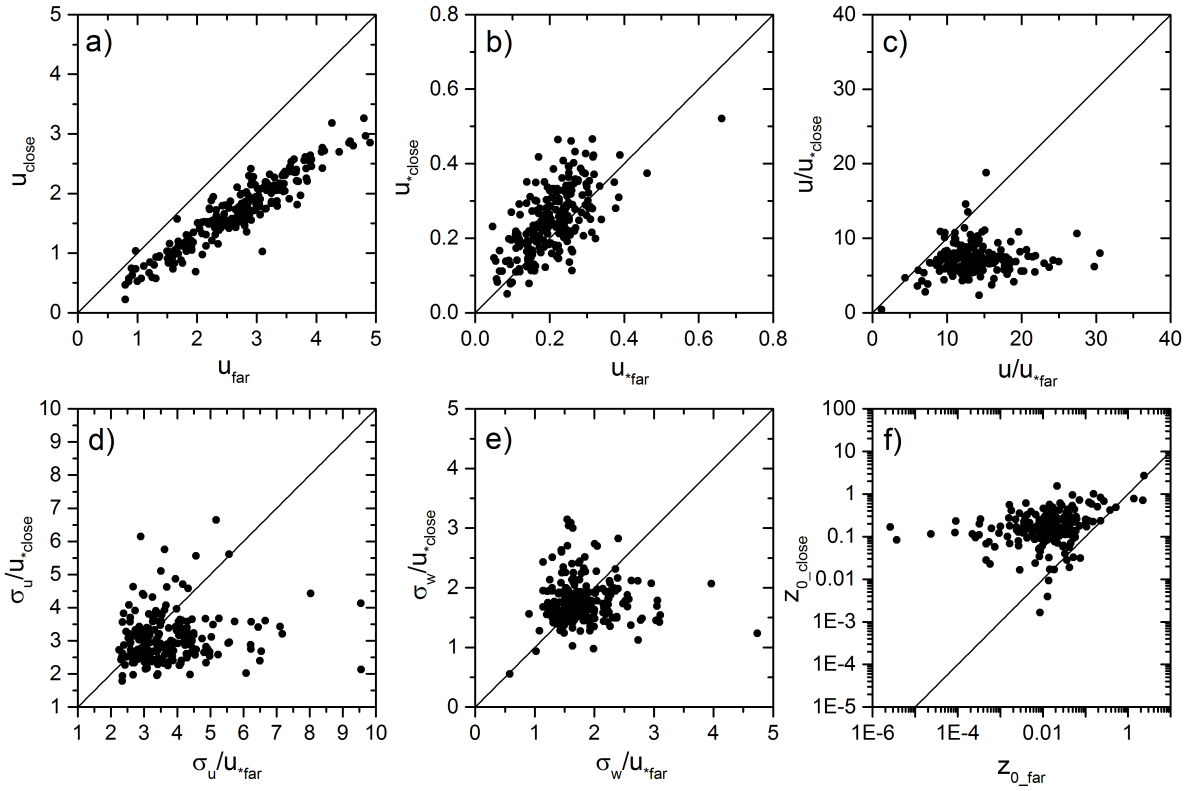

Figure 30: Turbulence parameters of the permanent tower (X_{far}) and the tower close to the forest edge (X_{close}): a) mean horizontal wind velocity u, b) friction velocity u_*, c) ratio u/u_*, d) integral turbulence characteristic σ_u/u_*, e) integral turbulence characteristic σ_w/u_* and f) apparent roughness length z_0 determined by the aerodynamic method (Eq. 32-34). Figure from Heidbach et al. (2017).

(Willmott et al., 1985) indicate an even better performance of KM at X_{close} while the index of agreement (d) (Willmott, 1981) and the coefficient of determination (R^2) do not show a clear tendency. This can be explained by the fact that the RMSE as well as the ratio $RMSE_s/RMSE_u$ are difference measures, determined out of mean absolute deviations, while d and R^2 represent relative statistical measures. In principle, the systematic RMSE ($RMSE_s$) of a perfect model should approach zero and thus the ratio $RMSE_s/RMSE_u$, should vanish. However, the index of agreement is bounded from 0 (bad performance) to 1 (perfect performance). As the statistical measures $RMSE_s/RMSE_u$, d, and R^2 show, the quality of the FFP model decreases for the measurements close to the forest edge. The performance of FSAM, using $z_0 = 0.01$ m at X_{close}, was slightly worse than at X_{far}, indicated by an increased ratio $RMSE_s/RMSE_u$, a lower index of agreement and a smaller R^2. Applying the local apparent roughness length did not improve model quality consistently in all cases. HS performed considerably worse at X_{close} than at X_{far}, irrespective of whether a constant or the local apparent roughness length was used.

However, at X_{close}, use of the apparent roughness length considerably increased model performance of HS, but not of FSAM. At X_{far}, the different determination of roughness length only slightly affected the quality of either model. Our measurements show that all models are sensitive to the sharp upwind change in roughness length close to the measurement system. The sensitivity is least pronounced for the KM model, while the strongest deterioration of model performance at X_{close} compared to X_{far} was found for HS.

Table 2: Statistics of the footprint model performance for the permanent tower X_{far} and the tower close to the forest edge X_{close}. Footprints of FSAM and HS were determined with $z_0 = 0.01$ and with the local apparent z_0 determined by Equations (32-34). No distinction of z_0 is made for the KM and the FFP model since it is not required as input parameter. Parameters presented are: number of observations (N), root mean square error (RMSE), the ratio of systematic to unsystematic RMSE, index of agreement (d) and the coefficient of determination (R^2). Table from Heidbach et al. (2017).

Model		N	RMSE $[m^{-2}]$	$RMSE_s$/ $RMSE_u$	d	R^2
KM	X_{far}	216	4.7E-4	2.2	0.56	0.20
	X_{close}	216	2.8E-4	1.8	0.57	0.17
FFP	X_{far}	216	3.3E-4	1.6	0.57	0.16
	X_{close}	216	3.0E-4	2.6	0.43	0.06
FSAM	$X_{far}\_z_0\_0.01$	216	3.8E-4	1.3	0.66	0.30
	$X_{far}\_z_0\_app$	216	3.6E-4	1.1	0.68	0.29
	$X_{close}\_z_0\_0.01$	216	4.0E-4	1.7	0.55	0.14
	$X_{close}\_z_0\_app$	216	2.9E-4	1.7	0.51	0.10
HS	$X_{far}\_z_0\_0.01$	216	3.9E-4	0.7	0.68	0.26
	$X_{far}\_z_0\_app$	216	3.5E-4	0.7	0.71	0.29
	$X_{close}\_z_0\_0.01$	216	4.4E-4	2.0	0.48	0.05
	$X_{close}\_z_0\_app$	216	2.9E-4	2.5	0.53	0.19

4.3.6 Summary and conclusions of the experimental evaluation[16]

This section presents an experimental evaluation of the flux footprint models of Kormann and Meixner (2001) (KM), Schmid (1994) (FSAM), Hsieh et al. (2000) (HS), and Kljun et al. (2015) (FFP) at an eddy covariance site in southern Germany. The experiments were conducted above grassland by releasing an artificial tracer gas (methane) out of a single surface source of relatively small size ($\sim 1m^2$). Due to the negligible natural flux at the site, measured methane fluxes could be attributed solely to the artificial tracer source. With different setups, we were able to evaluate upwind as well as downwind flux contributions, and to analyze the effect on model performance of a sharp change in

[16]Excerpts of the following paragraph are also contained, almost verbatim, in Heidbach et al. (2017).

roughness length upwind of the measurement tower.
Our experiments with an upwind source show that, for the whole ensemble of observations, FFP fits best to measured flux contributions, and FSAM, KM, and HS match observations roughly. HS considerably and consistently underestimates observations for near neutral to stable conditions while KM, FSAM, and FFP perform better and do not show such a clear behavior. As our experiments were conducted during daytime in summer and autumn, and thus mainly during unstable conditions (89%), the generally good performance of HS is biased. Especially during winter- and nighttime, the HS model would presumably perform much worse.
Analyzing only a narrow wind sector of $\pm 5°$ made it possible to examine the model performance in along-wind direction, and to evaluate the location of the footprint maximum. We found that KM, FSAM, and HS tend to underestimate flux contributions in the region downwind of the peak distance of the footprint (x_{max}). Measured flux contributions downwind of x_{max} were mostly much higher than even the estimated maximum flux contribution (f_{max}), which indicates that the three evaluated models not only underestimate f_{max} but also overestimate x_{max}. Such a behavior leads to a "flattening" of the real footprint and to an overestimation of the footprint extent. This problem can result in too strict data rejection, when integrated flux contributions of a specific area of interest are used for data screening. However, our measurements exceed FFP estimates of the peak contribution in fewer cases than estimates of the other three models, which leads to the conclusion that FFP predicts the maximum contribution of the real footprint better. As there are only few data available in regions downwind and around the predicted x_{max} we were not able to evaluate the footprints peak location of the FFP model.
We could show that there are measurable and non-negligible contributions to the flux from downwind sources. Although downwind contributions occurred only intermittently and not continuously, they should be taken into account, especially at sites with a heterogeneous source distribution in the vicinity of the flux measurement. Whether contributions from downwind sources are relevant at a specific site can be estimated by the along-wind turbulence intensity $\sigma_u/\overline{u}$. We found that downwind source contributions can be expected in periods with an along-wind turbulence intensity of 0.6 and higher. In summary, including along-wind diffusion in analytical flux footprint models would likely increase model quality, as not only downwind contributions would be considered, but also the peak distance would move closer to the measurement (Kljun et al., 2003; Rannik et al., 2000).
The third part of experiments comprised the comparison of model performances at two eddy covariance towers, one of which was located closer to a forest edge (X_{close}) than the other (X_{far}). With this setup we intentionally violated the model assumption of homoge-

neous turbulence and were able to examine whether a sharp change in roughness length close to the flux measurement affects model quality. To satisfy the effective roughness length at both towers, footprints of HS and FSAM were determined with two different roughness lengths: the estimated constant roughness length of X_{far}, and the local apparent roughness length determined by the aerodynamic method. It turned out that all evaluated models show sensitivity to an abrupt change in surface roughness and sensible heat flux in the nearby upwind area of the measurement tower. Nevertheless, KM appeared to be the model with the largest RMSE (and thus the largest error) and least sensitivity while FSAM, HS, and FFP showed a non-negligible decline in model quality. Therefore, as already required by the eddy covariance method, special attention should be paid to the site selection of an eddy covariance station to avoid distinct roughness changes or obstacles in the vicinity of the tower. As highly homogeneous sites are rare in real world conditions, all footprint estimates and related quality assessment should be handled with care.

4.4 Integration of streamwise turbulence effects in the analytical flux footprint model FSAM

As the crosswind integrated flux footprint ($\overline{f^y}$) corresponds to the crosswind integrated flux downwind of a unit surface point source, it is directly related to the crosswind integrated concentration distribution $\overline{C^y}$ and the mean wind speed profile $\bar{u}(z)$, through the two-dimensional advection-diffusion equation (Horst and Weil, 1992; Schmid, 1994):

$$\bar{u}(z)\frac{\partial}{\partial x}\overline{C^y} = -\frac{\partial}{\partial z}\overline{f^y} \tag{40}$$

where the usual micrometeorological coordinate system, aligned with the mean flow, is used. Integrating Equation (40) over z up to the measurement height z_m results in the crosswind integrated flux footprint

$$\overline{f^y}(x, z_m) = -\int_{z_0}^{z_m} \bar{u}(z)\frac{\partial}{\partial x}\overline{C^y}(x, z)dz. \tag{41}$$

Following Horst and Weil (1992) the crosswind integrated concentration distribution ($\overline{C^y}$) downwind of a unit surface point source can be written in the form

$$\overline{C^y}(x, z) = \frac{D_z(x, z)}{U(x)} \tag{42}$$

with the vertical concentration distribution function D_z and the plume advection velocity U, and x denotes the streamwise separation distance between sensor and source. Multiplying Equation (41) with the crosswind concentration distribution D_y gives the

two-dimensional flux footprint

$$f(x, y, z_m) = \overline{f^y}(x, z_m) D_y(x, y). \tag{43}$$

Equation (43) assumes that dispersion components in crosswind and vertical directions are statistically independent of each other, which is reasonable as surface layer $\overline{v'w'} \approx 0$ in the micrometeorological coordinate system.
As all analytical footprint models, FSAM (Schmid, 1994) assumes horizontally homogeneous turbulence and neglects streamwise turbulent diffusion. Therefore, like all such models it does also not account for flux contributions from sources located downwind of the measurement system. In order to define a more realistic description of turbulent fluctuations and to improve model quality, we extend the existing model FSAM (Schmid, 1994) by implementing an along-wind diffusion module. For this purpose, we introduce an along-wind dispersion component D_x and realize its implementation by a non-stationary convolution of the 2-dimensional footprint with the spatially varying kernel D_x. For simplicity, we define the upwind distance of the original non-convoluted footprint and the along-wind distance of the convoluted footprint as x and $\tilde{x}$, respectively.

$$f_x(\tilde{x}, y, z_m) = f(x, y, z_m) * D_x(x, \tilde{x} - x) = \int_0^\infty f(x, y, z_m) D_x(x, \tilde{x} - x) dx \tag{44}$$

where $f(x, y, z_m)$ is the initial 2-dimensional footprint and $f_x(\tilde{x}, y, z_m)$ the convoluted footprint. As D_x changes with along-wind distance x, but is independent of crosswind distance y, the convolution is performed in streamwise direction. Consequently, the footprint weighting factor at a specific along-wind distance now comprises the probability of a particle emitted at this point to reach the sensor as well as the probabilities of particles released from further or shorter distances, which may be transported faster or slower due to along-wind fluctuations.
In summary, the 2-dimensional footprint of the extended model, which we refer to as FSAMx, is defined as

$$f_x(\tilde{x}, y, z_m) = (\overline{f^y}(x, z_m) D_y(x, y)) * D_x(x, x - \tilde{x}) \tag{45}$$

Equation (45) is subject to the assumption that D_x and D_y as well as D_x and D_z are independent of each other. As mentioned, the former assumption is based on the finding that $\overline{v'w'} \approx 0$, while the latter simplification may be critical during near-neutral or stable conditions when u' and w' are correlated. However, in such cases, along-wind turbulent fluctuations, and thus the effect of the convolution with D_x, are expected to be small. For this reason and to keep the model practicable, we consider this assumption

as applicable.
Mathematically, the order of applying the convolution and multiplying with the crosswind distribution is not relevant. However, as is it not straightforward to define a crosswind distribution that is continuous from positive (upwind of the measurement system) to negative (downwind) along-wind distances resulting in a smooth footprint function, we apply the spread in crosswind direction before the convolution.
As the convolution is independent of other components of the model, it can be considered as a standalone module. In order to save computational demand, a "simplified convolution" can be applied to a two-dimensional discrete footprint array, where the integral in Equation (44) is replaced by a summation. Therefore, it can also be applied to the gridded outcome of any other footprint model.

4.4.1 Definition of crosswind distribution

In FSAM, as in most analytical footprint models, the Gaussian crosswind distribution is defined as a function of the standard deviation of the lateral wind component σ_v and the plume travel time x/U with x being the upwind distance and U the horizontal plume velocity:

$$\sigma_y(x) = \frac{\sigma_v x}{U} \tag{46}$$

However, in FSAMx we follow Pasquill (1971), and express the crosswind spread of a plume σ_y as

$$\sigma_y(x) = \sigma_v \tau F_y \left(\frac{\tau}{T_y}\right) \tag{47}$$

with the plume travel time τ, F_y is a function of the dimensionless travel time τ/T_y , and T_y is the Lagrangian time scale for crosswind turbulence. F_y implies the theory of Taylor (1921) that in the near-field (small τ), the spread of a plume is proportional to τ while in the far-field it is proportional to $\sqrt{\tau}$. In accordance with Deardorff and Willis (1975), F_y can be expressed as

$$F_y = \left[1 + \left(\frac{\tau}{2T_y}\right)^{\frac{1}{2}}\right]^{-1} \tag{48}$$

In Equation (46), the plume travel time includes only the horizontal component of the plume's path and neglects the vertical component which is inherent in the fact that particles are assumed to be released at the surface and the sensor measures at a specific height. To make this notion explicit, we define the travel time as being composed of a horizontal advective and a vertical diffusion component. To estimate the combined travel

distance, $\hat{X}$, and the combined travel velocity, $\hat{V}$, we applied the Pythagorean theorem for distance and velocity separately as it may not be used for travel times, such that

$$\tau = \frac{\hat{X}}{\hat{V}} = \frac{\sqrt{x^2 + z_m^2}}{\sqrt{U^2 + v_z^2}} \tag{49}$$

where z_m is the measurement height, U the horizontal plume velocity and v_z the vertical velocity of the plume required to reach z_m, expressed as the ratio of the measurement height and the vertical diffusive component of the plume travel time τ_D:

$$v_z = \frac{z_m}{\tau_D} \tag{50}$$

τ_D can be related to an eddy diffusivity K by

$$\tau_D \approx \frac{K}{\sigma_w^2} = \frac{k(z_m - z_0)u_*}{\phi_h(\frac{(z_m - z_0)}{L})\sigma_w^2} \tag{51}$$

with $K = k(z_m - z_0)u_*/\phi_h((z_m - z_0)/L)$, u_* is the friction velocity, and σ_w the standard deviation of the vertical wind component, which is assumed to be constant in the layer below z_m.

4.4.2 Definition of along-wind distribution

By analyzing turbulence data measured over the Xilinhaote prairie in Inner Mongolia of China Liu et al. (2011) show that the probability density functions of horizontal velocity fluctuations are nearly Gaussian over a wide range of stability conditions. Therefore, according to the crosswind dispersion, we introduce a Gaussian along-wind dispersion D_x

$$D_x(x, \tilde{x} - x) = \frac{1}{\sqrt{2\pi}\sigma_x} exp\left(-\frac{(\tilde{x} - x)^2}{2\sigma_x^2}\right) \tag{52}$$

with the along-wind distance x and its deviation $(x - \tilde{x})$. The standard deviation σ_x is defined similar to Equation (47), but in terms of along-wind turbulence intensity $\sigma_u/\bar{u}$

$$\sigma_x(x) = \frac{\sigma_u}{\bar{u}} \hat{V} \tau F_x \tag{53}$$

with the standard deviation of the along-wind component σ_u, and $F_x = F_y$, assuming that the Lagrangian time scale for lateral and along-wind dispersion is equal. For dimensional consistency, the additional velocity $\hat{V}$ was introduced, as already used in

Equation (49). With that modification, Equation (53) simplifies to

$$\sigma_x(x) = \frac{\sigma_u}{\bar{u}} \sqrt{x^2 + z_m^2} F_x. \tag{54}$$

The along-wind dispersion describes the probability of a particle released at a specific upwind distance x being transported faster or slower than expected by mean advection only. As the particle travel time increases with upwind distance, a particle released at further upwind distances experiences more along-wind diffusion processes than particles emitted at shorter distances. Therefore, the standard deviation of the Gaussian distribution increases for longer pathways (Fig. 31).

4.4.3 The effect of including along-wind turbulent fluctuations in FSAM

Incorporating along-wind turbulent fluctuations in footprint models has the effect that the source weight function is spread further in along-wind direction, and, as a result, extends into downwind regions. As indicated by Equation (53), this effect is strongest in cases when $\sigma_u/\overline{u} \gg 0$. Fig. 31 shows a crosswind integrated footprint of FSAM (without along-wind dispersion) compared to the corresponding footprint of FSAMx considering along-wind dispersion. Main differences between these two occur downwind of the measurement tower, at short upwind distances, and around the footprint maximum. Three main effects result from the D_x-convolution of footprint estimates:

- Estimates of contributions from downwind sources to the measured flux are possible
- Flux contributions at short upwind distances gain in importance
- The maximum source weight moves closer to the measurement system

These effect coincide with the results of our experiments which show that there are indeed measurable and non-negligible downwind flux contributions, and that KM, FSAM, and HS tent to underestimate flux contributions at short upwind distances ($<x_{max}$), and to overestimate the upwind distance of the footprint maximum x_{max}. The same effects apply to Lagrangian model results: Considering along-wind diffusion moves x_{max} closer to the measurement tower and increases the flux contribution from sources close to the measurement system (Rannik et al., 2000; Kljun et al., 2003). From x_{max} on, the influence of along-wind diffusion decreases as the source weight function flattens, and therefore the effect of convolution decreases.
Applying the D_x-convolution to the 2-dimensional, crosswind distributed footprint results in a footprint that continuously extends to negative along-wind distances (Fig. 32). This results from the fact that the crosswind distribution is defined only for positive distances (upwind regions) while negative distances (downwind regions) only emerge from the convolution.

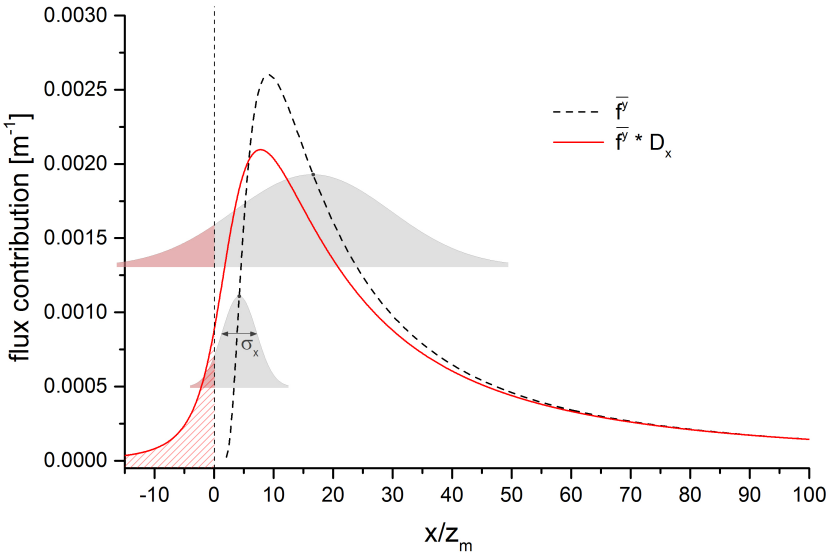

Figure 31: Example of an original crosswind integrated footprint of FSAM (black dashed line) and the crosswind integrated footprint after convolution with D_x (red line) as a function of non-dimensional upwind distance x/z_m with following input values: z_m/L=-0.02, u_*=0.3, u=3.5, z_0=0.1. Grey shaded areas show the Gaussian distributions D_x at the upwind distances 4.2 and 16.7. Axes of Gaussian distributions not shown.

4.4.4 Model comparison FSAMx vs. LPDM-B

In this section, the redefined model FSAMx is compared to the backward Lagrangian model LPDM-B (for more details see the Excursus below, and Kljun et al., 2002). Although Lagrangian models can be applied within a wide range of turbulence regimes and measurement heights, this inter-comparison focuses on the surface-layer, where Monin-Obukhov similarity theory and thus FSAM and FSAMx estimates are valid. To evaluate solely the effect of along-wind turbulence, we calculate crosswind integrated flux footprints of both models. This is possible as in FSAMx, the order of applying the convolution and multiplying with the crosswind distribution is mathematically not relevant (Section 4.4). Footprints of FSAM and FSAMx are both normalized as described in Section 3.2.1 to force the computed integral footprint to unity.
Crosswind integrated flux footprint estimates of LPDM-B, FSAM, and FSAMx were determined for two different stabilities ($z_m/L=-0.009$ and $z_m/L=-0.25$) and two roughness lengths (z_0=0.01 m and z_0=0.1 m). As horizontal wind velocity and along-wind turbulent fluctuations were calculated out of the logarithmic wind profile and Equation (55) following Rotach et al. (1996), respectively, different values for z_m and z_0 result in different values for $\overline{u}$ and $\sigma_u/\overline{u}$.

$$\sigma_u^2 = u_*^2 0.35 \left(-\frac{h}{kL}\right)^{\frac{2}{3}} + \left(5 - 4\frac{z_m}{h}\right) \tag{55}$$

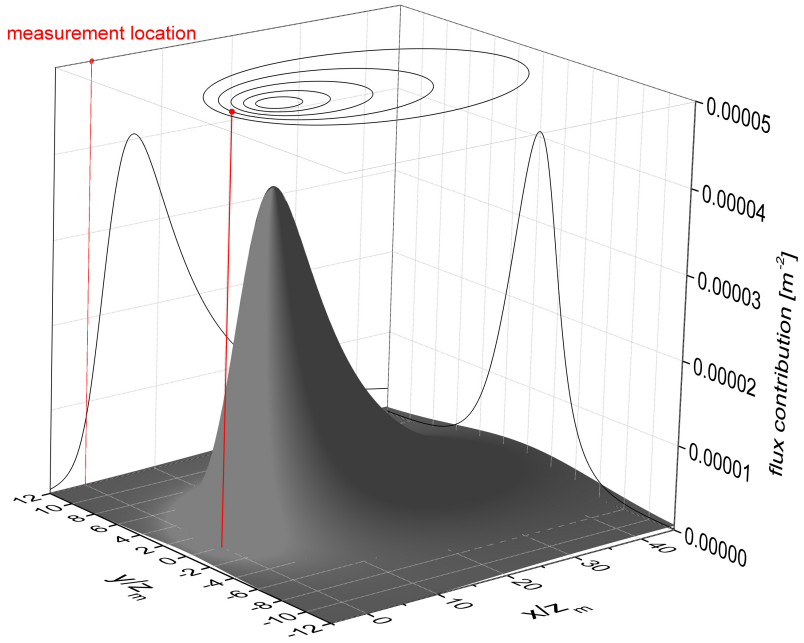

Figure 32: Example of a 3-dimensional flux footprint of FSAMx, using the same conditions as in Fig. 31. Planes show the centerline of the footprint, the crosswind distribution at x_{max} and source weight isopleths, while the red point/line represents the measurement location.

where k is the Von Kármán constant and h is the boundary layer height. In each run of LPDM-B, 70000 particles were released. All examples in Fig. 33 show that the footprint estimates of LPDM-B have a higher maximum contribution than those of FSAM and FSAMx. Our tracer experiments indicate an underestimation of f_{max} in all four evaluated models. Thus, it is likely that LPDM-B estimates f_{max} more accurately. Moreover, the distance between the maximum contribution and the measurement system, x_{max}, is smaller for LPDM-B than for the other two models. However, due to the consideration of along-wind diffusion, the footprint maximum contribution of FSAMx is in all cases closer to the measurement tower (and to x_{max} of LPDM-B) than that of FSAM. In general, differences in x_{max} of LPDM-B and the other two models are largest when $\sigma_u/\overline{u}$ is small (Fig. 33a) and decreases with increasing along-wind turbulence intensity.
Another new aspect of FSAMx is that flux contributions from downwind sources can be estimated. In the panels of Fig. 33, wind velocity decreases from 4.8 m/s (Fig. 33a) to 1.9 m/s in panel d, and thus $\sigma_u/\overline{u}$ increases accordingly. As a result, the relevance of downwind sources increases for footprint estimates of FSAMx, which is reflected in both, the downwind extent and the downwind integral of the footprint. For an along-wind turbulence intensity of 0.47 (Fig. 33a), the relevance of downwind flux contributions is negligible in FSAMx while it increases for $\sigma_u/\overline{u} = 0.76$ and is largest for $\sigma_u/\overline{u} = 1.22$. This coincides with our tracer experiments, which indicate that, from an along-wind

turbulence intensity of 0.6 and higher, downwind flux contributions gain considerably in importance (Section 4.3.4).
However, this dependence is not apparent in LPDM-B where downwind contributions first appear slightly in Fig. 33d where $\sigma_u/\overline{u} = 1.22$. The relevance of downwind flux

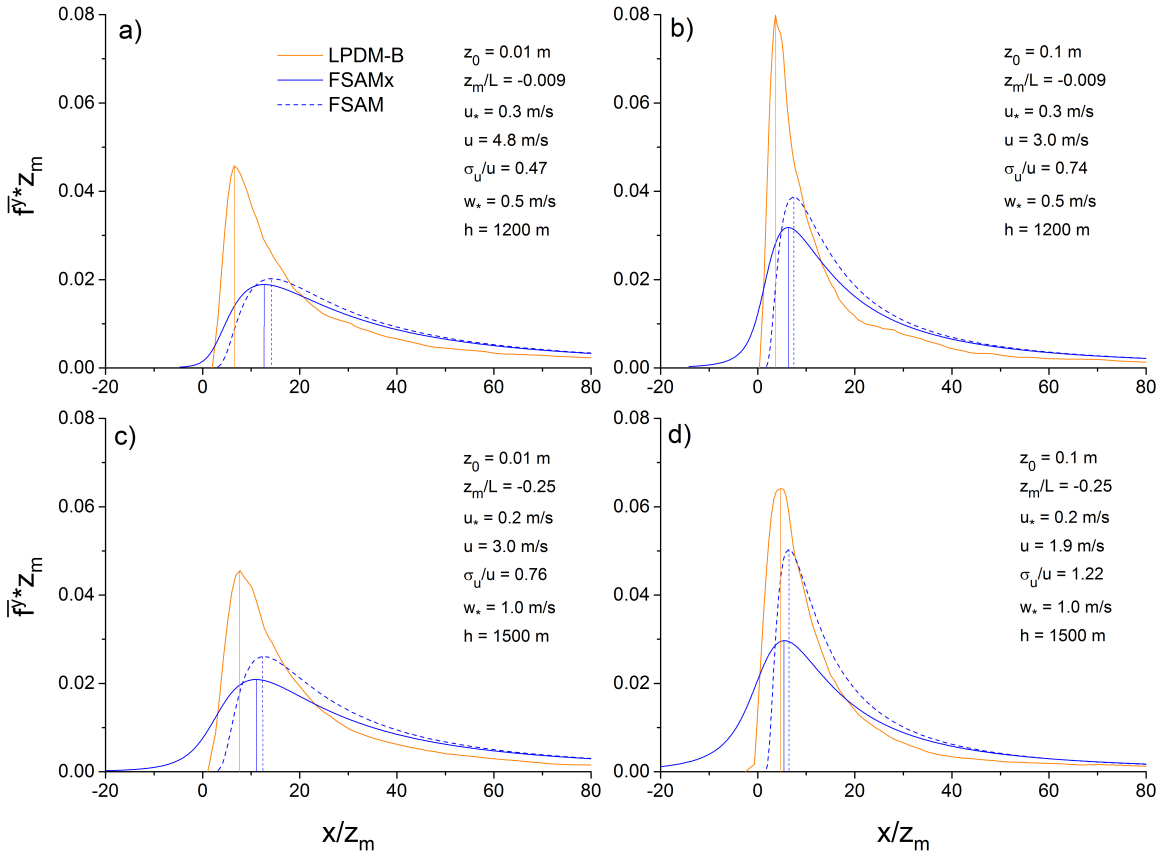

Figure 33: Inter-comparison of crosswind integrated footprint estimates of LPDM-B, FSAM, and FSAMx for different atmospheric conditions. Upwind distance and flux contribution were non-dimensionalized by dividing by and multiplying with measurement height z_m, respectively. The locations of the maximum flux contributions are indicated with vertical lines. In regions where touchdowns are sparse the curves of LPDM-B may have a irregular appearance due to smoothing issues.

contributions in LPDM-B further increases when stratification becomes more unstable. In Fig. 34, atmospheric conditions are quite similar to those in Fig. 33d, except for the stability parameter z_m/L. While for $z_m/L = -0.25$ the footprint estimate of LPDM-B reaches a downwind distance of $-2.2z_m$, it extends to $-5.9z_m$ for $z_m/L = -0.666$. In total, the relevance of downwind contributions is still smaller than in FSAMx, but the footprints of LPDM-B and FSAMx seem to converge in the downwind region for stronger along-wind diffusion and higher instabilities. Under the conditions given in Fig. 34, all three models estimate an almost identical x_{max}. Based on our measurements we can state

that LPDM-B underestimates the relevance of downwind flux contributions in slightly convective conditions with still moderate along-wind turbulence intensity. FSAMx seem to better reflect the dependence on $\sigma_u/\overline{u}$. However, due to the small amount of data and the limited size of the tracer source, it is not possible to evaluate model performance in downwind regions directly with our data.

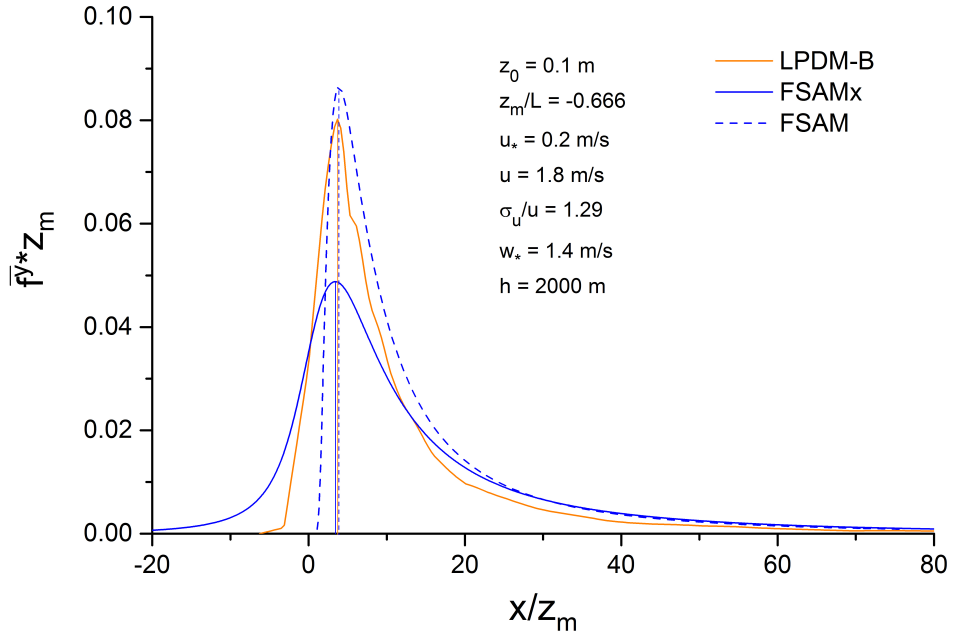

Figure 34: Inter-comparison of crosswind integrated footprint estimates of LPDM-B, FSAM, and FSAMx for strongly unstable conditions.

Excursus: LPDM-B

LPDM-B is a 3-dimensional Lagrangian footprint model that is based on the dispersion model of Rotach et al. (1996). It is applicable within a wide range of boundary-layer stratifications and receptor heights, even above the surface layer. In this model, stochastic backward trajectories of particles are used to determine the footprint. The advantage of this approach is that only trajectories of particles exactly reaching the measurement point need to be determined. This saves computation time in comparison to forward computations.
Several turbulence parameterizations are necessary so that particles follow appropriate trajectories, these are: the profiles of mean wind speed, Reynolds stress, the dissipation rate of turbulence kinetic energy, the particle velocity variances, the vertical velocity skewness, and the relative strengths of updrafts and downdrafts C_{up} and C_{down} (Kljun et al., 2002).
To determine the footprint distribution out of the dispersion model, a large number of particles are "released" at the receptor location with initial velocities randomly picked from specific distributions after a spin-up process and tracked backward in time until they touch the ground at a specific location with a specific vertical velocity (touchdown velocity). By means of touchdown locations and velocities the concentration footprint and the flux footprint can be estimated as detailed in Flesch (1996).

4.4.5 Summary and conclusions

Section 4.4 of this thesis introduces the new flux footprint model FSAMx, which is an extended version of the model FSAM (Schmid, 1994). FSAMx considers along-wind turbulent fluctuations and thus describes turbulence more realistically than FSAM or other simple, analytical models that do not incorporate along-wind diffusion (e.g., Kormann and Meixner, 2001; Hsieh et al., 2000). Consequently, FSAMx increases the relevance of flux contributions at short upwind distances, has its maximum contribution closer to the measurement system than the original model FSAM, and is able to estimate flux contributions from sources downwind of the measurement system. This is not surprising, as the same effects can also be found in Lagrangian simulation results by running the models with and without along-wind turbulence (Rannik et al., 2000; Kljun et al., 2003).
To include along-wind diffusion in FSAM, we first introduce a Gaussian along-wind dispersion component D_x following the definition of D_y, the crosswind dispersion. The standard deviation of D_x is defined as a function of travel time and along-wind turbulence intensity $\sigma_u/\overline{u}$ in order to reflect the dependence that our flux measurements

with a downwind tracer source showed. The implementation of D_x is realized by a non-stationary convolution of the 2-dimensional footprint with the spatially varying kernel D_x.

The main benefit of this approach is that it can be considered as a standalone module, because the convolution is independent of other model components. In this study, we applied a "simplified convolution" to the 2-dimensional discrete footprint array in order to save computation time. Accordingly, our introduced standalone module can also be applied to the outcome of any other footprint model.

Finally, we compared crosswind integrated flux footprint estimates of FSAM, FSAMx, and the backward Lagrangian model LPDM-B. LPDM-B estimates of f_{max} are consistently higher than those of FSAM and FSAMx. In combination with the experimental finding that FSAM and thus FSAMx underestimate f_{max}, we can conclude that f_{max} of LPDM-B is a more realistic estimate. However, compared to our measurements the probability of downwind flux contributions in LPDM-B is still small even under conditions with a considerable along-wind diffusion. This dependence is better reflected in FSAMx. Footprint estimates of LPDM-B and FSAMx seem to converge in the downwind region for stronger along-wind diffusion and higher instabilities.

Although FSAMx does not reach f_{max} of LPDM-B, it reflects the relevance of flux contributions from both, downwind sources and upwind regions close to the measurement system better than the original model FSAM. Because it accounts for along-wind turbulent fluctuations, the presented model FSAMx describes turbulence, and thus the footprint probability distribution, more realistically.

5 Summary and Conclusions

This thesis consists of two main innovative parts: The first part comprises the first direct experimental evaluation of the 2-dimensional flux footprint distribution in real field conditions. In the second part, an extended version of the flux footprint model FSAM (Schmid, 1994), FSAMx, is introduced. It contains a newly defined standalone module that can be applied to the output of any other simple, similarity-theory based footprint model to include streamwise turbulent fluctuations.

Experimental evaluation of flux footprint models
This part aimed at evaluating simple, computationally inexpensive flux footprint models that are commonly used for real time data analysis, although their assumption of horizontally homogeneous turbulence is usually violated in practical flux measurement conditions. The evaluation experiments were conducted at a site with nearly ideal conditions, and in a second stage with clearly non-ideal conditions. The TERENO site in Graswang was shown to offer ideal conditions for conducting tracer experiments with methane: first, the natural flux of the chosen tracer gas (methane) is negligible and second, due to the prevailing mountain-valley-breeze pattern, wind directions are predictable and a fixed tracer release setup could be implemented.
The performance of the analytical footprint models of Schmid (1994) (FSAM) and Kormann and Meixner (2001) (KM), as well as the footprint parameterizations of Hsieh et al. (2000) (HS) and Kljun et al. (2015) (FFP) are investigated by comparing estimated to measured flux contributions from a small ($\sim 1\mathrm{m}^2$) surface source of the artificially released tracer gas. By analyzing tracer flux contributions of different experiment setups the following conclusions can be drawn:

- The proposed experimental evaluation method is applicable and provides valuable information to evaluate 2-dimensional flux footprint functions.
- Considering the whole ensemble of observations, FFP fits best to measured flux contributions and FSAM, KM, and HS match observations roughly.
- HS considerably and consistently underestimates observations for near neutral to stable conditions.
- KM, FSAM, and HS considerably underestimate flux contributions in regions close to the measurement system (closer than x_{max}). No such analysis could be carried out for the FFP model as no data are available for an upwind distance smaller than x_{max} of FFP.
- KM, FSAM, and HS tend to underestimate f_{max} but also to overestimate x_{max}. The footprint peak location of the FFP model could not be evaluated.

- Flux contributions from downwind sources are measurable and non-negligible.
- The relevance of downwind flux contributions is dependent on the along-wind turbulence intensity $\sigma_u/\overline{u}$.
- All evaluated models are sensitive to an abrupt change in surface roughness and sensible heat flux in the upwind vicinity of the measurement tower. FSAM, HS, and FFP showed a non-negligible decline in model quality while KM appeared to be the model with least sensitivity (but the largest overall error).

The facts that flux contributions from downwind sources are not negligible in conditions with moderate and high along-wind turbulent intensities and that regions closer than x_{max} are underestimated by KM, FSAM, and HS are, in part, attributable to neglecting along-wind turbulent diffusion. Therefore, a standalone module is introduced in the second part of this thesis that can be used to incorporate along-wind turbulent fluctuations into footprint models.

Integration of along-wind diffusion in FSAM

In the second part of this thesis, a practicable approach that enables the integration of along-wind turbulent fluctuations into simple, similarity-theory based footprint models is presented. It consists of a standalone module that is superimposed on the two-dimensional output of the footprint model FSAM (Schmid, 1994), resulting in the extended version FSAMx. Its characteristics are summarized in the following:

- First, a Gaussian along-wind dispersion component D_x is defined.
- It's standard deviation is determined from along-wind turbulence intensity $\sigma_u/\overline{u}$ and travel time, and is therefore dependent also on upwind distance.
- The implementation of along-wind diffusion is realized by a non-stationary convolution of the 2-dimensional footprint with the spatially varying kernel D_x.
- By applying a simplified discrete convolution the module can be applied to the gridded outcome of any footprint model.
- Compared to the original model FSAM, FSAMx increases the relevance of flux contributions at short upwind distances, has its maximum contribution closer to the measurement system, and is able to estimate flux contributions from sources downwind of the measurement system.
- Although f_{max} is reduced compared to FSAM, FSAMx reflects the relevance of flux contributions from upwind regions close to the measurement system and from downwind sources better.

A comparison of footprint estimates of FSAMx with the Lagrangian model LPDM-B (Kljun et al., 2002) demonstrates that LPDM-B estimates of f_{max} are higher than those of FSAMx. Nevertheless, the dependence of flux contributions from downwind sources on along-wind turbulent fluctuations appear to be better reflected in FSAMx than in LPDM-B, as the number of particle touchdowns contributing to downwind flux necessarily remains limited in LPDM-B even in conditions with considerable along-wind diffusion. However, the evaluation of downwind fluxes needs to be handled with care as it is based on few data points only. We can conclude that, even though FSAMx most likely underestimates f_{max}, it describes the distribution of flux contributions in regions close to and downwind of the measurement system more realistically.

References

Amiro, B. (1998). Footprint climatologies for evapotranspiration in a boreal catchment. *Agricultural and Forest Meteorology*, 90(3):195–201.

Aubinet, M., Vesala, T., and Papale, D., editors (2012). *Eddy Covariance. A Practical Guide to Measurement and Data Analysis.* Springer.

Baldocchi, D. (1997). Flux footprints within and over forest canopies. *Boundary-Layer Meteorology*, 85(2):273–292.

Baldocchi, D., Falge, E., Gu, L., Olson, R., Hollinger, D., Running, S., Anthoni, P., Bernhofer, C., Davis, K., Evans, R., Fuentes, J., Goldstein, A., Katul, G., Law, B., Lee, X., Malhi, Y., Meyers, T., Munger, W., Oechel, W., U, K., Pilegaard, K., Schmid, H., Valentini, R., Verma, S., Vesala, T., Wilson, K., and Wofsy, S. (2001). Fluxnet: A new tool to study the temporal and spatial variability of ecosystem-scale carbon dioxide, water vapor, and energy flux densities. *Bull.Amer.Meteor.Soc.*, 82(11):2415–2434.

Baldocchi, D. D., Hincks, B. B., and Meyers, T. P. (1988). Measuring biosphere-atmosphere exchanges of biologically related gases with micrometeorological methods. *Ecology*, pages 1331–1340.

Burba, G. (2013). *Eddy covariance method for scientific, industrial, agricultural and regulatory applications: A field book on measuring ecosystem gas exchange and areal emission rates.* Li-Cor Biosciences.

Chatwin, P., Lewis, D., and Mole, N. (1996). Atmospheric diffusion: some new mathematical models. *Advances in Computational Mathematics*, 6(1):227–242.

Chen, B., Ge, Q., Fu, D., Yu, G., Sun, X., Wang, S., and Wang, H. (2010). A data-model fusion approach for upscaling gross ecosystem productivity to the landscape scale based on remote sensing and flux footprint modelling. *Biogeosciences*, 7(9):2943–2958.

Claussen, M. (1989). Subgrid-scale fluxes and flux divergences in a neutrally stratified, horizontally inhomogeneous surface-layer. *Contributions to atmospheric physics*, 62:236–245.

Cooper, D., Eichinger, W., Archuleta, J., Hipps, L., Kao, J., Leclerc, M., Neale, C., and Prueger, J. (2003). Spatial source-area analysis of three-dimensional moisture fields from lidar, eddy covariance, and a footprint model. *Agricultural and Forest Meteorology*, 114(3-4):213–234.

De Haan, P. and Rotach, M. W. (1998). A novel approach to atmospheric dispersion modelling: The puff-particle model. *Quarterly Journal of the Royal Meteorological Society*, 124(552):2771–2792.

Deardorff, J. and Willis, G. (1975). A parameterization of diffusion into the mixed layer. *Journal of Applied Meteorology*, 14(8):1451–1458.

Detto, M., Montaldo, N., Albertson, J. D., Mancini, M., and Katul, G. (2006). Soil moisture and vegetation controls on evapotranspiration in a heterogeneous mediterranean ecosystem on sardinia, italy. *Water Resources Research*, 42(8).

Dragoni, D., Schmid, H., Grimmond, C., and Loescher, H. (2007). Uncertainty of annual net ecosystem productivity estimated using eddy covariance flux measurements. *Journal of Geophysical Research: Atmospheres (1984–2012)*, 112(D17).

Dyer, A. (1974). A review of flux-profile relationships. *Boundary-Layer Meteorology*, 7(3):363–372.

Eugster, W., McFadden, J. P., and Chapin III, F. S. (1997). A comparative approach to regional variation in surface fluxes using mobile eddy correlation towers. *Boundary-Layer Meteorology*, 85(2):293–307.

Finkelstein, P. and Sims, P. (2001). Sampling error in eddy correlation flux measurements. *Journal of Geophysical Research-Atmospheres*, 106(D4):3503–3509.

Finn, D., Lamb, B., Leclerc, M., and Horst, T. (1996). Experimental evaluation of analytical and lagrangian surface-layer flux footprint models. *Boundary-Layer Meteorology*, 80(3):283–308.

Flesch, T. (1996). The footprint for flux measurements, from backward lagrangian stochastic models. *Boundary-Layer Meteorology*, 78(3-4):399–404.

Flesch, T., Wilson, J., and Yee, E. (1995). Backward-time lagrangian stochastic dispersion models and their application to estimate gaseous emissions. *J.Appl.Meteor.*, 34(6):1320–1332.

Foken, T. (2008). *Micrometeorology.*, volume 1. Springer, Berlin.

Foken, T. and Leclerc, M. (2004). Methods and limitations in validation of footprint models. *Agricultural and Forest Meteorology*, 127(3-4):223–234.

Foken, T., Mauder, M., Liebethal, C., Wimmer, F., Beyrich, F., Leps, J., Raasch, S., Debruin, H., Meijninger, W., and Bange, J. (2010). Energy balance closure for the litfass-2003 experiment. *Theoretical and Applied Climatology*, 101(1-2):149–160.

Gash, J. (1986). Observations of turbulence downwind of a forest-heath interface. *Boundary-Layer Meteorology*, 36(3):227–237.

Goeckede, M., Markkanen, T., Hasager, C. B., and Foken, T. (2006). Update of a footprint-based approach for the characterisation of complex measurement sites. *Boundary-Layer Meteorology*, 118(3):635–655.

Goeckede, M., Markkanen, T., Mauder, M., Arnold, K., Leps, J. P., and Foken, T. (2005). Validation of footprint models using natural tracer measurements from a field experiment. *Agricultural and Forest Meteorology*, 135(1-4):314–325.

Goeckede, M., Rebmann, C., and Foken, T. (2004). A combination of quality assessment tools for eddy covariance measurements with footprint modelling for the characterisation of complex sites. *Agricultural and Forest Meteorology*, 127(3-4):175–188.

Gryning, S.-E., Holtslag, A., Irwin, J. S., and Sivertsen, B. (1987). Applied dispersion modelling based on meteorological scaling parameters. *Atmospheric Environment (1967)*, 21(1):79–89.

Guo, X. and Cai, X. (2005). Footprint characteristics of scalar concentration in the convective boundary layer. *Advances in Atmospheric Sciences*, 22(6):821–830.

Hadfield, M. (1994). Passive scalar diffusion from surface sources in the convective boundary layer. *Boundary-Layer Meteorology*, 69(4):417–448.

Hanna, S. R., Briggs, G. A., and Hosker Jr, R. P. (1982). Handbook on atmospheric diffusion. Technical report, National Oceanic and Atmospheric Administration, Oak Ridge, TN (USA). Atmospheric Turbulence and Diffusion Lab.

Heidbach, K., Schmid, H. P., and Mauder, M. (2017). Experimental evaluation of flux footprint models. *Agricultural and Forest Meteorology*, 246:142 – 153.

Holtslag, A. and De Bruin, H. (1988). Applied modeling of the nighttime surface energy balance over land. *J.Appl.Meteor.*, 27(6):689–704.

Hommeltenberg, J., Mauder, M., Droesler, M., Heidbach, K., Werle, P., and Schmid, H. P. (2014a). Ecosystem scale methane fluxes in a natural temperate bog-pine forest in southern germany. *Agricultural and Forest Meteorology*, 198:273–284.

Hommeltenberg, J., Schmid, H., Droesler, M., and Werle, P. (2014b). Can a bog drained for forestry be a stronger carbon sink than a natural bog forest? *Biogeosciences*, 11(13):3477–3493.

Horst, T. (1979). Lagrangian similarity modeling of vertical diffusion from a ground-level source. *J.Appl.Meteor.*, 18(6):733–740.

Horst, T. and Weil, J. (1992). Footprint estimation for scalar flux measurements in the atmospheric surface-layer. *Boundary-Layer Meteorology*, 59(3):279–296.

Horst, T. and Weil, J. (1994). How far is far enough - the fetch requirements for micrometeorological measurement of surface fluxes. *J.Atmos.Oceanic Technol.*, 11(4):1018–1025.

Hsieh, C., Katul, G., and Chi, T. (2000). An approximate analytical model for footprint estimation of scaler fluxes in thermally stratified atmospheric flows. *Advances in Water Resources*, 23(7):765–772.

Huang, C. (1979). Theory of dispersion in turbulent shear-flow. *Atmospheric Environment*, 13(4):453–463.

Kaimal, J., Wyngaard, J., Izumi, Y., and Coté, O. (1972). Spectral characteristics of surface-layer turbulence. Technical report, DTIC Document.

Kaimal, J. C. and Finnigan, J. J. (1994). *Atmospheric boundary layer flows: their structure and measurement*. Oxford University Press, New York.

Kim, J., Guo, Q., Baldocchi, D., Leclerc, M., Xu, L., and Schmid, H. (2006). Upscaling fluxes from tower to landscape: Overlaying flux footprints on high-resolution (ikonos) images of vegetation cover. *Agricultural and Forest Meteorology*, 136(3-4):132–146.

Kljun, N., Calanca, P., Rotach, M., and Schmid, H. (2015). A simple two-dimensional parameterisation for flux footprint prediction (ffp). *Geoscientific Model Development*, 8(11):3695–3713.

Kljun, N., Calanca, P., Rotachhi, M., and Schmid, H. (2004a). A simple parameterisation for flux footprint predictions. *Boundary-Layer Meteorology*, 112(3):503–523.

Kljun, N., Kastner-Klein, P., Fedorovich, E., and Rotach, M. (2004b). Evaluation of lagrangian footprint model using data from wind tunnel convective boundary layer. *Agricultural and Forest Meteorology*, 127(3-4):189–201.

Kljun, N., Kormann, R., Rotach, M., and Meixer, F. (2003). Comparison of the lagrangian footprint model lpdm-b with an analytical footprint model. *Boundary-Layer Meteorology*, 106(2):349–355.

Kljun, N., Rotach, M., and Schmid, H. (2002). A three-dimensional backward lagrangian footprint model for a wide range of boundary-layer stratifications. *Boundary-Layer Meteorology*, 103(2):205–226.

Kormann, R. and Meixner, F. (2001). An analytical footprint model for non-neutral stratification. *Boundary-Layer Meteorology*, 99(2):207–224.

Kurbanmuradov, O. and Sabelfeld, K. (2000). Lagrangian stochastic models for turbulent dispersion in the atmospheric boundary layer. *Boundary-layer meteorology*, 97(2):191–218.

Kustas, W. P., Anderson, M. C., French, A. N., and Vickers, D. (2006). Using a remote sensing field experiment to investigate flux-footprint relations and flux sampling distributions for tower and aircraft-based observations. *Advances in Water Resources*, 29(2):355–368.

Le, H., Moin, P., and Kim, J. (1997). Direct numerical simulation of turbulent flow over a backward-facing step. *Journal of fluid mechanics*, 330(1):349–374.

Leclerc, M. and Foken, T. (2014). *Footprints in Micrometeorology and Ecology*. Springer, Dordrecht.

Leclerc, M., Karipot, A., Prabha, T., Allwine, G., Lamb, B., and Gholz, H. (2003a). Impact of non-local advection on flux footprints over a tall forest canopy: a tracer flux experiment. *Agricultural and Forest Meteorology*, 115(1-2):19–30.

Leclerc, M., Meskhidze, N., and Finn, D. (2003b). Comparison between measured tracer fluxes and footprint model predictions over a homogeneous canopy of intermediate roughness. *Agricultural and Forest Meteorology*, 117(3-4):145–158.

Leclerc, M., Shen, S., and Lamb, B. (1997). Observations and large-eddy simulation modeling of footprints in the lower convective boundary layer. *Journal of Geophysical Research-Atmospheres*, 102(D8):9323–9334.

Liu, J., Chen, J., Black, T., and Novak, M. (1996). E-epsilon modelling of turbulent air flow downwind of a model forest edge. *Boundary-Layer Meteorology*, 77(1):21–44.

Liu, L., Hu, F., and Cheng, X.-L. (2011). Probability density functions of turbulent velocity and temperature fluctuations in the unstable atmospheric surface layer. *Journal of Geophysical Research: Atmospheres*, 116(D12).

Luhar, A. K. (2013). *Turbulent Dispersion: Theory and Parameterization-Overview*, pages 14–18. American Geophysical Union.

Luhar, A. K. and Rao, K. S. (1994). Source footprint analysis for scalar fluxes measured in flows over an inhomogeneous surface. In *Air Pollution Modeling and Its Application X*, pages 315–323. Springer.

Marcolla, B. and Cescatti, A. (2005). Experimental analysis of flux footprint for varying stability conditions in an alpine meadow. *Agricultural and Forest Meteorology*, 135(1-4):291–301.

Markkanen, T., Steinfeld, G., Kljun, N., Raasch, S., and Foken, T. (2009). Comparison of conventional lagrangian stochastic footprint models against les driven footprint estimates. *Atmospheric Chemistry and Physics*, 9(15):5575–5586.

Markkanen, T., Steinfeld, G., Kljun, N., Raasch, S., and Foken, T. (2010). A numerical case study on footprint model performance under inhomogeneous flow conditions. *Meteorologische Zeitschrift*, 19(6):539–547.

Mauder, M., Cuntz, M., Druee, C., Graf, A., Rebmann, C., Schmid, H. P., Schmidt, M., and Steinbrecher, R. (2013). A strategy for quality and uncertainty assessment of long-term eddy-covariance measurements. *Agricultural and Forest Meteorology*, 169:122–135.

Mauder, M., Desjardins, R. L., Pattey, E., and Worth, D. (2010). An attempt to close the daytime surface energy balance using spatially-averaged flux measurements. *Boundary-layer meteorology*, 136(2):175–191.

Mauder, M. and Foken, T. (2004). Documentation and instruction manual of the eddy covariance software package TK2. Technical report, Universitaet Bayreuth, Abteilung Mikrometeorologie.

Metzger, S., Junkermann, W., Mauder, M., Beyrich, F., Butterbach-Bahl, K., Schmid, H., and Foken, T. (2012). Eddy-covariance flux measurements with a weight-shift microlight aircraft. *Atmospheric Measurement Techniques*, 5(7):1699–1717.

Moeng, C. (1984). A large-eddy-simulation model for the study of planetary boundary-layer turbulence. *J.Atmos.Sci.*, 41(13):2052–2062.

Moncrieff, J., Clement, R., Finnigan, J., and Meyers, T. (2004). Averaging, detrending, and filtering of eddy covariance time series. In *Handbook of micrometeorology*, pages 7–31. Springer.

Moncrieff, J., Massheder, J., deBruin, H., Elbers, J., Friborg, T., Heusinkveld, B., Kabat, P., Scott, S., Soegaard, H., and Verhoef, A. (1997). A system to measure surface fluxes

of momentum, sensible heat, water vapour and carbon dioxide. *Journal of Hydrology*, 189(1-4):589–611.

Myklebust, M., Hipps, L., and Ryel, R. J. (2008). Comparison of eddy covariance, chamber, and gradient methods of measuring soil co 2 efflux in an annual semi-arid grass, bromus tectorum. *agricultural and forest meteorology*, 148(11):1894–1907.

Neftel, A., Spirig, C., and Ammann, C. (2008). Application and test of a simple tool for operational footprint evaluations. *Environmental Pollution*, 152(3):644–652.

Nicolini, G., Fratini, G., Avilov, V., Kurbatova, J., Vasenev, I., and Valentini, R. (2015). Performance of eddy-covariance measurements in fetch-limited applications. *Theoretical and Applied Climatology*, pages 1–12.

Ogunjemiyo, S. O., Kaharabata, S. K., Schuepp, P. H., MacPherson, I. J., Desjardins, R. L., and Roberts, D. A. (2003). Methods of estimating co 2, latent heat and sensible heat fluxes from estimates of land cover fractions in the flux footprint. *Agricultural and Forest Meteorology*, 117(3):125–144.

Panofsky, H., Larko, D., Lipschutz, R., Stone, G., Bradley, E., Bowen, A. J., and Højstrup, J. (1982). Spectra of velocity components over complex terrain. *Quarterly Journal of the Royal Meteorological Society*, 108(455):215–230.

Pasquill, F. (1971). Atmospheric dispersion of pollution. *Quarterly Journal of the Royal Meteorological Society*, 97(414):369–395.

Pasquill, F. and Smith, F. (1983). *Atmospheric Diffusion.*, volume 3. Ellis Horwood limited, Chichester.

Paulson, C. (1970). The mathematical representation of wind speed and temperature profiles in the unstable atmospheric surface layer. *J.Appl.Meteor.*, 9(6):857–861.

Raasch, S. and Schröter, M. (2001). Palm–a large-eddy simulation model performing on massively parallel computers. *Meteorologische Zeitschrift*, 10(5):363–372.

Rannik, U., Aubinet, M., Kurbanmuradov, O., Sabelfeld, K., Markkanen, T., and Vesala, T. (2000). Footprint analysis for measurements over a heterogeneous forest. *Boundary-Layer Meteorology*, 97(1):137–166.

Rannik, U., Markkanen, T., Raittila, J., Hari, P., and Vesala, T. (2003). Turbulence statistics inside and over forest: Influence on footprint prediction. *Boundary-Layer Meteorology*, 109(2):163–189.

Rannik, U., Sogachev, A., Foken, T., Goeckede, M., Kljun, N., Leclerc, M., and Vesala, T. (2012). Footprint analysis. In Aubinet, M., Vesala, T., and Papale, D., editors, *Eddy Covariance: A Practical Guide to Measurement and Data Analysis*, number 8, pages –. Springer Atmospheric Sciences.

Reithmaier, L., Gockede, M., Markkanen, T., Knohl, A., Churkina, G., Rebmann, C., Buchmann, N., and Foken, T. (2006). Use of remotely sensed land use classification for a better evaluation of micrometeorological flux measurement sites. *Theoretical and Applied Climatology*, 84(4):219–233.

Reth, S., Gockede, M., and Falge, E. (2005). Co2 efflux from agricultural soils in eastern germany - comparison of a closed chamber system with eddy covariance measurements. *Theoretical and Applied Climatology*, 80(2-4):105–120.

Reynolds, A. (1998). A two-dimensional lagrangian stochastic dispersion model for convective boundary layers with wind shear. *Boundary-Layer Meteorology*, 86(2):345–352.

Richardson, A., Aubinet, M., Barr, A., Hollinger, D., Ibrom, A., Lasslop, G., and Reichstein, M. (2012). Uncertainty quantification. In Aubinet, M., Vesala, T., and Papale, D., editors, *Eddy Covariance: A Practical Guide to Measurement and Data Analysis*, pages 173–209. Springer, Dordrecht.

Roedel, W. (2011). *Physik unserer Umwelt: Die Atmosphaere.*, volume 3. Springer, Berlin, Heidelberg.

Rotach, M. W., Gryning, S.-E., and Tassone, C. (1996). A two-dimensional lagrangian stochastic dispersion model for daytime conditions. *Quarterly Journal of the Royal Meteorological Society*, 122(530):367–389.

Schmid, H. (1994). Source areas for scalars and scalar fluxes. *Boundary-Layer Meteorology*, 67(3):293–318.

Schmid, H. (1997). Experimental design for flux measurements: matching scales of observations and fluxes. *Agricultural and Forest Meteorology*, 87(2-3):179–200.

Schmid, H. (2002). Footprint modeling for vegetation atmosphere exchange studies: a review and perspective. *Agricultural and Forest Meteorology*, 113(1-4):159–183.

Schmid, H. and Bunzli, B. (1995). The influence of surface texture on the effective roughness length. *Q.J.R.Meteorol.Soc.*, 121(521):1–21.

Schmid, H., Cleugh, H., Grimmond, C., and Oke, T. (1991). Spatial variability of energy fluxes in suburban terrain. *Boundary-Layer Meteorology*, 54(3):249–276.

Schmid, H. and Lloyd, C. (1999). Spatial representativeness and the location bias of flux footprints over inhomogeneous areas. *Agricultural and Forest Meteorology*, 93(3):195–209.

Schmid, H. and Oke, T. (1990). A model to estimate the source area contributing to turbulent exchange in the surface-layer over patchy terrain. *Q.J.R.Meteorol.Soc.*, 116(494):965–988.

Schuepp, P., Leclerc, M., Macpherson, J., and Desjardins, R. (1990). Footprint prediction of scalar fluxes from analytical solutions of the diffusion equation. *Boundary-Layer Meteorology*, 50(1-4):353–373.

Slade, D. H. (1968). Meteorology and atomic energy, 1968. Technical report, Environmental Science Services Administration, Silver Spring, Md. Air Resources Labs.

Sogachev, A., Leclerc, M., Karipot, A., Zhang, G., and Vesala, T. (2005). Effect of clearcuts on footprints and flux measurements above a forest canopy. *Agricultural and Forest Meteorology*, 133(1-4):182–196.

Sogachev, A., Leclerc, M., Zhang, G., Rannik, U., and Vesala, T. (2008). Co2 fluxes near a forest edge: A numerical study. *Ecological Applications*, 18(6):1454–1469.

Sogachev, A. and Lloyd, J. (2004). Using a one-and-a-half order closure model of the atmospheric boundary layer for surface flux footprint estimation. *Boundary-Layer Meteorology*, 112(3):467–502.

Sogachev, A., Menzhulin, G., Heimann, M., and Lloyd, J. (2002). A simple three-dimensional canopy - planetary boundary layer simulation model for scalar concentrations and fluxes. *Tellus Series B-Chemical and Physical Meteorology*, 54(5):784–819.

Sogachev, A., Rannik, U., and Vesala, T. (2004). Flux footprints over complex terrain covered by heterogeneous forest. *Agricultural and Forest Meteorology*, 127(3-4):143–158.

Song, J. and Wesely, M. (2003). On comparison of modeled surface flux variations to aircraft observations. *Agricultural and forest meteorology*, 117(3):159–171.

Steinfeld, G. (2009). *Die Beurteilung von Turbulenzmess- und Analyseverfahren der Mikrometeorologie durch virtuelle Messungen innerhalb von Grobstruktursimulationen.*

dissertation, Leibniz Universitaet Hannover, Institute for Meteorology and Climatology.

Steinfeld, G., Raasch, S., and Markkanen, T. (2008). Footprints in homogeneously and heterogeneously driven boundary layers derived from a lagrangian stochastic particle model embedded into large-eddy simulation. *Boundary-Layer Meteorology*, 129(2):225–248.

Stockie, J. M. (2011). The mathematics of atmospheric dispersion modeling. *Siam Review*, 53(2):349–372.

Stull, R. (1999). *An introduction to boundary layer meteorology*. Kluwer Academic Publishers, Dordrecht.

Taylor, G. I. (1921). Diffusion by continuous movements. *Proceedings of the London Mathematical Society*, s2-20(1):196–212.

Thomson, D. (1987). Criteria for the selection of stochastic-models of particle trajectories in turbulent flows. *Journal of Fluid Mechanics*, 180:529–556.

van de Boer, A., Moene, A., Schuettemeyer, D., and Graf, A. (2013). Sensitivity and uncertainty of analytical footprint models according to a combined natural tracer and ensemble approach. *Agricultural and Forest Meteorology*, 169:1–11.

Van Ulden, A. (1978). Simple estimates for vertical diffusion from sources near the ground. *Atmospheric Environment*, 12(11):2125–2130.

Vesala, T., Kljun, N., Rannik, U., Rinne, J., Sogachev, A., Markkanen, T., Sabelfeld, K., Foken, T., and Leclerc, M. (2008). Flux and concentration footprint modelling: State of the art. *Environmental Pollution*, 152(3):653–666.

Webb, E., Pearman, G., and Leuning, R. (1980). Correction of flux measurements for density effects due to heat and water-vapor transfer. *Q.J.R.Meteorol.Soc.*, 106(447):85–100.

Willmott, C., Ackleson, S., Davis, R., Feddema, J., Klink, K., Legates, D., Odonnell, J., and Rowe, C. (1985). Statistics for the evaluation and comparison of models. *Journal of Geophysical Research-Oceans*, 90(NC5):8995–9005.

Willmott, C. J. (1981). On the validation of models. *Physical Geography*, 2(2):184–194.

Wilson, K., Goldstein, A., Falge, E., Aubinet, M., Baldocchi, D., Berbigier, P., Bernhofer, C., Ceulemans, R., Dolman, H., Field, C., Grelle, A., Ibrom, A., Law, B., Kowalski,

A., Meyers, T., Moncrieff, J., Monson, R., Oechel, W., Tenhunen, J., Valentini, R., and Verma, S. (2002). Energy balance closure at fluxnet sites. *Agricultural and Forest Meteorology*, 113(1-4):223–243.

Zacharias, S., Bogena, H., Samaniego, L., Mauder, M., Fuß, R., Pütz, T., Frenzel, M., Schwank, M., Baessler, C., Butterbach-Bahl, K., et al. (2011). A network of terrestrial environmental observatories in germany. *Vadose Zone Journal*, 10(3):955–973.

Zeeman, M., Mauder, M., Steinbrecher, R., Heidbach, K., Eckart, E., and Schmid, H. (2017). Reduced snow cover affects productivity of upland temperate grasslands. *Agricultural and Forest Meteorology*, 232:514–526.

List of Abbreviations and Symbols

D_x ..... Along-wind concentration distribution function
D_y ..... Crosswind concentration distribution function
D_z ..... Vertical concentration distribution function
F ..... Scalar Flux
L ..... Obukhov length
Q ..... Emission rate
U ..... Effective plume velocity
X_{close} ..... Mobile tower close to forest edge, configuration D
X_{far} ..... Permanent tower, configuration D
Γ ..... Gamma-function
Φ_h ..... Surface flux layer function describing the stability dependence of the eddy diffusivity of sensible heat
δ ..... Dirac-delta distribution function
ϵ_a ..... Model uncertainty resulting from the violation of model assumptions
ϵ_c ..... Measurement uncertainty as a result of instrument design and calibration errors
ϵ_f ..... Measurement uncertainty associated with spatial representativeness affected by variability of the source field within the footprint
ϵ_i ..... Measurement uncertainty due to the instrument system
ϵ_p ..... Measurement uncertainty resulting from data processing
ϵ_t ..... Turbulence sampling error
ϵ_{EC} ..... Measurement uncertainty due to unmet assumptions of the EC method
ϵ_{in} ..... Model uncertainty propagating from the uncertainty of input parameters
ϵ_{model} ..... Uncertainty of footprint model
ϵ_{obs} ..... Uncertainty of observations
ϵ_{th} ..... Model uncertainty resulting from an incomplete or deficient model theory
$\frac{\sigma_u}{\overline{u}}$ ..... Along-wind turbulence intensity
$\overline{C^y}$ ..... Crosswind integrated concentration
$\overline{F^y}$ ..... Crosswind integrated flux
$\overline{f^y}$ ..... Crosswind integrated footprint function
$\overline{u}$ ..... Mean horizontal wind velocity

$\overline{w'T'}$ ..... Sensible heat flux
$\overline{w'T'}$ ..... Standard deviation of D_y
$\overline{z}$ ..... Mean plume height
ψ ..... Surface flux layer function describing the stability dependence of the wind profile
ρ_a ..... Air density
σ_u ..... Standard deviation of the along-wind component u
σ_v ..... Standard deviation of the lateral wind component v
σ_w ..... Standard deviation of the vertical wind component w
σ_y ..... Standard deviation of D_y
$\sigma_{\overline{w'T'}}$ ..... Random error of sensible heat flux
σ_{u_*} ..... Random error of friction velocity
$\tilde{x}$ ..... Along-wind distance of the convoluted footprint
$\tilde{Q}$ ..... Spatial distribution of stationary surface sources/sinks
$\vec{F}_A$ ..... Advective component of a flux
$\vec{F}_D$ ..... Diffusive component of a flux
$\vec{u}$ ..... horizontal wind velocity
c ..... dry mole fraction of a specific gas in the air
f ..... 2-dimensional footprint function
f_x ..... 2-dimensional footprint function including along-wind diffusion
$f_{estimated}$ ..... Estimated flux contribution
f_{max} ..... Maximum contribution of the footprint
$f_{measured}$ ..... Measured flux contribution
h ..... Boundary layer height
k ..... Von Kármán constant
u ..... Along-wind component of the wind vector
$u*$ ..... Friction velocity
v ..... Crosswind component of the wind vector
w ..... Vertical wind component
x ..... Along-wind distance
x_{max} ..... Distance of maximum contribution of the footprint
y ..... Crosswind distance
z_0 ..... Roughness length
z_m ..... Aerodynamic measurement height
ASTER ..... **A**dvanced **s**paceborne **t**hermal **e**mission and **r**eflection **r**adiometer

C ..... Gas concentration
CH_4 ..... Methane
CO_2 ..... Carbon dioxide
d ..... Index of agreement
DEM ..... **D**igital **e**levation **m**odel
EC ..... **E**ddy **c**ovariance
FFP ..... **F**lux **F**ootprint **P**rediction of Kljun et al. (2015)
FLUXNET ... A global network of micrometeorological flux measurement sites
FSAM ..... Extended version of FSAM
FSAM ..... **F**lux **s**ource **a**rea **m**odel of Schmid (1994)
H_2O ..... Water
HS ..... Footprint model of Hsieh et al. (2000)
IRGA ..... **I**nfra**r**ed **G**as **A**nalyzer
ITS ..... Integral time scale
K ..... Diffusion Coefficient
KM ..... Footprint model of Kormann and Meixner (2001)
LAI ..... Leaf area index
LES ..... Large eddy simulation
LPDM-B ..... backward Lagrangian Particle Dispersion Model
LS ..... Lagrangian simulation
PALM ..... Parallelized large-eddy simulation model
R^2 ..... Coefficient of determination
RANS ..... **R**eynolds **a**veraged numerical **N**avier-**S**tokes simulation
RMSD ..... Root mean square deviation
RMSE ..... Root mean square error
$RMSE_s$ ..... Systematic root mean square error
$RMSE_u$ ..... Unsystematic root mean square error
RSSI ..... **R**eceived **s**ignal **s**trength **i**ndicator
S ..... source or sink strength of a gas
SAM ..... **S**ource **a**rea **m**odel of Schmid and Oke (1990)
SCADIS ..... **sca**lar **dis**tribution - a RANS model of Sogachev et al. (2002)
SF_6 ..... Sulfur hexafluoride
TERENO ..... **Ter**restrial **En**vironmental **O**bservatories
TKE ..... Turbulence kinetic energy
X_{close} ..... Designation of the EC-mast close to the forest edge

X_{far} ..... Designation of the permanent EC-mast

List of Figures

List of Tables

Acknowledgements

My research was conducted at the Karlsruhe Institute of Technology (KIT), Institute of Meteorology and Climate Research, Department of Atmospheric Environmental Research (IMK-IFU), located in Garmisch-Partenkirchen, in collaboration with the chair of Atmospheric Environmental Research, Technical University Munich.

I am very grateful to my supervisor, Professor Dr. Hans Peter Schmid, that he gave me the opportunity to shape my own PhD topic. I am happy that I could profit from his broad meteorological knowledge and his talent to show light at the end of the tunnel, no matter how long and curvy the tunnel is. I am thankful for the numerous chances to visit international conferences in San Francisco, Portland, Helsinki, and Berlin, which were a great addition and benefit for my PhD.

As a fellow of the Helmholtz Research School on Mechanisms and Interactions of Climate Change in Mountain Regions (MICMoR), I greatly benefited from various Summer Schools, Technical Short Courses and Professional Skills Courses as well as from the financial support for conference attendances. I wish to thank Petra Guppenberger, Karen Suppan, and Dr. Elija Bleher from the MICMoR coordination office for their enthusiasm and their perfect organisation of all events. Furthermore, I would like to thank Prof. Dr. Ralf Ludwig and Dr. Matthias Mauder for valuable discussions as part of my MICMoR 'Thesis Advisory Committee'.

I am grateful that I could utilize the measurements of the observation networks TERENO and ICOS-Ecosystems which are funded, in part, by the German Helmholtz Association and the German Federal Ministry of Education and Research (BMBF). This work was embedded in the Helmholtz-Association's climate initiative REKLIM (Topic 4 'The Land Surface in the Climate System') which I would like to acknowledge for additional funding.

I thank Dr. Matthias Mauder for his support in micrometeorological concerns and Dr. Peter Werle for fruitful and critical discussions. Thanks to Elisabeth, Carsten J., Carsten M. who helped me to install the field setup.

Without Janina, this thesis would never have been completed. I am very happy that we shared not only our office and scientific problems, but also every day-to-day challenge and any other question of life. Special thanks to Jo, Hong, and all other colleagues for our absolutely necessary daily meetings at 10:00 a.m.

Ganz besonders möchte ich meinen Eltern und meinem Bruder für ihre Unterstützung, ihre Neugier und ihren Stolz danken. Ohne Euch hätte ich es nicht so weit geschafft. Zu guter Letzt bedanke ich mich von Herzen bei Carsten für seine Unterstützung in schwierigen Zeiten und die richtigen Worte im richtigen Moment.